NEW POLYMER ELECTROLYTES OF BIO-BASED POLYURETHANE FOR DYE-SENSITIZED SOLAR CELL APPLICATIONS

SALMIAH BINTI IBRAHIM

INSTITUTE OF GRADUATE STUDIES
UNIVERSITY OF MALAYA
KUALA LUMPUR

2016

NEW POLYMER ELECTROLYTES OF BIO-BASED POLYURETHANE FOR DYE-SENSITIZED SOLAR CELL APPLICATIONS

SALMIAH BINTI IBRAHIM

THESIS SUBMITTED IN FULFILMENT OF THE REQUIREMENTS FOR THE DEGREE OF DOCTOR OF PHILOSOPHY

INSTITUTE OF GRADUATE STUDIES
UNIVERSITY OF MALAYA
KUALA LUMPUR

2016

UNIVERSITY OF MALAYA

ORIGINAL LITERARY WORK DECLARATION

Name of Candidate : **SALMIAH BINTI IBRAHIM**

I.C/Passport No :

Registration/Matric No: **HHC 110005**

Name of Degree : **DOCTOR OF PHILOSOPHY**

Title of Project Paper/Research Report/Dissertation/Thesis ("this Work"):

NEW POLYMER ELECTROLYTES OF BIO-BASED POLYURETHANE FOR DYE-SENSITIZED SOLAR CELL APPLICATIONS

Field of Study : **APPLIED SCIENCE**

I do solemnly and sincerely declare that:

(1) I am the sole author/writer of this Work;
(2) This Work is original;
(3) Any use of any work in which copyright exists was done by way of fair dealing and for permitted purposes and any excerpt or extract from, or reference to or reproduction of any copyright work has been disclosed expressly and sufficiently and the title of the Work and its authorship have been acknowledged in this Work;
(4) I do not have any actual knowledge nor do I ought reasonably to know that the making of this work constitutes an infringement of any copyright work;
(5) I hereby assign all and every rights in the copyright to this Work to the University of Malaya ("UM"), who henceforth shall be owner of the copyright in this Work and that any reproduction or use in any form or by any means whatsoever is prohibited without the written consent of UM having been first had and obtained;
(6) I am fully aware that if in the course of making this Work I have infringed any copyright whether intentionally or otherwise, I may be subject to legal action or any other action as may be determined by UM.

Candidate's Signature Date:

Subscribed and solemnly declared before,

Witness's Signature Date:

Name:

Designation:

ABSTRACT

In this research work, a new bio-based polyurethane (PU) based on castor oil was synthesized as host polymer in electrolytes for application in dye-sensitized solar cell (DSSC). In the first stage of this work, castor oil based polyol was synthesized via transesterification reaction under nitrogen gas atmosphere at room temperature. The polyol possessed acid value of 3.0 mg KOH g^{-1}, hydroxyl value of 190 mg KOH g^{-1} and molecular weight of 2786 g mol^{-1}, characteristics suitable for producing flexible PU. The polyol was reacted with 4,4'-diphenylmethane diisocyanate at room temperature in appropriate ratios to form flexible PU. The formation of urethane linkage was confirmed using Fourier transform infrared analysis by the disappearance of NCO peak and appearance of amine (secondary), carbonyl and ether group in PU chain. For the preparation of PU polymer electrolytes, the PU was added with sodium iodide (NaI) and lithium iodide (LiI) salts in different weight percentages to form PU-LiI and PU-NaI systems respectively. 3-propyl-1-methylimidazolium iodide (PMII) ionic liquid was added to the highest conducting sample of PU-NaI and PU-LiI systems to enhance the conductivity as well as the efficiency of DSSC. The characteristics of polymer electrolytes were analyzed using Fourier transform infrared spectroscopy, dynamic mechanical analysis, electrochemical impedance spectroscopy, transference number measurement and linear sweep voltammetry. Glass transition temperature of –15.8 °C of PU decreased upon addition of salts. The lowest glass transition temperature of PU-NaI system was –26.2 °C and PU-LiI system was –27.3 °C. The highest conductivity achieved for the systems were 4.28×10^{-7} S cm^{-1} and 1.41×10^{-6} S cm^{-1}, respectively. The inclusion of PMII ionic liquid to the PU-NaI and PU-LiI enhanced the ionic conductivity of the polymer electrolytes by one order of magnitude and also lowered the T_g value to ~ –33.0 °C. Ionic liquid is believed to act as plasticizer to soften the polymer backbone therefore increase the polymer segmental motion to ease ions migration which in turn increased the ionic conductivity. The conductivity for all PU electrolyte films increased with increase of temperature and follow the Arrhenius behaviour for PU-NaI, PU-LiI and PU-NaI-PMII systems, and Vogel-Tamman-Fulcher behaviour for PU-LiI-PMII. The calculation of activation energy, E_a from the gradient of Arrhenius and Vogel-Tamman-Fulcher plots showed that the trend of conductivity was consistent with the trend of E_a, i.e: the higher conducting sample possessed lower activation energy. The addition of ionic liquid to the PU-salt also enhanced electrochemical stability window of the polymer electrolytes. The electrochemical stability windows were ~ 2.0 V. DSSCs were fabricated employing PU based polymer electrolytes with configuration of FTO/TiO_2-dye/PU electrolytes-I_2/Pt/FTO. Photovoltaic parameters such as current density, open circuit voltage, fill factor and efficiency were calculated from photocurrent–voltage measurement. The highest efficiency employing PU-NaI and PU-LiI systems were 0.80% and 0.83%, respectively, whereas for PU-NaI-PMII was 1.06% and PU-LiI-PMII was 1.92%. These results revealed that the new bio polymer electrolytes have potential for application in DSSC.

ABSTRAK

Dalam penyelidikan ini, bio poliuretana (PU) baru berasaskan minyak jarak telah disintesis sebagai polimer perumah dalam elektrolit untuk diaplikasi dalam sel suria terpeka pewarna (DSSC). Pada peringkat awal kajian ini, poliol berasaskan minyak jarak telah disintesis melalui tindak balas transesterifikasi di bawah persekitaran gas nitrogen pada suhu bilik. Poliol yang dihasilkan mempunyai jumlah asid 3.0 mg KOH g^{-1}, jumlah hidroksil 190 mg KOH g^{-1} dan berat molekul 2786 g mol^{-1} iaitu ciri-ciri yang sesuai untuk menghasilkan poliuretana yang mudah dibentuk. Poliol telah ditindak balaskan dengan 4,4'-difenilmetilena diisosianat pada suhu bilik dalam nisbah yang sesuai untuk membentuk poliuretana mudah bentuk. Pembentukan jaringan uretana dibuktikan melalui analisis spektroskopi inframerah transformasi Fourier iaitu dengan kehilangan puncak NCO dan kemunculan amina (sekunder), karbonil dan kumpulan eter dalam rantaian PU. Untuk penyediaan elektrolit polimer, PU ditambah dengan garam natrium iodida (NaI) dan litium iodida (LiI) dalam peratusan jisim yang berbeza-beza untuk membentuk sistem-sistem PU-NaI dan PU-LiI. 3-propil-1-metilimidazolium iodida (PMII) cecair ionik telah ditambah kepada sampel yang mempunyai kekonduksian paling tinggi dari sistem PU-NaI dan sistem PU-LiI untuk meningkatkan kekonduksian serta kecekapan DSSC. Ciri-ciri elektrolit polimer dianalisis menggunakan spektroskopi inframerah transformasi Fourier, analisis dinamik mekanikal, rintangan elektrokimia spektroskopi, pengukuran nombor pindahan dan voltammetri sapuan linear. Suhu peralihan kaca PU iaitu –15.8 °C menurun apabila garam ditambah kepadanya. Suhu peralihan kaca yang paling rendah pada sistem PU-NaI adalah –26.2 °C dan pada sistem PU-LiI pula adalah –27.3 °C. Kekonduksian tertinggi yang diperolehi dari sistem-sistem ini ialah 4.28×10^{-7} S cm^{-1} dan 1.41×10^{-6} S cm^{-1}. Kemasukan cecair ionik PMII kepada PU-NaI dan PU-LiI telah meningkatkan kekonduksian ionik elektrolit polimer sebanyak satu magnitud dan juga menurunkan nilai T_g kepada ~ –33.0 °C. Cecair ionik dipercayai bertindak sebagai pemplastik untuk melembutkan polimer seterusnya meningkatkan pergerakan segmen polimer untuk memudahkan pergerakan ion-ion, dengan itu meningkatkan kekonduksian ionik. Kekonduksian untuk semua filem elektrolit PU meningkat dengan peningkatan suhu dan mematuhi hukum Arrhenius bagi sistem-sistem PU-NaI, PU-LiI dan PU-NaI-PMII, dan hukum Vogel-Tamman-Fulcher bagi system PU-LiI-PMII. Pengiraan tenaga pengaktifan, E_a dari kecerunan plot Arrhenius dan Vogel-Tamman-Fulcher menunjukkan bahawa nilai kekonduksian konsisten dengan nilai E_a, di mana sampel yang berkekonduksian tinggi mempunyai tenaga pengaktifan yang rendah. Penambahan cecair ionik kepada PU-garam juga meningkatkan tetingkap kestabilan elektrokimia elektrolit polimer. Nilai tetingkap kestabilan elektrokimia adalah ~ 2.0 V. DSSC telah difabrikasi menggunakan elektrolit polimer berasaskan PU dengan konfigurasi FTO/TiO_2-pewarna/PU elektrolit-I_2/Pt/FTO. Parameter-parameter fotovoltan seperti ketumpatan arus, voltan litar buka, faktor isi dan kecekapan telah dikira dari pengukuran fotoarus-voltan. Kecekapan tertinggi yang diperolehi menggunakan sistem-sistem PU-NaI dan PU-LiI adalah masing-masing 0.80% dan 0.83%, manakala bagi PU-NaI-PMII adalah 1.06% dan PU-LiI-PMII adalah 1.92%. Semua keputusan ini menunjukkan bahawa elektrolit bio polimer baru berasaskan poliuretana dari minyak jarak berpotensi untuk diaplikasi dalam DSSC.

ACKNOWLEDGEMENTS

Thank you Allah for giving me the strength and determination to complete my doctoral thesis.

I wish to express my deepest gratitude and profound appreciation to my supervisor Professor Dr. Nor Sabirin Mohamed from Centre for Foundation Studies in Science, University of Malaya for her assistance, guidance, concern, patience and encouragements that greatly enhanced the outcome of this thesis. I am also very thankful to my co-supervisor, Professor Dr. Azizan Ahmad from Universiti Kebangsaan Malaysia for his assistance, support, motivate and understanding.

I also want to thank the Ministry of Higher Education, Malaysia for MyPhD scholarship under MyBrain15 scheme and the University of Malaya for Postgraduate Research Fund Grant (PG073/2012B).

I also like to thank science officer at PASUM and her assistant, my colleagues and members of Electrochemical and Materials Research Group especially Akma, Siti, Amalina, Fatin, Lin, Saiful, Fizha, Watie, Zul, Yana and Wan for their helps and ideas. A very big appreciation to my close friends Azlina for helping me in the polymer synthesis part and Hamdah who always understands my problems. A note of thanks also goes to my friends from Polymer Electrolytes research group in UKM; Nad, Jue, Fatihah and Edison. Thanks to Sukor from Solar Energy Research Centre, UKM who helped me in DSSC fabrication stage.

Last but not least, special thanks to my beloved mother for her support and prayers. My sincere appreciation also extends to my sisters and brother for support and encouragement. Also, thank you to all people that I met during this journey. Thank you very much.

TABLE OF CONTENTS

CHAPTER 5: PU-SALT POLYMER ELECTROLYTES

CHAPTER 6: PU-SALT-PMII POLYMER ELECTROLYTES

CHAPTER 8: CONCLUSIONS AND SUGGESTIONS FOR FURTHER WORK

LIST OF FIGURES

LIST OF TABLES

LIST OF SCHEME

LIST OF SYMBOLS

A	Cross sectional area
C	Capacitor
E_a	Activation energy
FF	Fill factor
I_f	Final current
I_I or I_o	Initial current
I_{ss}	Steady state current
I_T	Total current
J_{sc}	Short-circuit current density
$J–V$	Current density-voltage
k_B	Boltzmann constant
l	Thickness
M_w	Molecular weight
P_{in}	Incident power

P_{max}	Maximum power
R	Resistance
R_{b}	Bulk resistance
R_{ct}	Charge-transfer resistance
R_{o}	Bulk resistance before polarization
R_{ss}	Bulk resistance after polarization
R_{w}	Warburg diffusion impedance
T	Temperature
t_{ele}	Electronic transference number
T_{g}	Glass transition temperature
t_{ion}	Ionic transference number
$t_{\mathrm{Li+}}$	Lithium transference number
$t_{\mathrm{Na+}}$	Sodium transference number
V_{oc}	Open-circuit voltage
wt %	Weight percentage
Z	Impedance
Z_{R}	Real part of impedance
η	Energy conversion efficiency
σ	Conductivity
σ_o	Pre-exponential factor of conductivity

LIST OF ABBREVIATIONS

AC	Alternating current
$AlCl_4^-$	Tetrachloroaluminate
AM	Air Mass
ASTM	American Society for Testing and Materials
ATR	Attenuated Total Reflectance
BD	1,4-Butanediol
BMII	1-butyl-3-methylimidazolium iodide
Br^-/Br_2	Bromine/bromide
CB	Conduction band
CE	Counter electrode
CO	Castor oil
$CoNi_2S_4$	Cobalt nickel sulfide
CO-p	Castor oil-polyol
CoTe	Cobalt telluride

CPE	Constant phase element
CZTS	Copper-zinc tin sulfide
DBP	Dibutyl phthalate
DC	Direct current
DEC	Diethyl carbonate
DEG	Diethylene glycol
DEP	Diethyl phthalate
DMA	Dynamic Mechanical Analysis
DMII	1,3-dimethylimidazolium iodide
DMPII	1,2-dimethyl-3-propylimidazolium iodide
DMPP	2,2-dimethoxy-2-phenylacetophenone
DSSC	Dye-sensitized solar cells
EC	Ethylene Carbonate
EGMEM	Ethylene glycol methyl ether methacrylate
EIS	Electrochemical impedance spectroscopy
$EMIBF_4$	1-ethyl-3-methylimidazolium tetrafluoroborate
EMII	1-ethyl-3-methylimidazolium iodide
EMImTFSI	1-ethyl-3-methylimidazolium bis(trifluoromethylsulfonyl)imide
EMISCN	1-ethyl-3-methylimidazolium thiocyanate
FTIR	Fourier transform infrared
FTO	Fluorine-doped tin oxide, SnO_2:F
GMA	Glycidyl methacrylate
GPC	Gel permeation chromatography
GPE	Gel polymer electrolyte
$H_{12}MDI$	4,4′-methylenebis(cyclohexyl isocyanate)
HBPU	Hyperbranched polyurethane
Hex_4NI	Tetrahexylammonium iodide
HMII	1-hexyl-3-methylimidazolium iodide

I^-/I^{3-}	Iodide-triiodide
I_2	Iodine
IL	Ionic liquid
IPDI	Isophorone diisocyanate
KI	Potassium iodide
KOH	Potassium hydroxide
Li_3N	Lithium nitride
$LiAl_2O_3$	Lithium aluminum oxide
$LiAsF_6$	Lithium hexafluoroarsenate (V)
$LiBF_4$	Lithium tetrafluoroborate
LiBr	Lithium bromide
$LiCF_3SO_3$	Lithium trifluoromethane sulfonate
$LiClO_4$	Lithium perchlorate
LiI	Lithium iodide
$LiN(SO_2CF_3)_2$	Lithium bis(tri-fluoromethanesulfonyl)imide
LiTf	Lithium triflate
LiTFSI	Lithium bis(tri-fluoromethanesulfonyl)imide
LSV	Linear sweep voltammetry
MDI	4,4’-diphenylmethane diisocyanate
MgI_2	Magnesium iodide
MMT	Montmorillonite
N3	cis-Bis(isothiocyanato) bis(2,2’-bipyridyl-4,4’-dicarboxylato ruthenium(II)
N-719	di-tetrabutylammonium cis-bis(isothiocyanato) bis(2,2’-bipyridyl-4,4’-dicarboxylato) ruthenium (II) dye
NaI	Sodium iodide
NaTf	Sodium trifluoromethanesulfonate
Nb_2O_5	Niobium pentoxide

NCO	Isocyanate
$NiTe_2$	Nickel telluride
NMBI	*N*-methylbenzimidazole
NR	Natural rubber
OH	Hydroxyl
P(EO-EPI)	Poly(ethylene oxide-*co*-epichlorohydrin)
P(MMA-*co*-EMA)	Poly(methyl methacrylate-*co*-ethyl methacrylate)
PA	Phthalic anhydride
PAN	Polyacrylonitrile
PC	Propylene carbonate
PDMS-g PEO	Poly[dimethylsiloxane-g-poly(ethylene oxide)]
PEDOT	Poly(3,4-ethylenedioxythiophene)
PEDOT:PSS	Poly(3,4-ethylenedioxythiophene):poly(styrene sulfonate)
PEG	Poly(ethylene glycol)
PEM	Poly(methoxy polyethylene glycol monomethacrylates)
PEMA	Poly(ethyl methacrylate)
PEMPS	Polyether modified polysiloxane
PEO	Poly(ethylene oxide)
PEs	Polymer electrolytes
PET	Poly(ethylene terphthalate)
PHEA	Poly(hydroxyethylacrylate)
PMII	3-propyl-1-methylimidazolium iodide
PMMA	Poly(methyl methacrylate)
PPG	Poly(propylene) glycol
Pr_4NI	Tetrapropylammonium iodide
Pt	Platinum

PTMG	Poly(tetramethylene glycol)
PU	Polyurethane
PVA or PVAc	Polyvinyl acetate
PVC	Poly(vinyl chloride)
PVDF	Poly(vinylidene fluoride)
PVDF-HFP	Poly(vinylidene fluoride-*co*-hexafluoropropylene)
PVP	Poly(vinyl pyrolidone)
$PYRA_{12O1}TFSI$	N-ethyl(methylether)-N-methylpyrrolidinium trifluoromethanesulfonimmide
RE	Reference electrode
RS	Rice starch
$(SeCN)_2$	Selenocyanogen
SiO_2	Silicon oxide
SnO_2	Tin oxide
SPE	Solid polymer electrolyte
SS	Stainless steel
TBAI	Tetrabutylammonium iodide
TBP	4-*tert*-butylpyridine
TCO	Transparent conducting oxide
TDI	Toluene diisocyanate
TGA	Thermogravimetric analysis
THF	Tetrahydrofuran
TiO_2	Titanium oxide
TPU	Thermoplastic polyurethane
VTF	Vogel-Tamman-Fulcher
WE	Working electrode
ZnO	Zinc oxide

CHAPTER 1: INTRODUCTION

1.1 Introduction

Dye-sensitized solar cell (DSSC) is an alternative source to photoelectrochemical solar cells. It came in consideration after the novel work of Grätzel and co-workers in 1991 (O'Regan & Grätzel, 1991; Grätzel, 2001). DSSC is one of the promising candidates for the next generation solar cells due to their simple structure, high conversion efficiency and inexpensive fabrication procedures compared to amorphous silicon solar cells (Goetzberger et al., 2002). The overall performance of the cell depends on many factors such as substrate, photoanode including oxide semiconductor, dye sensitizer, electrolytes, counter electrode with catalyst, effect of processing parameters on structure and properties of individual components (Jena et al., 2012).

To date, DSSC still depends on liquid electrolytes to increase its efficiency. Technique for sealing of the cell must be perfectly established to prevent the evaporation of the components of electrolytes, especially for outdoor application. In order to overcome the leakage of the liquids, electrolytes based on polymers have been studied. Indeed, extensive studies have been conducted in order to improve polymer based DSSC efficiency (Nogueira et al., 2001; Kang et al., 2008; Benedetti et al., 2010). However, most of the researches still looking for petrochemical-based polymers, which are not environmental friendly such as polyethylene oxide (PEO) rather than bio-based polymers (Wang, 2007).

Polyurethane (PU) is a polymer that has potential to be used as host polymer in electrolytes for application in DSSC. This polymer has a unique multiphase structure formed from soft and hard segments of the polymer chain contributed by the polyols (OH) and isocyanates (NCO) respectively. The soft segment acts as a polymeric solvent to solvate the cations while the hard segment responsible for dimensional stability acting as physical cross-link sites. Furthermore, the low glass transition temperature, T_g and high segmental motion of the polyether soft segments lead to higher mobility of the dissolved ions. The hard segment domains, which are in glassy state and either distributed or interconnected throughout the rubbery phase of the soft segment, act as reinforcing filler and hence contribute to the dimensional stability of the polymer electrolytes (Wen et al., 2000; Wang, 2007).

1.2 Problem Statements

In DSSC studies, some issues related to DSSC based on liquid electrolytes such as leakage and volatilization of solvents, possible desorption and photodegradation of the attached dyes, high temperature instability and sealing issues have been reported. The possible approach to overcome this problem is by replacing these electrolytes with polymer electrolytes.

Studies on polymer electrolytes for application in DSSC have been reported in the literature (Wang et al., 2003b; Ileperuma et al., 2004; Kang et al., 2004; Wang et al., 2004; Yang et al., 2008a). However, the studies were done on petrochemical based polymers, which are associated to the environmental issues and high cost. In order to reduce the dependence of petrochemical based polymer for electrolytes, application of bio based polymers as host polymers may be used.

There has been growing interest in the use of renewable bio-based resources for development of electrolyte materials (Su'ait et al., 2009; Noor et al., 2010; Kumar et al., 2012; Samsudin et al., 2014). However, research on the potential of bio-based polyurethane as polymer electrolyte systems are limited in number. Daud et al., (2014) and Su'ait et al., (2014) have studied polymer electrolytes developed using PU from palm kernel oil-polyol. Their studies showed that PU is an interesting polymer to be further explored for the development of polymer electrolytes for DSSC. Moreover, application of bio-based PU as host polymer electrolytes in DSSC may expand the application of the bio-based polymers as an alternative to synthetic polymers while maintaining good properties of the materials. Bio-based polymers are also eco and environmental-friendly materials in terms of decomposition.

1.3 Research Objectives

This work was undertaken with the following objectives:

1. To synthesize bio-based polyurethane from castor oil with different weight ratios of the NCO:OH and study their properties in order to obtain PU with the characteristics suitable for use as host in polymer electrolytes.

2. To develop polymer electrolyte from bio-based polyurethane with various weight percentages (wt %) of salt and ionic liquid, and study the effects of the salt and

ionic liquid concentrations on thermal, optical, electrical and electrochemical properties in order to identify polymer electrolyte with the best properties for application in DSSC.

3. To fabricate and characterize DSSCs performance employing the bio-based electrolytes with better or at least comparable performance compared to synthetic polymer based DSSC.

1.4 Scope of Study

In this study, bio based polyurethane was prepared using castor oil-polyol (CO-p) by steps of polymerization reaction between polyester polyols and 4-4’ diphenylmethane diisocyanate in organic solvent. At the first stage, castor oil based polyol was synthesized via transesterification method and confirmed by Fourier transform infrared spectroscopy (FTIR). The percentage of the mixture to form polyol was fixed according to the Patton formula (Patton, 1962). The formation of PU depends on the ratio of NCO:OH reactive groups and some properties of the PU will be discussed in the later chapter.

For the preparation of bio-based polyurethane polymer electrolytes, the NCO:OH weight ratio was fixed and added with sodium iodide (NaI) and lithium iodide (LiI) salts in different weight percentages (wt %). In this work, iodide based salt was chosen as it is expected to give a redox process in the presence of iodine in the systems. 3-propyl-1-methylimidazolium iodide (PMII) ionic liquid was also added to the highest conducting polymer-salt system to enhance the conductivity as well as the efficiency of DSSC. All electrolytes in this study were prepared using solution casting technique. This technique was employed due to its simplicity of handling and low cost compared to the other techniques.

Last but not least is the application of the bio polymer electrolytes for fabrication of DSSC. The main components in DSSC are transparent conducting oxide glass coated with semiconductor and monolayer dye as working electrode, electrolytes containing redox mediator and catalyst deposited over transparent conducting oxide glass as counter electrode.

1.5 Thesis Organization

The research work has been done with the objectives mentioned in Section 1.3. Chapter 2 presents an overview on dye sensitized solar cells. This is followed by an overview of polyurethane, bio-based polyurethane and castor oil. This chapter also includes an overview of polymer electrolytes, polyurethane based polymer electrolytes, ionic liquid and polymer electrolytes based DSSC.

Chapter 3 covers the methodology to synthesize castor oil based polyol followed by polymerization of polyurethane. It also explained the characterization techniques for the polyol and polyurethane polymer electrolytes studied in this work. The characteristics of the materials were determined using gel permeation chromatography (GPC), Fourier transform infrared spectroscopy (FTIR), thermal gravimetric analysis (TGA), dynamic mechanical analysis (DMA), scanning electron microscopy (SEM), electrochemical impedance spectroscopy (EIS), transference number measurement and linear sweep voltammetry (LSV). Chapter 3 also described the experimental work to fabricate dye-sensitized solar cell using polyurethane polymer electrolytes including preparation of working and counter electrodes for DSSC.

Experimental results are presented in the following four chapters. Chapter 4 presents the results and discussion of the synthesized castor oil-polyol with determination of acid number, hydroxyl number and molecular weight. The polyurethane based on castor oil was analyzed using FTIR, GPC, TGA, DMA and SEM. Chapter 5 discusses the results for castor oil-polyol based polyurethane added with different wt % of NaI and LiI. In Chapter 6, the results and discussion of the highest conducting sample of PU-NaI and PU-LiI systems added with different wt % of 3-propyl-1-methylimidazolium iodide (PMII) ionic liquid are given. Chapter 7 covers the application part, which includes overall performance of the fabricated polyurethane polymer electrolytes based DSSCs meanwhile, Chapter 8 states the conclusions of this thesis as well as a few suggestions for further works.

CHAPTER 2: LITERATURE REVIEW

2.1 Introduction to Dye-Sensitized Solar Cell

Dye sensitized solar cell (DSSC) is a device that converts the solar energy directly into electricity by photovoltaic effects. DSSCs have been considered one of the promising alternatives to conventional solar cells, because of their low cost, easy fabrication and relatively high energy conversion efficiency (Nogueira et al., 2004; Wang, 2009). Since these solar cells can be produced from low-cost materials using simple manufacturing processes, overall manufacturing expenditures are expected to be comparatively low.

Generally, typical DSSC consists of a dye-coated mesoporous TiO_2 nanoparticle film sandwiched between two conductive transparent electrodes and a liquid electrolyte, usually containing iodide/triiodide (I^-/I_3^-) redox couple to fill the pores of the film and contact the nanoparticles. The photovoltaic effect in a DSSC originates from the interface between a redox electrolyte containing iodide and triiodide ions and a dye-adsorbed mesoscopic TiO_2 electrode (Grätzel, 2000, 2001). The electrolyte is one of the key components that provides internal electrical conductivity by diffusing within the mesoporous TiO_2 layer that affect in determining the performance of the cell (Wang et al., 2005a). However, an appropriate method and materials of the components in DSSC also influence the overall performance of DSSC.

2.2 Materials in DSSC

A schematic configuration of a DSSC device is illustrated in Figure 2.1. A typical DSSC consists of four major components: transparent conductive oxide (TCO) glass with deposited TiO_2 metal oxide as working electrode, dye sensitizer, electrolyte containing redox mediator and TCO with platinum (Pt) layered as counter electrode.

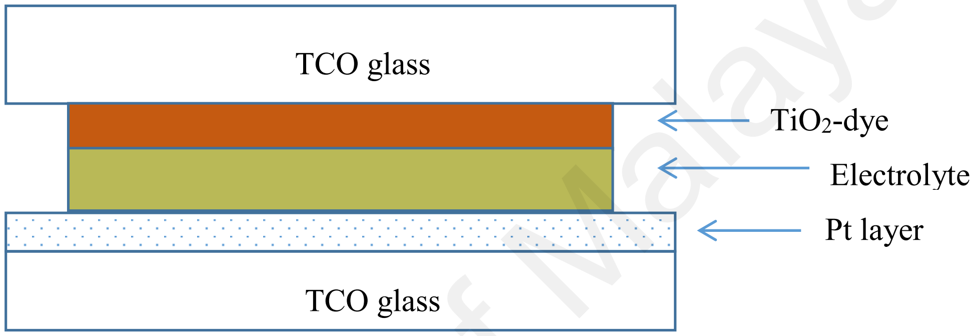

Figure 2.1: Schematic diagram of dye-sensitized solar cell

2.2.1 Working electrode

Working electrode (WE) consists of a mesoporous layer of metal oxide semiconductor, typically titanium oxide (TiO_2), screen printed onto the conducting glass substrates, usually fluorine-doped tin oxide (FTO). Metal oxide TiO_2 has been widely used in DSSC. Other metal oxides that have been used in DSSCs are zinc oxide (ZnO), niobium pentoxide (Nb_2O_5) and tin oxide (SnO_2) (Lee et al., 2011).

2.2.2 Sensitizer

Sensitizer or also known as dye is one of the important materials in DSSC. The function of dye is to absorb light and inject the excited electrons into the semiconductor conduction band. Dye also accepts electrons from the redox mediator in the electrolyte (Buraidah et al., 2011). A monolayer of the sensitizer is attached onto the surface of working electrode by chemical bonding. There are mainly two categories of sensitizers: metal complexes mainly ruthenium based complexes and metal-free organic sensitizers. A large number of ruthenium complexes such as cis-Bis(isothiocyanato) bis(2,2’-bipyridyl-4,4’-dicarboxylato ruthenium(II) (N3), di-tetrabutylammonium cis-bis(isothiocyanato)bis(2,2’-bipyridyl-4,4’-dicarboxylato)ruthenium(II) (N-719) and black dye are usually used, and have shown excellent efficiencies to date. Natural dye colorants from chlorophyll, betalains, carotenoid and anthocyanin have also been explored by researchers as alternatives to synthetic dye (Hug et al., 2014).

2.2.3 Electrolytes

The efficiency of cell performance depends on many factors and one of them is electrolytes. Electrolytes generally consist of a redox couple and additives dissolved in a solvent. The electrolytes undertake the responsibility of dye regeneration and charge transport between the working and counter electrodes. Usually electrolytes containing iodide and triiodide were used. However, other redox couples have also been investigated for use in DSSCs such as Br^-/Br_2 (Wang et al., 2005b), $(SeCN)_2/SeCN^-$ (Bergeron et al., 2005) and bipyridyl cobalt (III/II) (Sapp et al., 2002). Several types of electrolytes have been used in DSSC such as liquid electrolytes and solid electrolytes. The presence of polymer would form electrolytes in solid state or gel-like solid state form. The usage of polymer electrolytes in DSSC prevents leakage and volatile components (De Freitas et al., 2009). The choices of polymer and redox mediator would affect the performance of DSSC. An appropriate method and other component materials also influence the performance of efficiency in DSSC.

2.2.4 Counter electrode

Counter electrode (CE) is typically prepared by depositing a thin layer of platinum (Pt) catalyst onto the transparent conductive oxide (TCO) substrates. The function of CE is mainly to regenerate the electrolyte, with the oxidized electrolyte diffusing towards the CE. The CE transports the electron that arrives from the external circuit back to the redox electrolyte system. For efficient charge transfer, the counter electrode should exhibit a high catalytic activity and high electrical conductivity to accelerate the reduction reaction (Suhaimi et al., 2015). Pt is a superior catalyst as a counter electrode for I_3^- reduction because of its high exchange current density, good catalytic activity and transparency (Gao et al., 2012). Several other materials have also been used as CE such as conducting polymers, carbon materials and cobalt sulphide.

2.3 Operation Principles

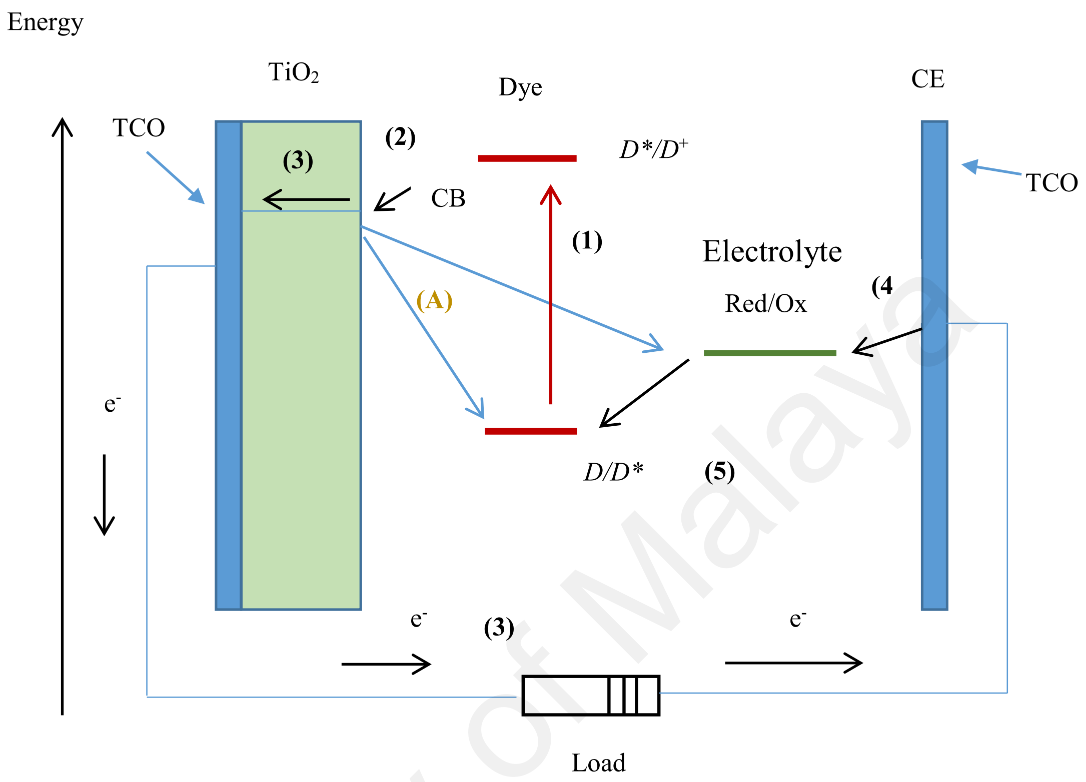

Figure 2.2: Schematic representation of the principle of the dye-sensitized solar cell. *D* stands for dye, D^* is electronically excited dye and D^+ is oxidized dye (Adapted from Hagfeldt and Graetzel, (1995))

The idea of DSSC was initially inspired from the photosynthesis of the leaves. The process involves two steps: light absorption and charged carrier transportation. Figure 2.2 explained the mechanism in DSSC. The incident light goes through the transparent substrate and gets absorbed by the dye sensitizer. (1) The dye is photoexcited. (2) The excited electrons are injected into the conduction band (CB) in the TiO_2. (3) The electrons penetrate through the nanocrystalline TiO_2 film to the back contact of the conducting substrate and flow through the external circuit to the CE. (4) At the CE, the oxidized component of redox couple in the electrolyte is reduced. (5) The oxidized form of the dye is finally regenerated by the reduced component of redox couple in the electrolyte. In this overall process, there are two major recombination loss processes that limit the total conversion efficiency within the DSSCs; the photoinjected electrons in TiO_2 can recombine directly with the oxidized dye molecules or with the oxidized form of the redox couple in the electrolyte (6). The schematic reaction of the overall process as follows:

$$\mathrm{TiO_2}\,|\,D + hv \longrightarrow \mathrm{TiO_2}\,|\,D^* \tag{1}$$

$$\mathrm{TiO_2}\,|\,D^* \longrightarrow \mathrm{TiO_2}\,|\,D + \mathrm{e}^-_{\mathrm{cb}} \tag{2}$$

$$\mathrm{TiO_2}\,|\,D^+ + e^-_{\mathrm{cb}} \longrightarrow \mathrm{TiO_2}\,|\,D \tag{3}$$

$$\mathrm{TiO_2}\,|\,D^+ + (3/2)\,\mathrm{I}^- \longrightarrow \mathrm{TiO_2}\,|\,D + (1/2)\,\mathrm{I}_3^- \tag{4}$$

$$(1/2)\mathrm{I}_3^- + \mathrm{e}^-_{\mathrm{pt}} \longrightarrow (3/2)\,\mathrm{I}^- \tag{5}$$

$$\mathrm{I}_3^- + 2\mathrm{e}^-_{\mathrm{cb}} \longrightarrow 3\,\mathrm{I}_3^- \tag{6}$$

2.4 Characterization Technique of DSSC

Basic characterization techniques for DSSC is Photocurrent density-photovoltage (*J–V*) measurement. The *J–V* measurement can be performed using Keithley 2400 source meter, WonaTech multichannel analyzer or any other multimeters under simulated sunlight. A typical *J–V* curve is shown in Figure 2.3. During the *J–V* measurement, the open circuit photovoltage, V_{oc}, short circuit photocurrent J_{sc}, fill factor, *FF* and efficiency, η can be determined.

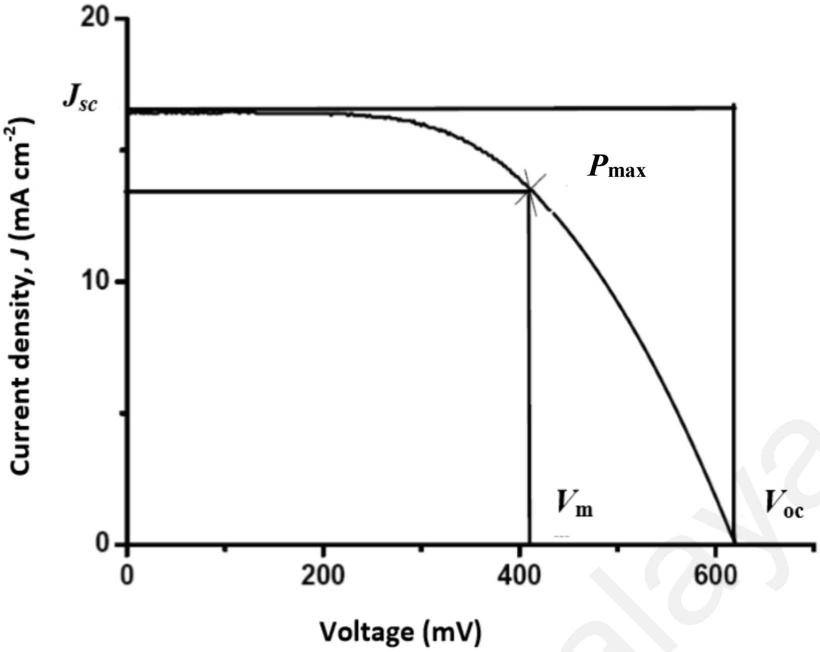

Figure 2.3: Example of *J–V* curve of DSSC

The performance of DSSC usually evaluated by the following parameters:

a) **Open circuit photovoltage (V_{oc})**: cell voltage measured when current within the cell is equal to zero.

b) **Short circuit photocurrent (I_{sc})**: the cell photocurrent measured at zero voltage. In general, it is presented in the form of the short circuit current density (J_{sc}) defined as the short circuit photocurrent divided with the active cell area.

c) **Fill factor (*FF*)**: the ratio of the maximum power output (P_{max}) to the product of short circuit photocurrent density and open circuit photovoltage

$$FF = \frac{P_{max}}{J_{sc}.V_{oc}} = \frac{J_{mpp}.V_{mpp}}{J_{sc}.V_{oc}} \tag{2.1}$$

where I_{mpp} and V_{mpp} are the photocurrent and photovoltage corresponding to the maximal power point, respectively in *J–V* curve.

d) Energy conversion efficiency (η): the ratio of P_{max} to the incident radiation power, P_{in} on the solar cell surface. It is the product of open circuit voltage of V_{oc}, short circuit photocurrent density, J_{sc} and fill factor, *FF* divided by the incident irradiation power.

$$\eta(\%) = \frac{P_{max}}{P_{in}} \times 100\ \% \ = \ \frac{J_{sc}.V_{oc}.FF}{P_{in}} \times 100\ \% \tag{2.2}$$

η is a function of J_{sc}, V_{oc} and *FF*. DSSC performance is achieved by optimization these three parameters and η is also dependent on the incident irradiation power, P_{in}.

2.5 Polyurethane

Polyurethane (PU) was first discovered by Professor Otto Bayer in 1937 (Rogers & Long, 2003). Research and development in the field of polyurethanes are increasing year to year showing the rapid growing in the polyurethane industry. PUs are versatile materials and widely used in industry and everyday life. PU can be used for many applications, such as tubing, footwear, industrial machinery, coatings and paints, elastic fibers, rigid insulations, soft-flexible foam, medical devices and many others (Chattopadhyay & Webster, 2009; Firdaus & Meier, 2013; Szycher, 2013). The polymer are mainly produced by the isocyanation of isocyanate with polyol of various molecular weights (Hepburn, 1992). An isocyanate is a molecule with two or more isocyanate functional groups R-$(N=C=O)_n$ where n ≥ 2. It will react with any compound containing an active hydrogen (Howard, 2002). Isocyanate can be aliphatic, cycloaliphatic, polycyclic or aromatic in nature, such as toluene diisocyanate (TDI), methylene diphenyl diisocyanate (MDI), xylene diisocyanate (XDI), tetramethyl-m-xylylene diisocyanate (TMXDI) and hydrogenated xylene diisocyanate (HXDI). Meanwhile, polyol is a molecule with two or more hydroxyl functional groups $(R\text{-}OH)_n$, where $n \geq 2$.

Two major isocyanates employed in polyurethane manufacturing are TDI and MDI. Both are aromatic isocyantes. The chemical structure of TDI and MDI with different isomer is shown in Figure 2.4.

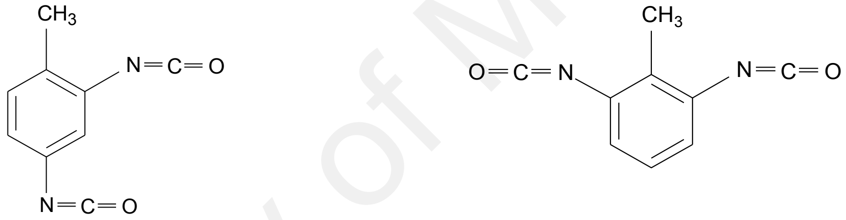

2,4’-Toluene diisocyanate 2,6’-Toluene diisocyanate

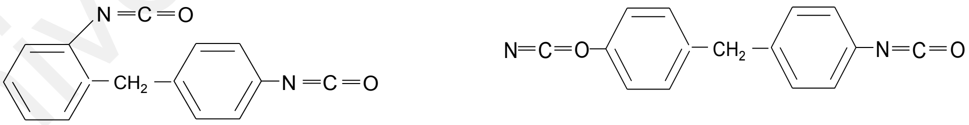

2,4’-Diphenylmethane-diisocyanate 4,4’-Diphenylmethane-diisocyanate

Figure 2.4: Chemical structure of TDI and MDI

The simplest formula for linear PU is represented by

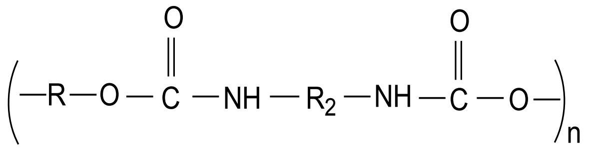

$$\left(-R-O-\overset{\overset{O}{\|}}{C}-NH-R_2-NH-\overset{\overset{O}{\|}}{C}-O- \right)_n$$

Figure 2.5: Linear polyurethane

where R represents hydrocarbon containing OH group, R_2 is a hydrocarbon chain and n is number of repetitions.

Polyurethanes serve the mankind in its various roles such as flexible, rigid, semi-rigid, elastomers, surface coatings and adhesives. The properties of PU are dependent on certain factors such as the content of the reactive groups, the degree of crosslinking, and the entanglement of the reacting monomers. In order to meet specific requirement, their structures can be tailored by selecting appropriate polyols and polyisocyanates. In industry, only a few diisocyanates or polyisocyanates are commonly used, while a variety of polyols are available. Therefore, the choice of polyol typically determines the properties of the created polyurethanes (Pfister et al., 2011). In addition to petroleum-based polyols, vegetable oils such as soybean oil, canola oil, palm oil, sunflower oil, corn oil, linseed oil and nahar seed oil (Louwrier, 1998; Badri et al., 2004; Dutta et al., 2004) have been extensively studied as bases for various polyols for the manufacture of PUs for different applications.

2.5.1 Bio-based Polyurethane

The preparation of polymers from vegetable oils is currently receiving increasing attention because of the economic and environmental concerns (Alfani et al., 1998; Uyama et al., 2003; Petrovic et al., 2005; Mutlu & Meier, 2010). Raw materials based on vegetable oils have a number of excellent properties for producing valuable polymers such as polyurethane, alkyd, polyester, amide and epoxy resins. Vegetable oils are triglycerides of fatty acids. In order to use these compounds as starting materials for polyurethane synthesis, it is necessary to functionalize them to form polyols before reacting with diisocyanate.

2.5.2 Castor oil

Castor oil (*Ricinus communis)* from the family of *Euphorbiaceae* is a promising starting raw material for polyurethane due to its low toxicity and availability as a renewable agricultural resource. Its major constituent, ricinoleic acid (12-hydroxy-cis-9-octadecenoic acid), is a hydroxyl containing fatty acid. The most common chain lengths in these fatty acids are 18 or 20 carbon atoms which can be either saturated or unsaturated, where unsaturation of the double bonds are located at the 9th, 12th and 15th carbon. By using enzymes or chemicals to modify the unsaturated fatty acid and introducing hydroxyl functional groups, castor oils could be converted into polyol (Sun, 2005). There are many literatures on modified castor oil polyurethane for application in bridge decking, adhesives and thermal insulation (Vu, 1989; Somani et al., 2003; Cardoso et al., 2012). However, modification of polyurethane for use as host in polymer electrolytes has not yet been reported in the literature. Figure 2.6 shows the structure of castor oil.

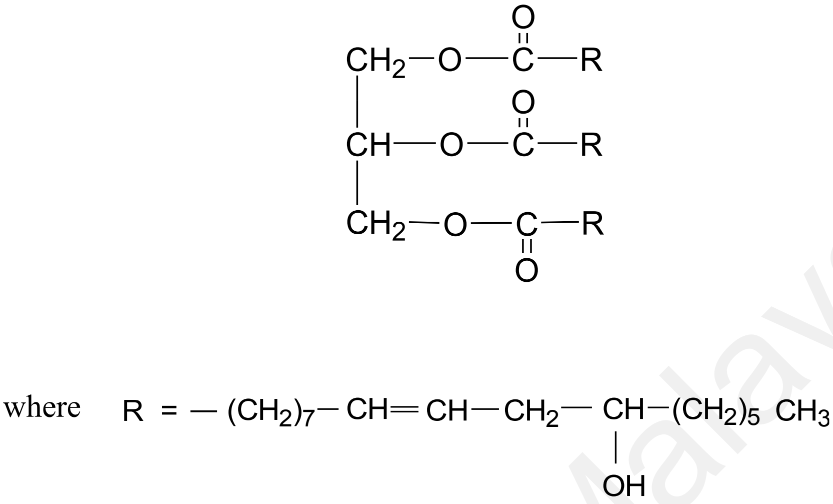

where $R = -(CH_2)_7-CH=CH-CH_2-\underset{\displaystyle OH}{\underset{|}{CH}}-(CH_2)_5\ CH_3$

Figure 2.6: Structure of castor oil

2.6 Polymer Electrolytes

The research in polymer electrolytes was started by Wright (1975) using polyethylene oxide (PEO) and has invoked after Armand and co-workers proposed applications of these materials as battery electrolytes (Armand et al., 1979). Polymer electrolytes can be defined as conducting materials in which charge carriers are mainly ions either positively or negatively charged ions. Polymer electrolytes are promising materials for the ever-growing need for high energy density power sources: battery, supercapacitor, fuel cell, dye-sensitized solar cell, etc. With the application of polymer electrolytes in high specific energy and high specific power, flexibility in packaging and low cost of fabrication can be expected.

The use of solid polymer electrolytes can also avoid problems related to liquid electrolytes such as leakage and gas formation that arises from solvent decomposition. There are many kinds of polymers that have been used as host in polymer electrolytes such as polyethylene oxide (PEO) (Bhattacharja et al., 1986; Quartarone et al., 1998), poly(vinylidene fluoride) (PVDF) (Periasamy et al., 2000; Mohamed & Arof, 2004), PVDF-HFP (Ibrahim et al., 2010; Puguan et al., 2015), poly (methyl methacrylate) (PMMA) (Sedlaří et al., 2001; Kuo et al., 2013), polyacrylonitrile (PAN) (Dissanayake et al., 2002; Chen-Yang et al., 2009) and polyurethane (Wang & Min, 2010).

Nowadays, research on polymer electrolytes still receives great attention. In addition to synthetic polymers, biopolymer electrolytes are also extensively studied in order to save cost and towards more environmental friendly while maintaining their good chemical and physical properties. Biopolymer that has been used in polymer electrolytes such as chitosan (Mohamed et al., 1995), modified natural rubber (NR) (Idris et al., 2001), corn starch (Ning et al., 2009), cellulose (Rani et al., 2014) and blending of kappa-carrageenan and cellulose derivatives (Rudhziah et al., 2015b).

2.6.1 Ionic Liquid

In order to further enhance their conductivity, additives such as plasticizers and ionic liquids (ILs) are incorporated into the polymer-salt electrolytes. IL is a liquid that contains essentially ions. Ionic liquid is also known as room temperature molten salts with melting points below 100 °C. It is non-volatile, non-flammable, thermally and chemically stable, high ionic conductivity, high solvating capability and wide electrochemical windows

(Ueki and Watanabe, 2008; Lee et al., 2013). Addition of IL is likely to further enhance the chain flexibility thus enhanced the conductivity. According to Noda and Watanabe (2000), ILs have dual roles in polymer; as charge carrier and plasticizer. The conductivity of PEO-KI, (Bhattacharya et al., 2007) increases with the addition of low viscosity ionic liquid. This due to IL that acts as plasticizer hence soften the polymer backbone enhancing mobility of ions.

To date, many ILs have been synthesized. A typical IL has a bulky organic cation (e.g., N-alkylpyridinium, N-N -dialkylimidazolium) that is weakly coordinated to an organic or inorganic anion, such as BF_4^-, Cl^-, I^-, $CF_3SO_3^-$ and $AlCl_4^-$ (Singh et al., 2012). In this research work, 3-propyl-1-methylimidazolium iodide (PMII) was used. The chemical structure of PMII is shown in Figure 2.7. PMII is considered a very promising ionic liquid in enhancing conductivity of electrolytes due to its low viscosity among the room temperature ionic liquid iodide imadazolium salts, good ionic conductivity and wide electrochemical stability. As mentioned in literature, the viscosity of IL affects the performance of the DSSC by affecting the mobility and ionic conductivity of the electrolytes. The viscosity of IL depends on the length of the alkyl chain group that also depends on the molecular weight of the IL (Cho et al., 2011).

Ng et al., (2015) reported that the ionic conductivity of P(VP-*co*-VAc)-KI gel polymer electrolyte increases from 1.7×10^{-3} S cm^{-1} to 3.13×10^{-3} S cm^{-1} upon addition of PMII ionic liquid as well as enhanced the efficiency of DSSC (Ng et al., 2015). Imidazolium cations based ILs have been found to be comparable to their liquid counterpart when they were used in DSSC (Wang et al., 2003a). Figure 2.8 shows other chemical structures of ionic liquid based on imidazolium iodide have been used in DSSCs.

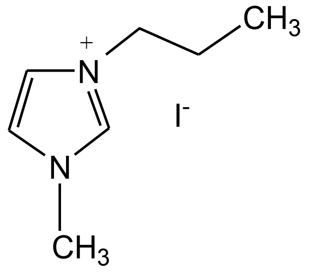

Figure 2.7: Chemical structure of 3-propyl-1-methylimidazolium iodide

1-ethyl-3-methylimidazolium iodide (EMII)

1-butyl-3-methylimidazolium iodide (BMII)

1-hexyl-3-methylimidazolium iodide (HMII)

1,2-dimethyl-3-propylimidazolium iodide (DMPII)

Figure 2.8: Chemical structures of ionic liquid based on imidazolium iodide used in DSSCs (Cho et al., 2011)

2.6.2 Polyurethane Polymer Electrolytes

Generally, PU is characterized by two-phase morphology i.e, soft and hard segments. Soft segment constitutes of aliphatic polyether or polyester and hard segment by isocyanate. Wang et al., (2000) and Kuo et al., (2002) reported their studies on PU electrolytes for rechargeable lithium ion batteries In PU electrolytes, the rubbery soft phase of PU acts as a polymeric solvent to solvate doping salts. This polyether soft segment also has low glass transition temperature, T_g and higher segmental motion which facilitates the mobility of ions. Meanwhile, the PU hard segment domain which is distributed or interconnected throughout the rubbery phase of the soft segment acts as a physical cross-links and filler to the soft segment matrix and hence contribute to the dimensional stability of the polymer electrolytes. Therefore, it is suitable to be used as host polymer electrolytes for fabrication of electrochemical devices (Wang and Min, 2010).

Polyurethane polymer electrolytes based on petrochemical polymers have been studied by many researchers (Wen et al., 1999a; Wen et al., 2000; Kuo et al., 2002b; Hong et al., 2003; Basak and Manorama, 2004; Chiu & Wu, 2005; Lavall et al., 2010; Wang and Min, 2010; Liu et al., 2014; Zhou et al., 2014). However, research on bio-based polyurethane polymer electrolytes are limited in number. In 2014, Su'ait et al., (2014) reported the potential of palm kernel-oil based solid polymer electrolyte for photoelectrochemical cell application. Table 2.1 lists some of polyurethane electrolytes and their conductivities.

Table 2.1: Polyurethane based polymer electrolytes

Polyurethane polymer electrolytes	**Conductivity, σ (S cm^{-1})**	**Reference**
MDI + PPG + $LiClO_4$ H_{12}MDI + PPG + $LiClO_4$ IPDI + PPG + $LiClO_4$ TDI + PPG + $LiClO_4$	$>10^{-5}$	Wen, T.-C et al., 2000
MDI:BD:PEO + LiClO4	2.7×10^{-7} (GPE)	Hong et al., 2003
TPU(PEG/PTMG + MDI) + EC + $LiClO_4$-liquid electrolytes	$\sim10^{-4}$	Chen et al., 2004
PEG + HDI + HBMA + $LiClO_4$	7.5×10^{-6}	Santhosh et al., 2006
PEG + MDI + $MgClO_4$	$\sim10^{-5}$	Choi et al., 2009
TPU (Irogram PS455-203-Huntsman Polyurethane) + $PYRA_{12O1}$TFSI ionic liquid/LiTFSI/PC	$\sim10^{-4}$	Lavall et al., 2010
PEG + MDI + $LiClO_4$ or LiTFSI	$\sim10^{-5}$ - 10^{-6}	Bandyopadhyay et al., 2010
PTMG + 4-4'MDI + BDO + LiTFSI	$\sim10^{-5}$	Wang et al., 2010
TPU (PTMG + MDI)/PEMPS + LiCl / $LiClO_4$ / LiTFSI / $LiN(SO_2CF_3)_2$	TPU/PEMPS + LiTFSI (2.49×10^{-5})	Wang and Min, 2010
HBPU + $LiClO_4$ in PC/DEC + MMT	$\sim10^{-4}$	Deka et al., 2012
PEG + 4,4'-MDI + $LiClO_4$	1.1×10^{-4}	Liu et al., 2014
TPU + EC/PC + $LiClO_4$ TPU/PVDF + EC/PC + $LiClO_4$	4.2×10^{-4} (GPE) 4.1×10^{-3} (GPE)	Zhou et al., 2014
Palm kernel oil-based monoester-OH (PKO-p) + 2,4'-MDI + EC + LiI	7.6×10^{-4}	Su'ait et al., 2014

2.6.3 Polymer Electrolytes based DSSC

Electrolyte is one of the key components that affects the DSSC overall conversion efficiency. The presence of liquid electrolytes in DSSC was considered as a drawback, especially considering the long term stability. To avoid leakage and evaporation of organic solvent in liquid-electrolytes, many efforts have been made to replace the liquid electrolyte by solid-state medium. The use of polymer electrolytes has shown promising potential. Therefore, extensive studies have been conducted in order to improve the efficiency of polymer based DSSCs as well as to overcome the shortcoming problems (Kang et al., 2008; Benedetti et al., 2010; Tsai et al., 2013).

The first DSSC assembled with a polymer electrolyte was reported by De Paoli and co-workers (Nogueira et al., 1999). They used poly(epichlorohydrin-*co*-ethylene oxide) copolymer containing NaI/I_2 as electrolyte and poly(*o*-methoxyaniline) as sensitizer. The photon-to-current conversion efficiency was 1.3 % with 410 nm and 0.1 % with 600 nm irradiation. The same electrolyte was applied in a device using a ruthenium complex as sensitizer, leading to an open circuit voltage, V_{oc} of 0.71 V, short-circuit current density, J_{sc} of 0.46 mA cm^{-2} and overall conversion efficiency, η of 0.22 % under 120 mW cm^{-2} of white-light illumination (Nogueira and De Paoli, 2000). Since then, various polymers have been used in DSSC such as polyacrylonitrile (PAN) (Ileperuma et al., 2002), poly(acrylonitrile-*co*-styrene) (Lan et al., 2006), PVDF-HFP (Kim et al., 2006), poly (ethylene oxide) (PEO) (Bhattacharya et al., 2007; Shen et al., 2008) and poly(methyl methacrylate-ethyl methacrylate) P(MMA-*co*-EMA) (Dzulkurnain et al., 2015).

Addition of IL to polymer electrolytes is one of the methods to enhanced conductivity as well as efficiency of DSSCs. There are many ILs have been used for DSSCs such as 1-ethyl-3-methylimidazolium bis(trifluoromethylsulfonyl)imide (EMImTFSI), 1-hexyl-2,3-dimethylimidazolium iodide (HDMII), 1-ethyl-3-methylimidazolium thiocyanate (EMISCN), etc. Iodide based ILs have been found to play the role of iodide source as well as non-volatile plasticizers in DSSC applications (Singh et al., 2009; Singh et al., 2011). Table 2.2 lists some of polymer electrolytes with/without IL in DSSCs.

Table 2.2: Different types of polymer electrolytes based DSSC with/without IL

Polymer electrolytes based DSSC	**Conductivity, σ (S cm^{-1})**	**Efficiency, η (%)**	**Reference**
PAN+ EC/ PC + $Pr_4N^+I^-$/ I_2	2.95×10^{-3}	2.99	Ileperuma et al., 2002
Poly(acrylonitrile-*co*-styrene) + NaI + I_2	2.37×10^{-3}	2.75	Lan et al., 2006
PVDF-HFP + TiO_2 + LiI/I_2 + HDMII	-	4.26	Kim et al., 2006
Poly(ethylene oxide-*co*-epichlorohydrin) P(EO-EPI) + NaI/I_2 + γ-butyrolactone (GBL)	~10^{-4}	1.80	De Freitas et al., 2006
PEO:KI:I_2 + EMISCN	2.25×10^{-3}	0.63	Bhattacharya et al., 2007
PEO:KI:I_2 + EMImTFSI	8.82×10^{-5}	1.75	Singh et al., 2008
PEO + PMII	3.56×10^{-4}	0.81	Singh et al., 2009

Table 2.2 continued…

Polymer electrolytes based DSSC	**Conductivity, σ (S cm^{-1})**	**Efficiency, η (%)**	**Reference**
PEO +KI/I_2	8.4×10^{-5}	2.0	De Freitas et al., 2009
PAN/EC/PC + MgI_2/$Hex_4N^+I^-$	6.86×10^{-5}	3.50	Bandara et al., 2012
Poly (citric acid-ethylene glycol) + LiI/I_2	5.43×10^{-5}	1.22	Liang et al, 2013
P(GMA) + $LiClO_4$ + EC + LiI/PMII/TBP	4.2×10^{-5}	0.679	Imperiyka et al., 2014
PVDF-HFP + NaI + EC/PC	1.53×10^{-4}	1.85	Noor et al., 2014
GMA + EGMEM + DMPP + EC + TBP + NaI/I_2	-	3.97	Bella et al., 2014
PVDF + NaI/I_2 PVDF + EC/PC + NaI/I_2	2.34×10^{-3} 1.00×10^{-3}	0.87 1.32	Wang et al, 2015
PEMA + NH_4I	1.80×10^{-5}	0.43	Singh et al., 2015
P(MMA-*co*-EMA) + NaI/I_2	5.19×10^{-6}	0.62	Dzulkurnain et al., 2015

As alternative to existing synthetic polymers, bio based polymers are used. Bio polymer electrolytes based DSSC was reported by Buraidah et al., (2010), Singh et al., (2010a) Alias and Mohamad, (2013), Bella et al., (2013), Chiappone et al., (2014), Khanmirzaei and Ramesh, (2014), Singh et al., (2014b) and Bella et al., (2015). Table 2.3 lists some biopolymer electrolytes, their conductivity and efficiency of DSSCs utilizing these electrolytes.

Table 2.3: DSSCs utilizing biopolymer electrolytes, their conductivity and efficiency

Bio polymer electrolytes based DSSC	**Conductivity, σ (S cm^{-1})**	**Efficiency, η (%)**	**Reference**
Chitosan + NaI	-	0.13	Singh et al., 2010
Chitosan + NH_4I	3.73×10^{-7}	-	Buraidah et al., 2010
Chitosan + NaI + EMImSCN	2.60×10^{-4}	0.73	Singh et al., 2010
Chitosan + NH_4I + BMII	3.43×10^{-5}	0.22	Buraidah et al., 2010
Agarose + LiI	3.98×10^{-3}	-	Alias and Mohamad, 2013
Agarose + KI	9.02×10^{-3}	0.54	Singh et al., 2013
RS + LiI + MPII	3.63×10^{-4}	0.17	Khanmirzaei and Ramesh, 2014
k-carrageenan + NaI + EC	1.40×10^{-3}	1.80	Bella et al., 2015
k-carrageenan/Carboxymethyl cellulose + NH_4I/I_2	2.41×10^{-3}	0.13	Rudhziah et al., 2015

CHAPTER 3: EXPERIMENTAL

3.1 Materials

Castor oil, glycerol (99.9 %), ethanol (99.5 %), methanol, potassium hydrogen phthalate, phthalate anhydride (PA), potassium hydroxide (KOH), phenolphthalein, ethylene carbonate (EC) and tetrahydrofuran (THF) were supplied by R&M Marketing, Essex, U.K. 4,4'-diphenylmethane diisocyanate (MDI), iodine (I_2) and 3-propyl-1-methylimidazolium iodide (PMII) were obtained from Merck (Germany) while sodium iodide (NaI), lithium iodide (LiI), sodium metal and lithium metal from Sigma Aldrich (St. Louis, Mo, USA). DSSC components; titanium (TiO_2) paste (Dyesol, Australia), di-tetrabutylammonium cis-bis(isothiocyanato) bis(2,2'-bipyridyl-4,4'-dicarboxylato) ruthenium (II) dye (N-719), platinum (Pt) paste under commercial name Platisol T, and 2.2 mm thick fluorine-doped tin oxide, SnO_2:F (FTO) with 7 Ω/sq as transparent conductive oxide were purchased from Solaronix (Aubonne, Switzerland). All the reagents were of analytical grade and used without further purification.

3.2 Preparation of Samples

The development of PU based on castor oil polymer electrolytes for application in DSSC involves 3 main steps:

i) Synthesis and characterization of castor oil-polyol based polyurethane.
ii) Development of castor oil-polyol based polyurethane polymer electrolytes.
iii) Fabrication of dye-sensitized solar cell.

3.2.1 Synthesis and characterization of castor oil-polyol (CO-p) based polyurethane

i) Synthesis of castor oil-polyol (CO-p)

Castor oil-polyol was synthesized via transesterification in nitrogen atmosphere. The apparatus setup consisted of four necked glass reactor of 1000 mL capacity with 250 mm height and 150 mm in diameter equipped with a mechanical stirrer. Heating was carried out by means of 1000 ml heating mantle. Nitrogen was supplied at a constant flow rate to avoid any oxidation reaction within the reactor. One of the necks of the reactor was equipped with a reflux condenser. The reactor was filled with castor oil and 15 wt % of glycerol was added to it. The percentage of the mixture was fixed according to Patton formula (Patton, 1962) to obtain the hydroxyl value of below 200 mg KOH g^{-1}. The mixture was slowly heated until it reached 210 °C. The temperature was maintained at this value under constant stirring at 200 rpm. The small amount of reaction mixture was added to methanol in the ratio of 1:4 to check the solubility of the mixtures. A clear and homogeneous solution was obtained indicating the formation of monoglycerides. Then, it was allowed to cool to 120 °C. Then the mixture was later continuously stirred at ~200 – 220 °C after addition of an appropriate amount of phthalate anhydride. The progress of condensation reaction and its stability were confirmed by examining its acid value according to the procedure recommended in ASTM D1639-90E. For this purpose, samples were taken out at regular interval and checked for an acid value using titration method and phenolphthalein was used as indicator. For titration method, 0.1 N KOH in 99 % ethanol solution and 1% phenolphthalein solution in 99 % ethanol were prepared. The time required to complete the reaction was about 10 hours. The resulted polyol was stored in dark bottles away from direct sun light.

ii) Synthesis of the castor oil-polyol (CO-p) based polyurethane

The produced polyol which confirmed by FTIR analysis was mixed thoroughly with MDI using digital magnetic stirrer at room temperature condition. Different weight percentage ratio of NCO:OH (20:80 and 40:60) were tried to get the flexible PU. MDI was slowly added to polyol and THF was used as the solvent. The complete reaction of PU was confirmed by the disappearance of NCO peak at 2270 cm^{-1} in FTIR spectra. The resulting solution was poured into a teflon mould and left at room temperature for slowly evaporation of solvent. To ensure complete curing, the films produced were kept in a desiccator before they were characterized.

3.2.2 Development of CO-p based polyurethane polymer electrolytes

i) Preparation of polymer-salts electrolytes

For polymer electrolytes preparation, the weight percentage, wt % ratio of isocyanate to polyol (NCO:OH/ 20:80) which formed polyurethane was dissolved in THF and stirred for 30 minutes before added with sodium iodide in the different wt % (10 to 40 wt %). Sodium iodide was dissolved separately in 6 ml THF. The solutions were mixed together and continue stirred for another 4 hours before cast into teflon petri dishes and left at room temperature for slowly drying until free-standing films were obtained. The films were kept in desiccators for further drying before characterization. These methods were repeated by changing sodium iodide with lithium iodide. Samples of polymer-salts added with sodium iodide and lithium iodide were designated as listed in Table 3.1.

Table 3.1: Weight percentage, wt % and designation of polyurethane-salt electrolyte systems

Polyurethane - Sodium iodide		**Polyurethane - Lithium iodide**	
NaI (wt %)	Designation	LiI (wt %)	Designation
10	PU-10NaI	10	PU-10LiI
20	PU-20NaI	20	PU-20LiI
30	PU-30NaI	30	PU-30LiI
40	PU-40NaI	40	PU-40LiI

ii) Preparation of polymer-salt-ionic liquid electrolytes

The composition of PU-salt, which gave the highest conducting film was chosen for the preparation of polymer-salt-ionic liquid electrolyte films. Ionic liquid (IL) used in this work is 3-propyl 1-methylimidazolium iodide (PMII). The weight ratio of PU: salt was fixed while the amount of IL varied from 10-30 wt %. PU and salt were dissolved separately and stirred together until homogeneous solutions were obtained. Ethylene carbonate (EC) was fixed at 20 wt % and added to the solution as co-solvent. The mixtures were continued stirred for 4 hours and added with IL in different wt %. The homogeneous solutions were cast in petri dishes and left at room temperature for slow drying. Table 3.2 lists the wt % of PMII and designation of polyurethane-salt-IL electrolyte systems. Only up to 30 wt % IL has been incorporated into the polymer-salt since the addition of more than that did not form a homogeneous solution.

Table 3.2: The wt % and designation of polyurethane-salt-IL electrolyte systems

Polyurethane-sodium iodide-ionic liquid		**Polyurethane-lithium iodide-ionic liquid**	
PMII (wt %)	Designation	PMII (wt %)	Designation
10	PU-NaI-10PMII	10	PU-LiI-10PMII
20	PU-NaI-20PMII	20	PU-LiI-20PMII
30	PU-NaI-30PMII	30	PU-LiI-30PMII

3.2.3 Fabrication of DSSC

Transparent conductive glass plates, fluorine doped tin oxide (FTO glass) with sheet resistance of 7 Ω/sq, were cut into 2.5 cm × 2.5 cm and used as a substrate for the deposition of a commercial TiO_2 porous film from a paste (DSL 18NR-AO, Dyesol) and for the fabrication of platinized counter-electrodes. For the photoanode preparation, FTO covered glasses were rinsed in acetone and ethanol in an ultrasonic bath for 15 minutes. A TiO_2 paste layer with a rectangular shape was deposited on FTO glass by doctor-blade supported by adhesive tape on both sides. The adhesive tape having a thickness ~50 μm controlled the thickness of the TiO_2 paste layer. After removing the adhesive tape a portion of 1.0×1.0 cm^2 was selected as the active area by removing the side portions by scraping. The deposited TiO_2 on FTO glass were then sintered at 450 °C for 30 minutes. The photoelectrodes were then soaked into 0.3 mM di-tetrabutylammonium cis-bis(isothiocyanato) bis(2,2’-bipyridyl-4,4’-dicarboxylato) ruthenium (II) (N-719) dye solution in ethanol for 24 hours at ambient temperature in the dark. The counter electrodes, platinized FTO were prepared by brush-painting technique of H_2PtCl_6 solution onto FTO glasses and sintered at 450 °C for 30 minutes. Polymer electrolytes containing iodine with molar ratio of 10:1 were then cast on top of titania photoelectrode. Iodine was added to the electrolytes to produce redox couple (I^-/I_3^-). The two electrodes were then clipped together with two binder clips. Figure 3.1 illustrates the assembling of FTO/TiO_2-dye/Polymer electrolytes-I_2/Pt/FTO dye sensitized solar cell while Figure 3.2 is a photograph of DSSC assembling in the laboratory.

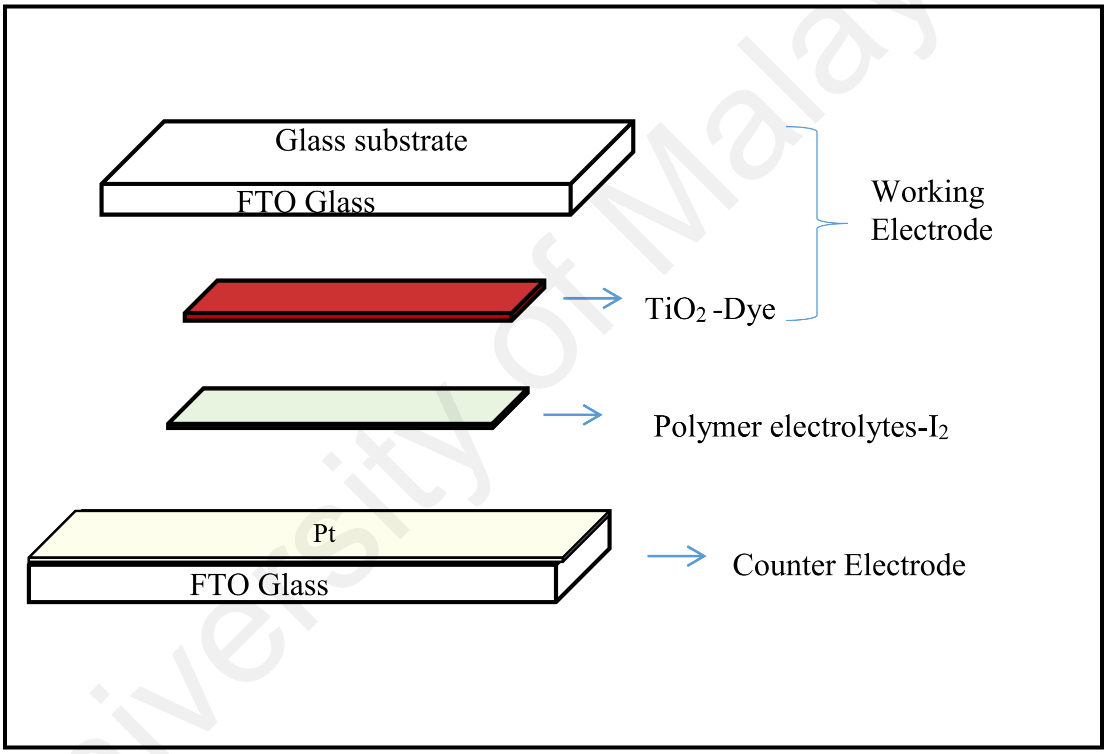

Figure 3.1: Assembling procedure of FTO/TiO_2-dye/ Polymer electrolytes-I_2/Pt/FTO dye-sensitized solar cell

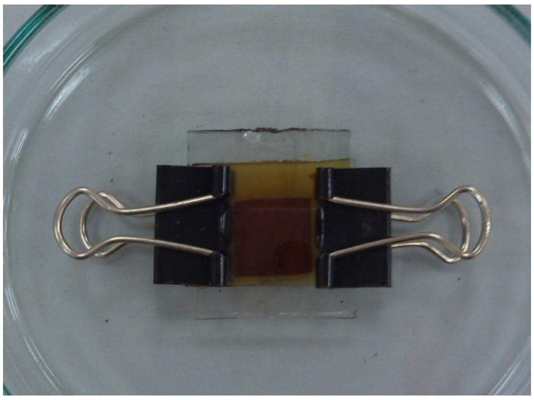

Figure 3.2: Photograph of FTO/TiO_2-dye/ Polymer electrolytes-I_2/Pt dye-sensitized solar cell fabrication

3.3 Analytical Measurements

3.3.1 Fourier Transform Infrared Spectroscopy (FTIR)

The interactions among the constituents of samples can be studied using Fourier Transform Infrared Spectroscopy (FTIR). The resulting spectrum represents the molecular absorption and transmission of the samples. In this work the spectroscopic analysis of the produced castor oil-polyol were performed using Perkin-Elmer Frontier FT-IR/FIR Spectrometers through Attenuated Total Reflectance (ATR) to confirm the formation of polyol. This analysis was also done to study the formation of polyurethane and interactions between polyurethane-salts and polyurethane-salts-ionic liquid. The samples were placed onto the ATR crystal and scanning from 550 to 4000 cm^{-1} wavenumber with resolution of 2 cm^{-1}.

3.3.2 Gel Permeation Chromatography (GPC)

Gel permeation chromatography (GPC) is a type of size exclusion chromatography (SEC) that separates analytes on the basis of size. GPC is often used to determine the distribution of molecular weights (M_w), number average molecular weight (M_n) and polydispersity index (PDI) of polymers. These three parameters of castor oil, polyol and polyurethane were determined by GPC technique using the Waters equipment with refractive index detector, Water 717 plus Autosampler and Water 600 Controller. THF was used as the eluent with flow rate of 1 ml min^{-1} at 16 bars. Sample of 0.02 g was solubilized in 5 ml THF for 24 hours before measurement.

3.3.3 Dynamic Mechanical Analysis (DMA)

Dynamic mechanical analysis (DMA) was performed in order to determine glass transition temperature, T_g of the synthesized polyurethane and polymer electrolytes. The analysis was performed using Perkin Elmer DMA 8000 dynamic mechanical analyser with a film-tension mode of 1 Hz. Rectangular film specimens of approximately 20 mm × 10 mm × 0.60 mm (length × thickness × width) were used for the analysis. The samples were cooled and held isothermally at −60 °C before the temperature was increased to 180 °C at a rate of 2 °C min^{-1}. The T_g values of the samples were obtained from the peaks of the tan δ curves.

3.3.4 Thermogravimetric Analysis (TGA)

The thermogravimetric analysis (TGA) was carried out in order to study the thermal stability of polymer films as well as the compositional information. The TGA was done using the Setaram LABSYS EVO simultaneous thermal analyser. Samples were carefully weighed to 15 ± 2 mg in alumina crucible placed in the centre of heating chamber. TGA scans were carried out under nitrogen atmosphere from 30 °C to 600 °C at 10 °C min^{-1} heating rate. The data were analysed using Calisto software TGA analysis determines the degradation temperature of polymer based on the mass loss.

3.3.5 Scanning Electron Microscopy (SEM)

The morphology of the cross-section of polymer film was observed using ZEISS EVO MA 10 scanning electron microscope at 2000 × magnification with 10 kV incident electron beam. Samples were immersed in liquid nitrogen before fractured. The fractured samples were mounted to the aluminium sample holder and coated with gold using sputter coating machine for 90 s before the analysis.

3.3.6 Linear Sweep Voltammetry (LSV)

The electrochemical stability of an electrolyte during oxidation and reduction cycles is one of the essential parameters for practical use in energy storage systems or electrochromic devices. The electrochemical stability of the electrolyte systems in this study was carried out at room temperature using linear sweep voltammetry over the potential range from −2.5 V to 4.0 V at a scan rate of 0.5 mV s^{-1}. The LSV was performed using Wonatech ZIVE MP2 multichannel electrochemical workstation. The configuration of the cell for the LSV measurements was SS/Polymer electrolytes/SS. Stainless steel was used as working, reference and counter electrodes. In LSV technique, the current at the working electrode is measured while the potential between the working electrode and the reference electrode is swept linearly with time. Only the highest conducting sample for each system was employed for LSV measurement.

3.3.7 Transference Number Measurement

Ionic transference number also called ion transport number is another important parameter for polymer electrolyte materials. Transference number of moving charges is defined as the ratio of the total current carried in an electrolyte by a given ions (cations/anions). For ionic transference number measurement of this work, stainless steel (SS) blocking electrodes were used and the polymer electrolytes were polarized under a fixed DC voltage of 1.0 V. The value of current is monitored until it reaches the steady state condition. The ionic (t_{ion}) and electronic transference numbers (t_{ele}) were evaluated by means of Wagner's polarization technique. The ionic and electronic transference numbers are estimated using equations.

$$t_{ion} = \frac{I_I - I_f}{I_I} \tag{3.1}$$

$$t_{ele} = \frac{I_f}{I_I} \tag{3.2}$$

where I_{I} is the initial current and I_{f} is the final residual current.

For cationic transference number measurement, the combination of AC and DC techniques as proposed by Brunce and Vincent (Bruce et al., 1988) was used. In this technique, the sample is held between two reversible electrodes for the cation whose contribution is to be estimated. For this purpose, the cations of interest are Li^+ and Na^+ and hence the sample geometry used are Li/(PU-LiI)/Li and Li/(PU-LiI-PMII)/Li for sample containing lithium salt, meanwhile, Na/(PU-NaI)/Na and Na/(PU-NaI-PMII)/Na for sample containing sodium salt. The cell was assembled in a glove box (H_2O and O_2 < 0.1 ppm). The transference number of Li^+ or Na^+ can be calculated using the equation

$$t_+ = \frac{I_{ss}}{I_0}\left[\frac{\Delta V - I_0 R_0}{\Delta V - I_{ss} R_{ss}}\right] \tag{3.3}$$

where R_o is bulk resistance before polarization and R_{ss} bulk resistance after polarization determined from complex impedance plot using ion-reversible electrodes. ΔV is the applied DC voltage, I_o and I_{ss} are the initial and steady state current under a DC bias voltage, respectively. In this work, the applied voltage was fixed at 1.0 V.

3.3.8 Electrochemical Impedance Spectroscopy (EIS)

Complex impedance measurements of the polymer electrolytes were done using impedance spectroscopy, Solartron SI 1260 Impedance/Gain-Phase Analyzer. The samples of 20 mm in diameter and average thickness of (0.6 - 0.9) mm were sandwiched by two polished stainless steel electrodes. The measurements were performed over frequency range of 10 Hz - 5 MHz with amplitude of 100 mV at room temperature. Ionic conductivity of polymer electrolyte samples was calculated using equation

$$\sigma = \frac{l}{R_b A} \tag{3.4}$$

where l is the thickness of the electrolyte and A is the electrolyte-electrode contact area. The values of the bulk resistance, R_b of the electrolytes were determined from the intersection of complex impedance plot in the real impedance axis.

The temperature dependence of conductivity was done with the aid of Espec SU-242, temperature and humidity chamber as thermal controller system. The polymer electrolyte films were sandwiched between stainless steel electrodes and placed in the chamber. The impedance measurements were recorded at room temperature and 5 °C intervals up to 80 °C. The cell was kept at the desired temperature for at least 15 minutes to reach the equilibrium temperature of the sample prior to reading the data. The bulk resistance of sample at different temperatures was obtained and used to calculate ionic conductivity. The results of ionic conductivity against the reciprocal of absolute temperature (1000/T (K^{-1})) were plotted to exhibit the temperature dependence conductivity of the samples.

3.3.9 Current-Voltage Measurement

The Current-Voltage curves of FTO/TiO_2-dye/PU electrolytes-I_2/Pt/FTO DSSC fabrication were recorded using WonaTech ZIVE MP2 multichannel work station interconnected with Solar light UVA/UVB simulator using xenon light source under illumination of AM 1.5G (100 mW cm^{-2}). The performance of dye-sensitized solar cells was evaluated in terms of short circuit current density (J_{sc}), open circuit voltage (V_{oc}), fill factor (FF) and energy conversion efficiency (η). The J_{sc} is defined as the current density that is measured under short-circuit conditions, i.e. when the voltage equals zero. The J_{sc} yields information on how efficiently the photogenerated charges are generated. The V_{oc} is the voltage generated by the cell when no external load is present. It yields information on how efficiently charges are separated. The fill factor is the ratio of the maximum power output (P_{max}) to the product of short circuit current density and open circuit voltage. The energy conversion efficiency, η is the ratio of P_{max} to the incident radiation power (P_{in}) on the solar cell surface. The values of fill factor and efficiency were calculated from the following equations.

$$FF = \frac{P_{max}}{J_{sc}.V_{oc}} = \frac{I_{mpp}.V_{mpp}}{J_{sc}.V_{oc}} \tag{3.5}$$

$$\eta = \frac{P_{max}}{P_{in}} = \frac{J_{sc}.V_{oc}.FF}{P_{in}} \tag{3.6}$$

where I_{mpp} and V_{mpp} represent the photocurrent and photovoltage corresponding to the maximal power point, respectively in J-V curve.

CHAPTER 4: CASTOR OIL BASED POLYURETHANE FOR POTENTIAL APPLICATION AS HOST IN POLYMER ELECTROLYTES

4.1 Introduction

This chapter revealed the results of the PU from renewable resource, castor oil, which was synthesized for application as host material in polymer electrolytes. The synthesis was carried out at room temperature without additives, crosslinkers and chain extenders. The work comprises of the transesterification of castor oil followed by polymerization of polyurethane. The castor oil based polyol was characterized in terms of acid value, hydroxyl number and molecular weight. The polymer was characterized in the aspects of optical, morphological and thermal properties.

4.2 Results of the castor oil-polyol (CO-p)

Scheme 4.1 shows the transesterification of castor oil based polyol. Esterification began after phthalate anhydride was added to the mixture of oil and glycerol and after some time, water was collected and the mixture turned into a clear brownish. From the titration that was done at a certain interval of time during the heating and stirring processes, the calculated acid value of the reaction was found to decrease gradually throughout the reaction. This proves that the reaction has progressed and polyester polyol was formed. The polyol obtained has an acid value of 3.0 mg KOH g^{-1}. The hydroxyl value of the polyol was obtained using 848 Titrino Plus equipment and its value is 190 mg KOH g^{-1}. According to Petrović, (2008), polyols with OH numbers of about

200 mg KOH g^{-1} and less give semi-rigid polyurethanes of moderate or low crosslinking density when crosslinked with diisocyanate.

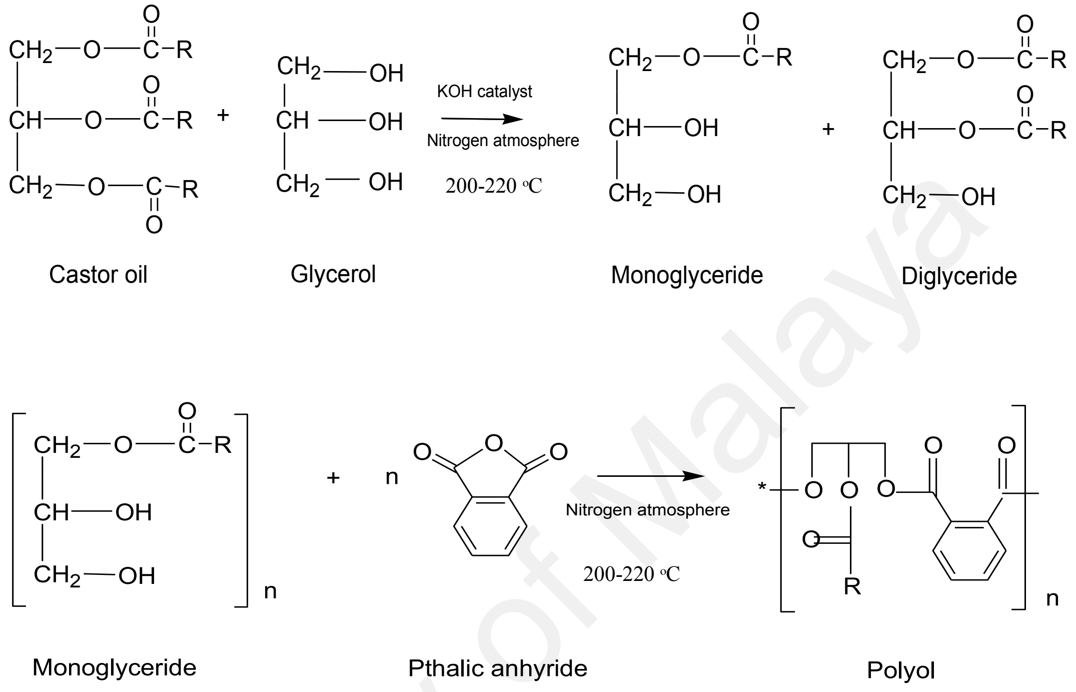

where

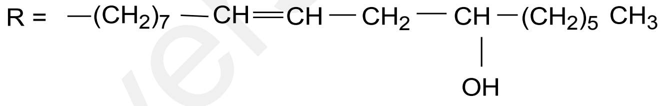

$$R = -(CH_2)_7-CH{=}CH-CH_2-\underset{\displaystyle OH}{\underset{|}{CH}}-(CH_2)_5\,CH_3$$

Scheme 4.1: Schematic representation of the preparation of castor oil based polyol

Figure 4.1 shows FTIR spectra of castor oil and synthesized castor oil based polyol. The characteristic band of ester group C=O stretching appears at 1730 cm^{-1} and that of the O-H functional group at 3550 cm^{-1}. The peak at around 3500 cm^{-1} seems to be weak and broad due to bonded hydrogen in the structure. These bands confirm the esterification reaction of polyol. The peaks at 2926 cm^{-1} and 2854 cm^{-1} are due to stretching vibrations of C-H for castor oil and polyol. Less intense peak at 1238 cm^{-1} due to C-O stretching vibration of castor oil is observed as sharp peak at 1266 cm^{-1} in the spectrum of castor oil based polyol. Two peaks at 1120 cm^{-1} and 1070 cm^{-1} correspond to C-O-H stretching vibration of secondary alcohol.

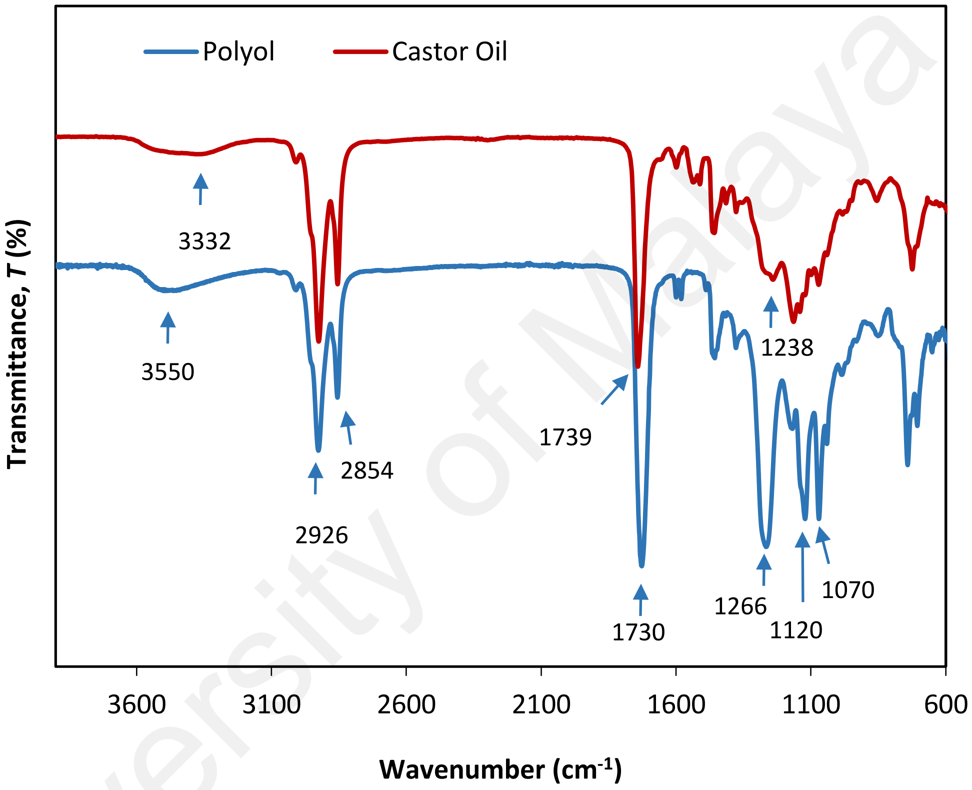

Figure 4.1: FTIR spectra of castor oil and polyol

4.3 Results of castor oil-polyol (CO-p) based polyurethane

As mentioned earlier, PU films were produced by the reaction of MDI with castor oil based polyol. Two different polyurethane formulations were used (Table 4.1). Formulation 1 contains NCO and OH in the weight ratio of 20:80 while Formulation 2 contains NCO and OH of weight ratio of 40:60. The PU of Formulation 1 is soft and flexible while that of Formulation 2 is rigid and brittle.

Table 4.1: Weight ratio of NCO:OH in different formulations

Formulation	NCO:OH	Physical observation
Formulation 1	20:80	Soft and flexible
Formulation 2	40:60	Rigid and brittle

4.3.1 FTIR Analysis

Figure 4.2 presents the FTIR spectra of the synthesized castor oil based polyurethane in the region 550 cm^{-1} to 4000 cm^{-1}. For Formulation 2, the presence of peak at 2270 cm^{-1} indicates that the isocyanate (NCO) has not completely reacted. The absence of the peak is an indicative of the absence of NCO groups in the structure of Formulation 1, (NCO:OH (20:80)). On the other hand, new peaks at 1512 cm^{-1} and 3369 cm^{-1} corresponding to -NH vibration (-NH-C=O-) and absorbance band around 1740 cm^{-1} of the C=O group are present in the FTIR spectra (Smith, 1998). According to Narine et al., (2007), the band around 1740 cm^{-1} indicates that the hydrogen bonded C=O group vibration region is overlapped with the free C=O group vibration region. The absence of isocyanate peak and the appearance of amine and carbonyl peaks suggest a complete conversion of monomers to urethane (Mortley et al., 2007; Xu et al., 2008; Rashmi et al., 2013).

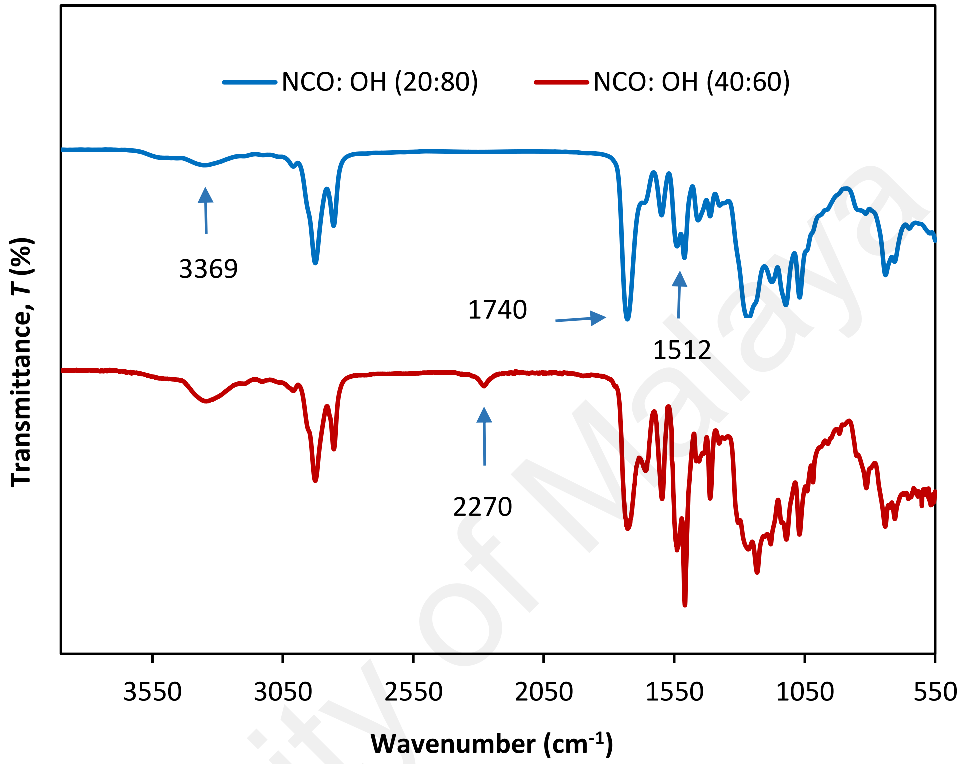

Figure 4.2: FTIR spectra of castor oil based polyurethane

Therefore, for further investigation, only Formulation 1 was used. The photograph of castor oil based polyurethane film is shown in Figure 4.3.

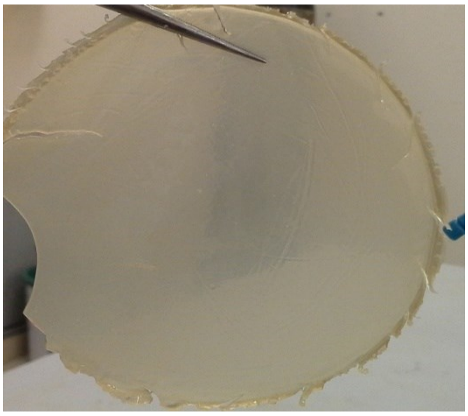

Figure 4.3: Photograph of castor oil based polyurethane with Formulation 1

4.3.2 GPC Result

In this work, molecular weight M_w, number average molecular weight, M_n and polydispersity index, PDI of castor oil, polyol and polyurethane were determined using gel permeation chromatography (GPC). Table 4.2 summarizes the value of M_w, M_n and PDI of the samples. The molecular weight of castor oil is 1023 g mol^{-1}, close to the value reported by other researchers which is 963 g mol^{-1} (Somani et al., 2003). The synthesized castor oil based polyol gives a molecular weight of 2786 g mol^{-1}. This value is suitable to form flexible polyurethane (Badri, 2012; Júnior et al., 2013). The molecular weight of the synthesized polyurethane in this work is 11942 g mol^{-1}.

Table 4.2: Value of molecular weight, number average molecular weight and polydispersity index of castor oil, polyol and polyurethane

Sample	**Molecular weight, M_w (g mol^{-1})**	**Number average molecular weight, M_n (g mol^{-1})**	**Polydispersity index, PDI (M_w/M_n)**
Castor oil	1023	880	1.16
Polyol	2786	1296	2.15
Polyurethane	11942	2540	4.70

4.3.3 Dynamic Mechanical Analysis

Figure 4.4 depicts the plot of storage modulus, E and tan δ versus temperature of polyurethane film. E is slightly decreased from –60 °C to –40 °C, then decreases rapidly after –40 °C until a rubbery plateau is observed in higher temperature. This change corresponds to glass-rubber transition and tan δ reaches its maximum peak simultaneously. The plot shows a tan δ peak, which indicates homogeneous nature of the film. The value of glass transition temperature, T_g is given by the peak (α relaxation) of the tan δ versus temperature curve. The T_g value obtained for the polyurethane film is –15.8 °C. T_g values of polyurethanes depend on the properties of the synthesized polyols, therefore the values could vary from –50 °C to 80 °C. Júnior et al., (2013) reported the T_g value of thermoplastic polyurethane based on castor oil of –30.0 °C whereas Liu and co-workers., (2008) obtained a T_g value of 22.3 °C for castor oil-based polyurethane. On the other hand, Yeganeh and Shamekhi, (2006) obtained values of T_g between 47 °C to 61 °C for the polyurethanes synthesized from different compositions of castor oil and glycolysed poly(ethylene terphthalate) (PET).

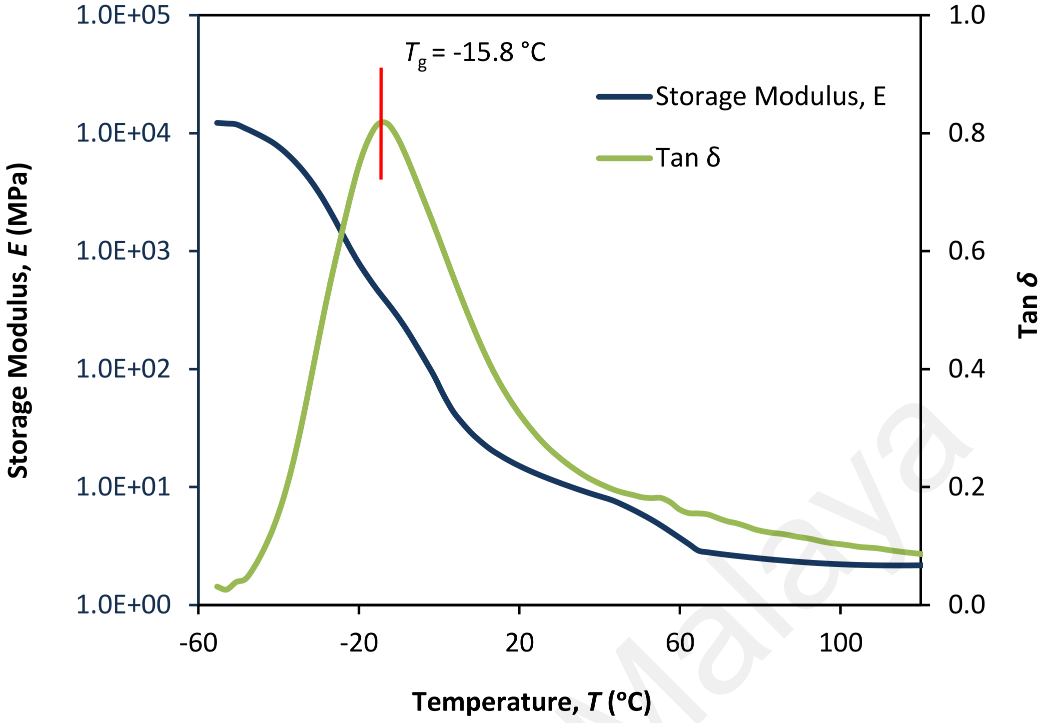

Figure 4.4: Tangent δ and storage modulus as a function of temperature for castor oil based polyurethane

4.3.4 Thermogravimetric Analysis

Illustrated in Figure 4.5 are thermogravimetric and derivatives thermogravimetric curves for castor oil based polyurethane. Three decomposition stages are observed. Table 4.3 lists the decomposition temperatures, T_d and percentage weight loss of each decomposition stage. The first degradation stage, T_{d1} is observed at 259 °C which achieves a maximum temperature, T_{max} at 271 °C. The T_{d1} is corresponding to the degradation of urethane linkages. From the first degradation stage, it can be concluded that the film is thermally stable from room temperature until the temperature started to decompose. The second step of thermal degradation, T_{d2} is observed from 313 °C up to 429 °C. The third step of thermal degradation, T_{d3} begins at 429 °C to 490 °C. T_{d2} corresponds to the liberation of free isocyanate and T_{d3} is attributed to the decomposition of soft segment of the polyurethane (Corcuera et al., 2011; Su'ait et al., 2014b). The TGA result suggests that the polyurethane is stable from ambient temperature up to 259 °C.

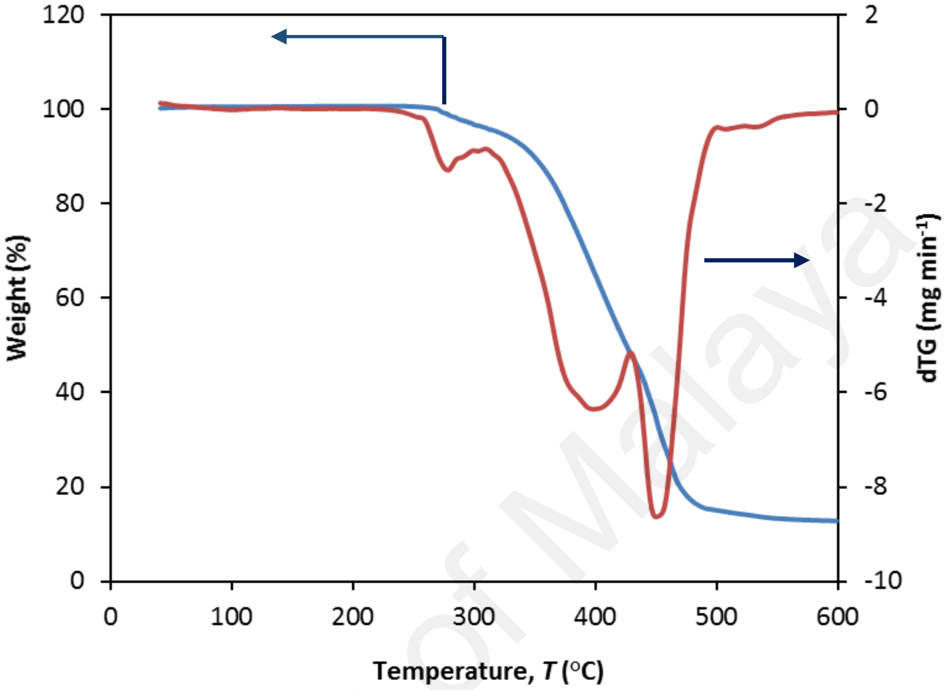

Figure 4.5: Thermogravimetric and derivative thermogravimetric curves of polyurethane

Table 4.3: Decomposition temperatures, T_d and percentages weight losses of polyurethane film

Weight loss (%)			**Total weight loss (%)**	**Residue after 600 °C (%)**
T_{d1} 259–313 °C	T_{d2} 313–429 °C	T_{d3} 429–490 °C		
4.7	47.7	34.8	87.2	12.8

4.3.5 Morphological Analysis

The morphology of cross-sectional area of the castor oil based polyurethane film is shown in Figure 4.6. As seen in the figure, the film is smooth and no phase separation is observed. The smooth morphology of the film shows that the film is highly amorphous. This characteristic is favourable for a host of polymer electrolytes since ion conduction occurs in amorphous region.

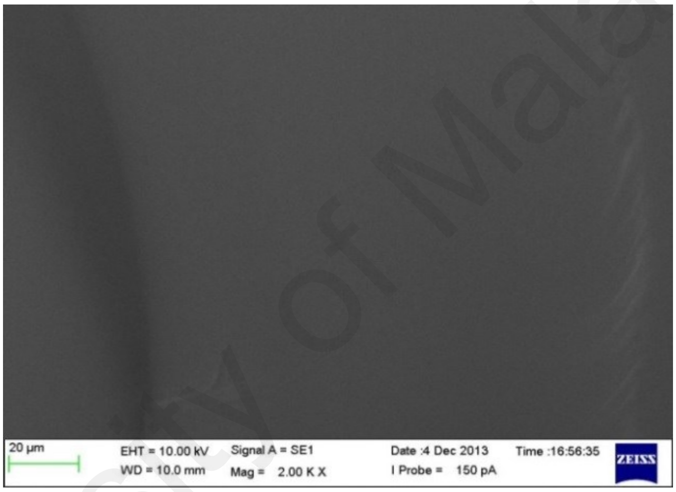

Figure 4.6: SEM image of cross-section of castor oil based polyurethane film

4.4 Summary

Castor oil based polyol was successfully synthesized via transesterification. The polyol has an acid value of 3.0 mg KOH g^{-1}, OH number of 190 mg KOH g^{-1} and molecular weight of 2786 g mol^{-1}. Using this polyol, polyurethane was successfully synthesized as confirmed by FTIR results. The film prepared using the synthesized polyurethane demonstrated highly amorphous character, low T_g value of −15.8 °C and was free standing as well as good thermal stability, up to 259 °C. These results indicated that the castor oil based polyurethane possessed favourable properties for application as host in polymer electrolytes. Although there are many methods and sources to synthesize polyurethane, the transesterification of polyol from castor oil could give highly amorphous polyurethane with low molecular weight and low glass transition temperature, T_g, thus give flexible PU. It is believed that flexible PU is highly amorphous that allows the enhancement of segmental motion of polymer to facilitate ion migrations.

CHAPTER 5: PU-SALT POLYMER ELECTROLYTES

5.1 Introduction

This chapter discusses the characteristics of castor oil based polyurethane electrolytes. The ratio of NCO:OH (20:80) for the formation of PU was fixed throughout the experiment. The PU was added with sodium iodide and lithium iodide in different wt % to form PU-NaI and PU-LiI polymer electrolyte systems, respectively. The electrolytes were analysed using FTIR spectroscopy, DMA, EIS, transference number measurement and LSV.

5.2 FTIR Analysis

FTIR has been employed to identify the constituent interactions in polymer-salt films. Three important regions of the spectrum are considered in the polyurethane polymer electrolytes systems; (a) N-H stretching vibration (3100–3700 cm^{-1}), (b) carbonyl stretching vibration (1680–1780 cm^{-1}) and (c) ether stretching vibration (1050–1100 cm^{-1}). According to Wen et al., (2002), the deconvoluted FTIR spectra in the NH stretching vibration have three strong absorption bands which are assigned to free -NH stretching vibration (3500–3505 cm^{-1}), -NH stretching vibration where the -NH groups are H bonded to the carbonyl oxygen of the hard segment (3305–3327 cm^{-1}) and -NH stretching where the -NH groups are H bonded to the ether oxygen of the soft segment (3253–3266 cm^{-1}). Meanwhile, in carbonyl band, the deconvoluted FTIR shows three peak for free or non-hydrogen bonded, disordered hydrogen bonded and ordered hydrogen bonded (Wen et al., 2002).

Figure 5.1 and Figure 5.2 show the FTIR spectra of PU electrolyte films with different wt % of NaI and LiI, respectively in the spectral region of 4000–1000 cm^{-1}. All the PU electrolyte films investigated in this study show similar spectra with a slight shift of some of the band positions. Obvious band shift is observed in the 3700–3100 cm^{-1} wavenumber, the region for free and H-bonded -NH stretching vibration.

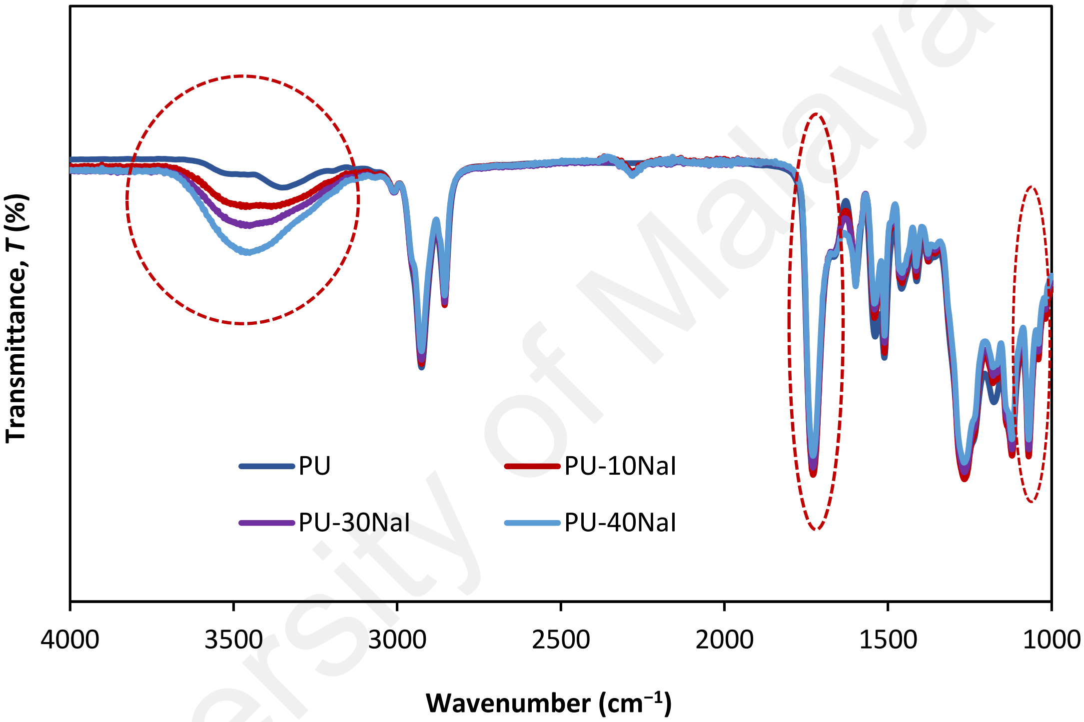

Figure 5.1: FTIR spectra of PU electrolytes with different wt % of NaI

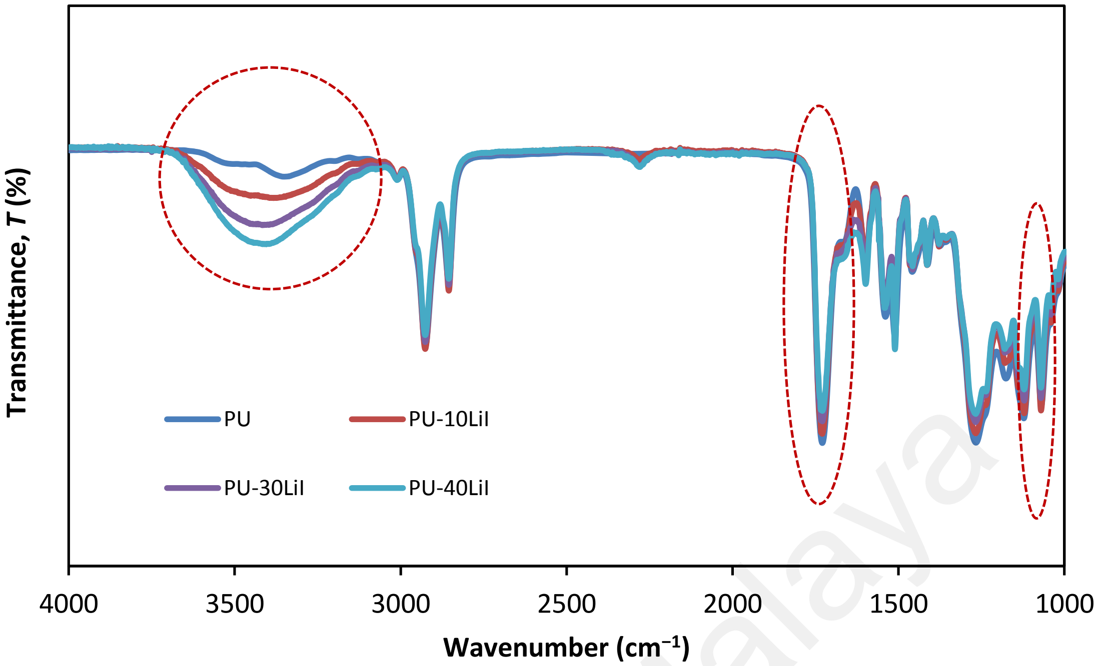

Figure 5.2: FTIR spectra of PU electrolytes with different wt % of LiI

In this work, the FTIR spectrum of pristine polyurethane shows the three peaks in the NH stretching region as observed in Figure 5.3 (a) and Figure 5.4 (a) (enlargement of range 3800–3100 cm^{-1}). Region 1 (3600–3430 cm^{-1}) corresponds to free NH stretching, region 2 (3430–3240 cm^{-1}) is the region for hydrogen bonded NH group to the carbonyl oxygen atom while region 3 (3240–3150 cm^{-1}) for hydrogen-bonded NH group to ether oxygen. With addition of NaI and LiI, peaks in a NH region become broader, shifted to higher or lower wavenumbers and might be overlapped with each other as suggested by Wen et al., (2001) and Digar et al., (2002). The shift of peak to lower wavenumber with the addition of salt (region 1) could be due to the interactions between Na^+ or Li^+ cations and lone pair of electrons on the nitrogen atom, leading to N-H bond length be reduced as seen in Scheme 5.1 (a). The shift of peak in region 2 is attributed to the coordination of Na^+ and Li^+ ions with the lone pair electrons of carbonyl oxygen atoms that leads to weakening of H bond strength (Scheme 5.1 (b)). This in turn increases the N-H bond strength, hence the peak position shifted to higher wavenumbers and overlapped with region 1. The shift of region 3 to higher wavenumber could be explained in terms of the phenomenon that the ether oxygen is coordinated by Na^+ or Li^+ ions leading to weakening the hydrogen-bonded strength between NH and ether oxygen (Scheme 5.1 (c)) (Wen et al., 1999b; Chen et al., 2004). It seems that region 2 and region 3 have collapsed and region 1 become broad and shift to lower wavenumber.

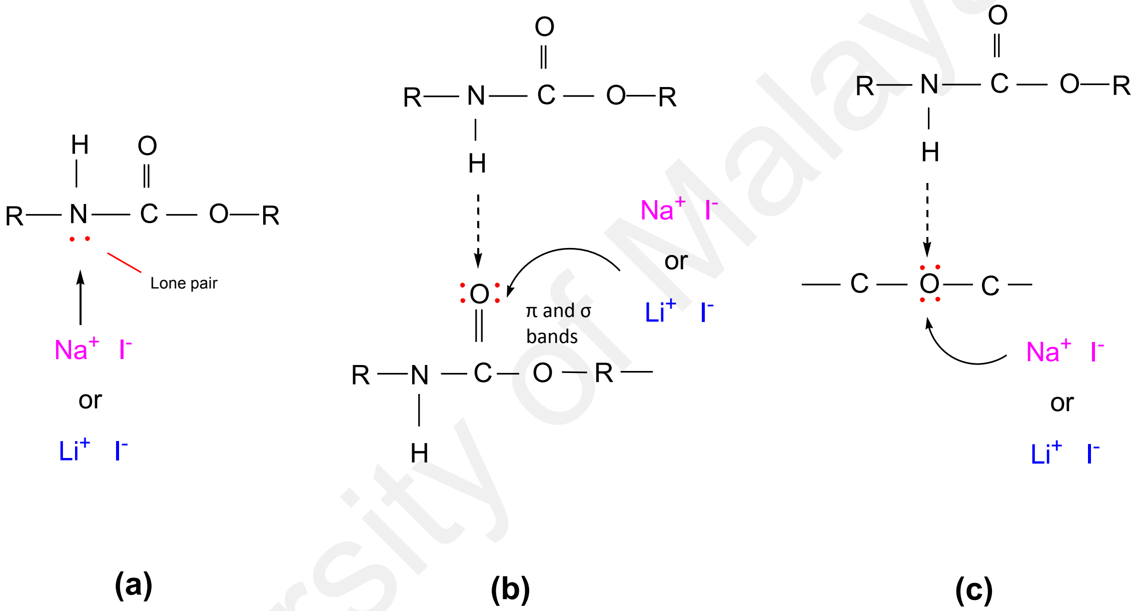

Scheme 5.1: Schematic for suggested coordination of salt with: (a) the nitrogen atoms of free -NH groups, (b) the hydrogen bonded carbonyl oxygen and (c) the hydrogen bonded ether oxygen of PU

Other important characteristic regions in FTIR spectrum for the study of the interaction in PU electrolytes are the region between 1760 and 1680 cm^{-1} (the carbonyl symmetric stretching vibration or amide band) and region between 1045 and 1085 cm^{-1} (ether stretching vibration). According to Chen et al., (2004), the convoluted FTIR spectra in the C=O stretching region have three peaks due to free or non-hydrogen-bonded C=O (1727–1735 cm^{-1}), disordered hydrogen-bonded C=O (1718–1721 cm^{-1}) and ordered hydrogen bonded C=O (1703–1704 cm^{-1}) vibrations, respectively. The disordered hydrogen-bonded C=O corresponds to the hydrogen-bonding interactions with –NH groups in both amorphous and crystalline regions, whereas the ordered hydrogen-bonded C=O occurs within the crystalline hard domain of the PU (Van Heumen & Stevens, 1995).

Figure 5.3 (b) and Figure 5.4 (b) depict the enlargement of carbonyl FTIR spectral region of PU whereas Figure 5.3 (c) and Figure 5.4 (c) are the ether stretching regions of PU with addition of NaI and LiI, respectively. This slight shift of the band to lower wavenumbers and decrease in intensity with the addition of salts might be due to coordination of Li^+ and Na^+ ions with carbonyl oxygen atoms. The shifting also indicates the existences of intermolecular interaction between lithium/sodium ions with oxygen atoms in the polymer. The oxygen atoms from carbonyl functional group in the PU act as electron donor atoms and hence form a coordinate bond with lithium and sodium ions from doping salts (Wen et al., 2000). From these FTIR results, it can be deduced that the interactions between host polymer and salts occurred both in the hard segment (C=O and N–H) and soft segment (C–O–C) of PU.

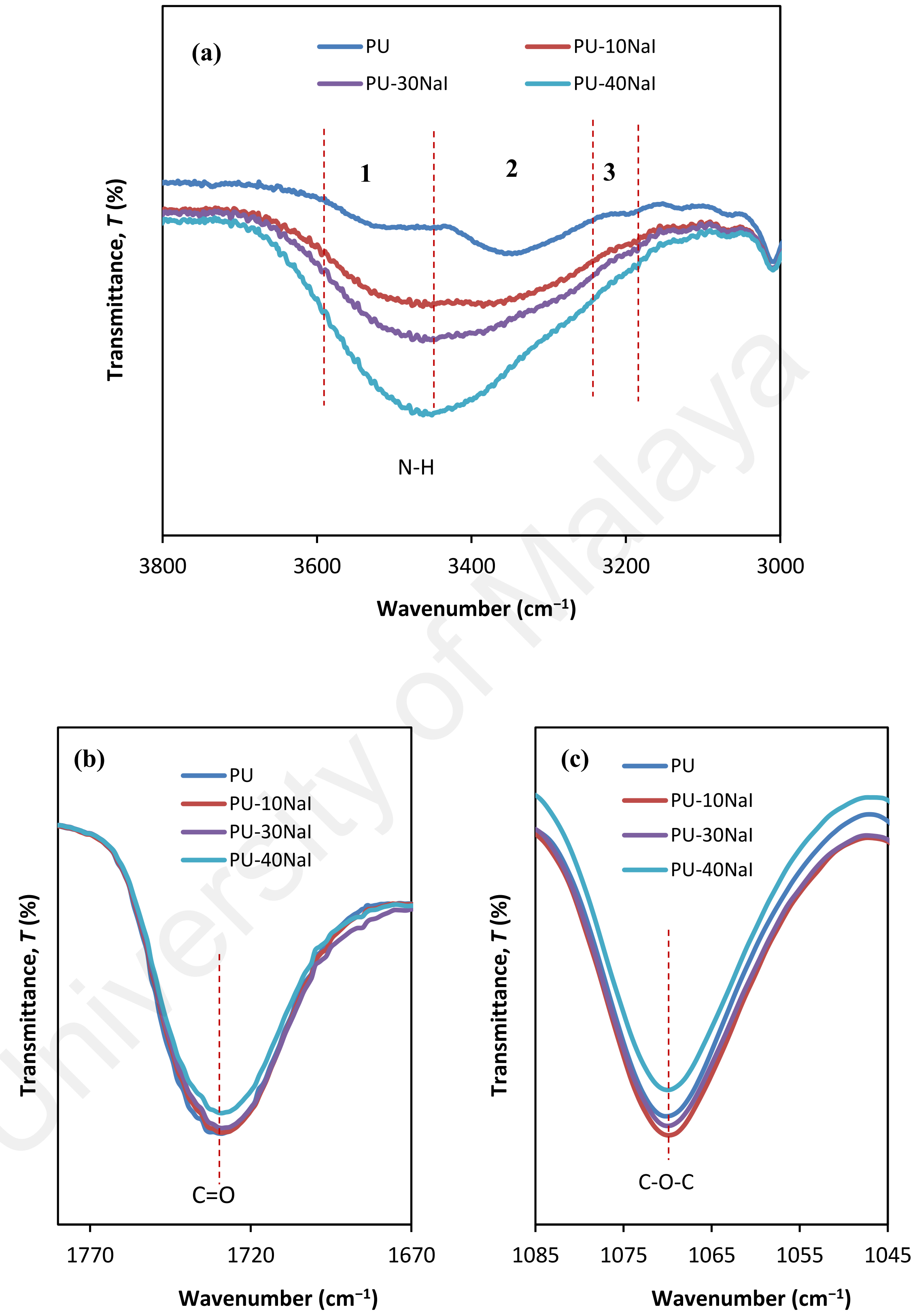

Figure 5.3: FTIR spectra of (a) NH, (b) carbonyl and (c) ether stretching region of PU-NaI electrolytes

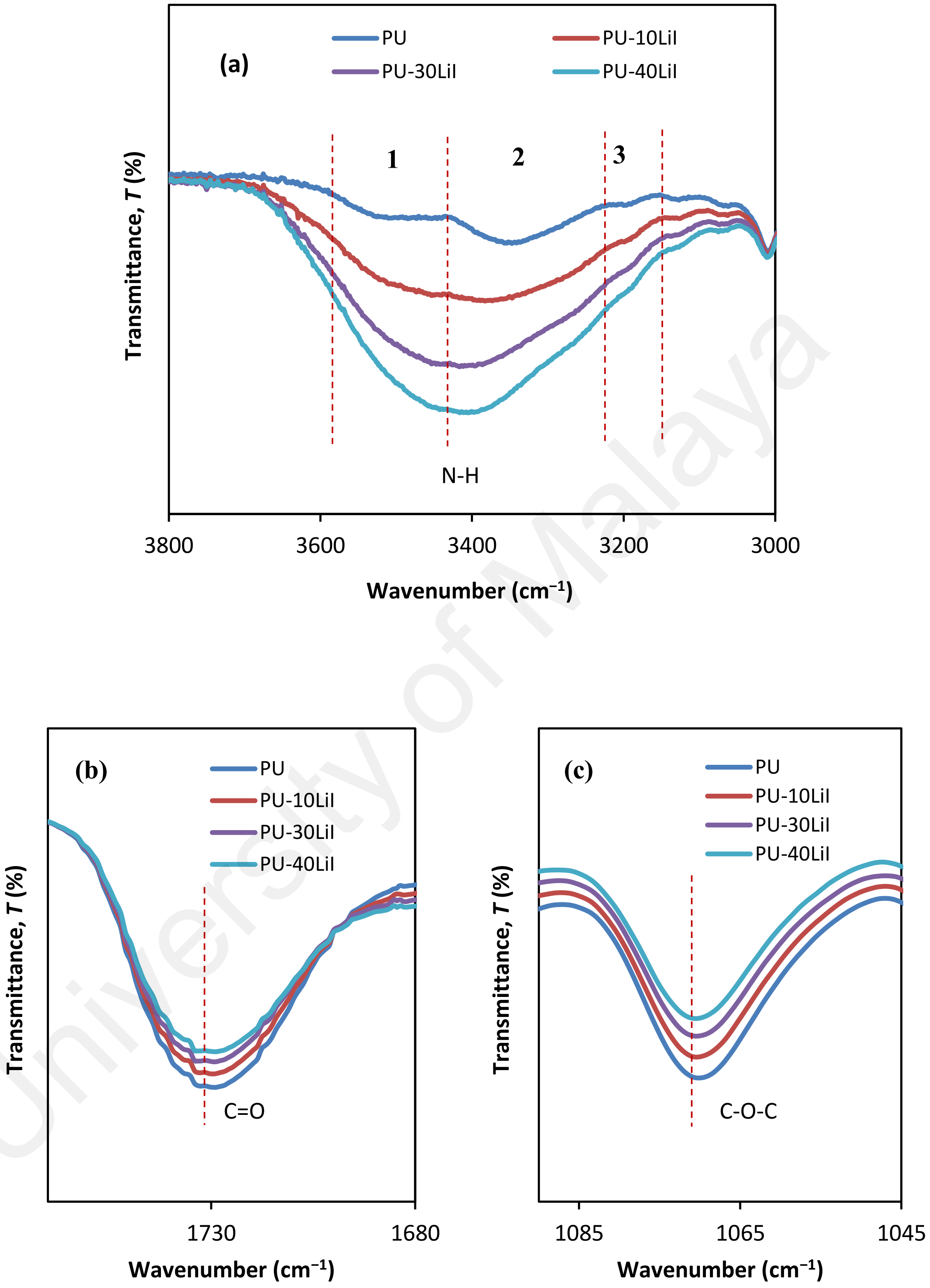

Figure 5.4: FTIR spectra of (a) NH, (b) carbonyl and (c) ether stretching region of PU-LiI electrolytes

5.3 Dynamic Mechanical Analysis

Dynamic mechanical analysis was performed in order to determine glass transition temperature, T_g of the PU polymer electrolyte films. Figure 5.5 and Figure 5.6 present the plots of tangent delta as a function of temperature for the studied electrolyte films and their glass transition temperature values are listed in Table 5.1 and Table 5.2. The temperature at the maximum peak (α relaxation) of tan δ corresponds to the T_g of the films. Small hump exists at higher temperature for the PU containing salt may be due to the phase transition of soft segment of PU. T_g of polyurethane film of –15.8 °C decreases to lower values upon addition of salt. This suggests that the segmental mobility of PU increases upon addition of salt and the segments become less rigid (Lavall et al., 2010; Wu et al., 2010). The incorporation of salt into the PU matrix might have weakened the dipole-dipole interactions between the PU chains leading to higher segmental mobility. However, for sample PU with 40 wt % LiI, T_g was found to be higher than that of salt free of PU. The T_g increased to –7.8 °C. This might be due to strong interaction between polymer and salt that created transient cross-linking between PU and LiI salt, thus increased the T_g value (Hong and Shi, 2007).

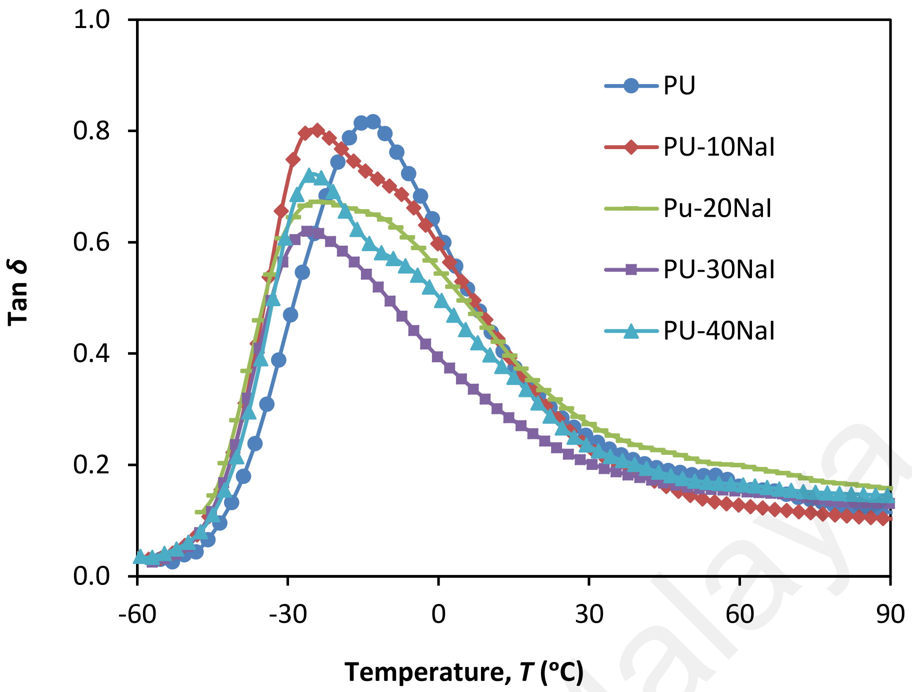

Figure 5.5: Tangent δ as a function of temperature for PU-NaI polymer electrolyte films

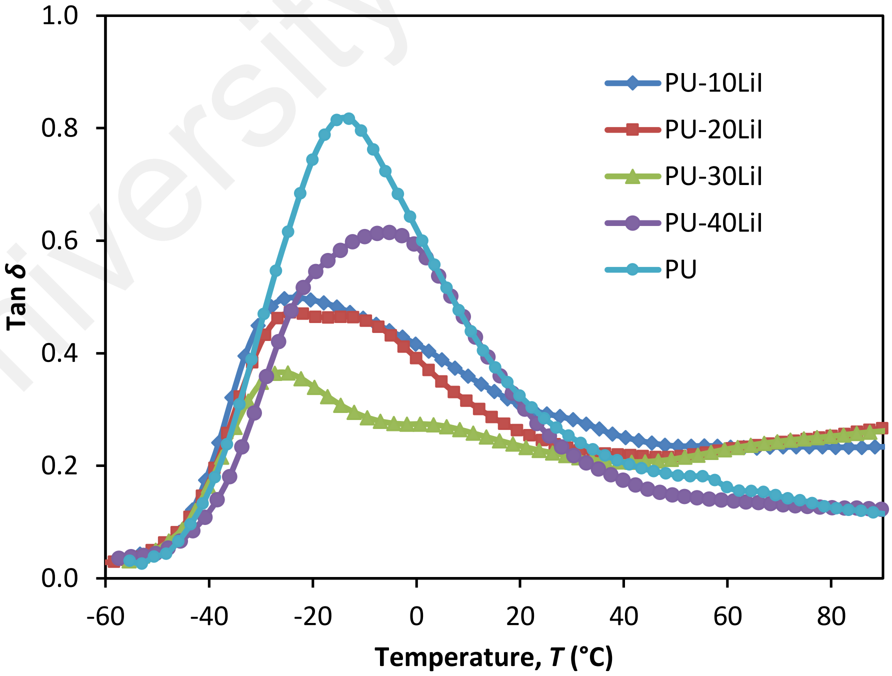

Figure 5.6: Tangent δ as a function of temperature for PU-LiI polymer electrolyte films

Table 5.1: Glass transition temperature, T_g of PU-NaI systems

Sample	**T_g (°C)**
PU	–15.8
PU-10NaI	–24.1
PU-20NaI	–24.3
PU-30NaI	–26.2
PU-40NaI	–25.8

Table 5. 2: Glass transition temperature, T_g of PU-LiI systems

Sample	**T_g (°C)**
PU	–15.8
PU-10LiI	–22.9
PU-20LiI	–24.3
PU-30LiI	–27.3
PU-40LiI	–7.8

5.4 Ionic Conductivity Study

5.4.1 Room Temperature Conductivity

Ionic conductivity of polymer electrolytes is a very important analysis. Like other researchers, the conductivity of the PU based electrolytes was also determined by impedance spectroscopy. The plots of room temperature conductivity of polymer electrolytes as a function of salt concentration are shown in Figure 5.7. The conductivity of both systems increases with the salt concentration, reaching a maximum value of 1.41×10^{-6} S cm^{-1} and 4.28×10^{-7} S cm^{-1} at 30 wt % of LiI and NaI, respectively, and decreases thereafter. The conductivity increase is due to the increase in charge carriers or mobile ions when the salt content increases. At high salt concentration, the distance between dissociated ions became too close to each other enabling them to recombine into neutral ion-pairs and do not contribute to conductivity. Such phenomenon has also been reported in the literature (Wen et al., 2002; Niitani et al., 2005; Rodrigues et al., 2007). According to Wang et al., (2010), ionic conductivity of PU was attributed to the existence of large amount of charge carriers and interaction between Li^+ and soft and hard segments of PU.

The conductivity was also correlated to the T_g of polymer electrolytes. The highest conductivity has the lowest T_g and vice versa for both systems, PU-NaI and PU-LiI, except for the PU containing 40 wt % LiI. Addition of salt disrupts the molecular structure of PU and decreased the T_g value of the polymer host. The shift of T_g value towards lower temperature suggests that the segmental mobility of PU increases upon addition of salts and the segment become less rigid. It is also could be due to the plasticization of the electrolyte with addition of salts by weakening the dipole-dipole interactions between the

PU chains, which makes the ions move freely through the polymer chain network when an electric field is applied and hence increase the conductivity.

However, for the PU-40LiI system, T_g value is –7.8 °C is higher than that of PU-10LiI. As mentioned earlier, transient cross-linking might be created in the PU with 40 wt % LiI resulting in higher T_g value. In the system, the cross-links are well separated in space and move with respect to each other to a certain extent thereby contributing to higher ionic conductivity as compared to that of the PU-10LiI (Zainal et al., 2013).

By comparing the systems containing LiI and NaI, the conductivity is higher for PU-LiI compared to that for PU-NaI. This might be due to the size of cations. The cation size of Li^+ and Na^+ are 0.76 and 1.02 Å, respectively (Bhattacharya et al., 2009). According to Bhattacharya et al., (2009), systems containing salt with smaller cation exhibit higher conductivity due to higher mobility of the cation. Therefore, the higher conductivity value of PU-LiI compared to the PU-NaI is due to higher mobility of Li^+.

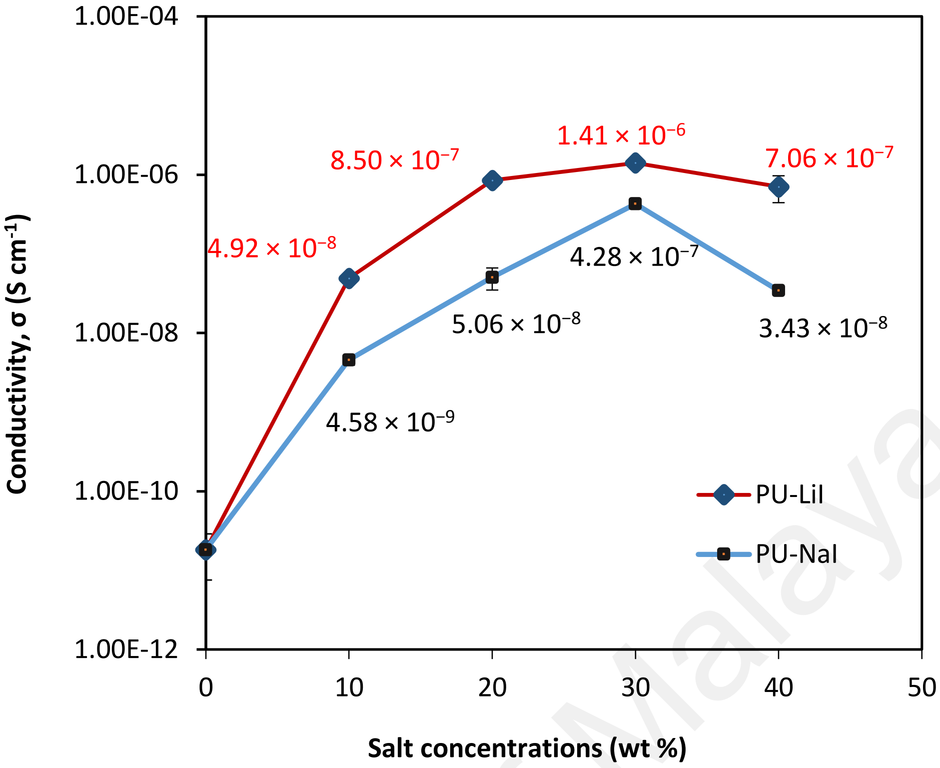

Figure 5.7: Conductivity behaviour of PU based polymer electrolytes with different wt % of LiI and NaI

From the electrolyte dissociation model, the number of dissociated charge carriers, n is given as

$$n = n_o \exp\left(-\frac{U}{2\varepsilon k_B T}\right) \tag{5.1}$$

where U is the bond dissociation energy of salt, k_B is the Boltzmann constant, ε is the dielectric constant of the system and T is temperature in Kelvin. The salt is assumed to be completely dissociated when dissolved in the polymer. From the equation, the charge carrier concentrations, n depends upon both on the dissociation energy involved and dielectric constant. The bond dissociation energy for LiI is 352 kJ/mol and NaI is 301 kJ/mol (Dean, 1985). Figure 5.8 and Figure 5.9 show the relative number of charge carrier (n/n_o) with different wt % of NaI and LiI, respectively at frequency of 50 Hz measured at room temperature. At low concentration of salts the relative value of n/n_0 is minimum and the value reaches a maximum at 30 wt % and decreases when the amount is 40 wt % for both systems. This supports the explanation of conductivity behaviour given earlier.

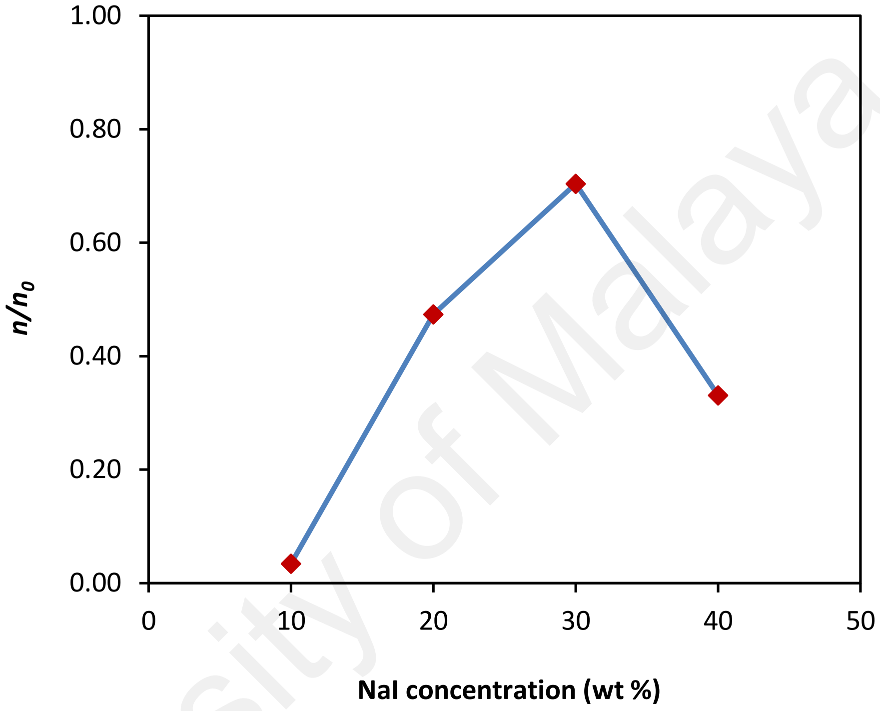

Figure 5.8: Change in relative number of charge carrier with different wt % of NaI at frequency of 50 Hz

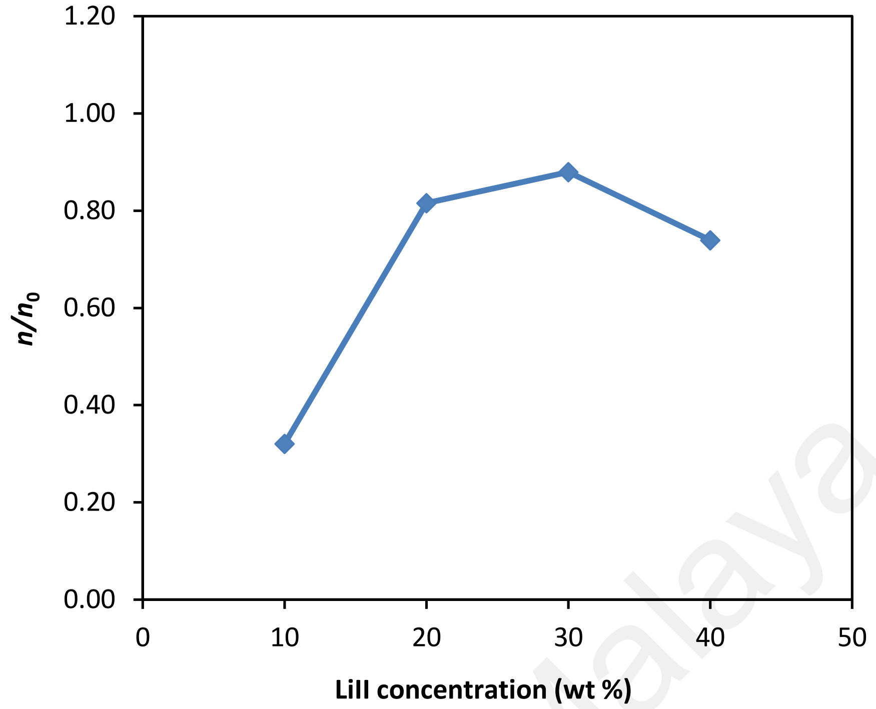

Figure 5.9: Change in relative number of charge carrier with different wt % of LiI at frequency of 50 Hz

5.4.2 Temperature Dependent Conductivity

Temperature dependence of ionic conductivity measurements were carried out to analyze the mechanism of ionic conduction in the studied polymer electrolyte films. Figure 5.10 displays the variation of ionic conductivity with the reciprocal of temperature for the PU-NaI and PU-LiI polymer electrolytes. The ionic conductivity values are found to increase w5hen the temperature increases from room temperature to 80 °C. The regression, R^2 values for all plots for both systems are ~ 1 indicating that the points lie in almost straight line revealing that the ionic conduction mechanism obeys the Arrhenius theory.

The increase of conductivity with temperature is interpreted as an ion hopping mechanism between coordinating sites, local structural relaxations and segmental motions of the polymer-salt complexes (Rajendran et al., 2006). As the temperature increases, the polymer chains acquire faster internal modes in which bond rotations produce segmental motion, facilitate hopping inter-chain and intra-chain ion movements thus increase the conductivity of the polymer electrolyte (Baskaran et al., 2006; Vieira et al., 2007). According to Rajendran et al., (2004), polymers can expand easily and produce a free volume when heated, therefore, ions, solvated molecules, or polymer segments can move to the free volume hence increase the conductivity. The Arrhenian conductivity-temperature relationship has also been observed in other polyurethane based polymer electrolytes (Wen et al., 2000; Wang & Min, 2010). Arrhenius equation is expressed as

$$\sigma = \sigma_o exp\left(\frac{-E_a}{k_B T}\right) \tag{5.2}$$

where σ_o is a pre-exponential factor, E_a is the activation energy, T is the absolute temperature in Kelvin and k_B is Boltzmann constant (8.6173324×10^{-5} eV K^{-1}). The activation energy values were calculated from the slope of log σ versus $1000/T$ graph. The activation energy is the minimum energy that is required by the ions to hop from one coordination site to another coordination site. The values of E_a of PU-salt electrolytes are given in Table 5.3. The trend of E_a-salt content is opposite to the trend of σ-salt content shown in Figure 5.7. This is in agreement with the fact that the amount of charge carrier in polymer electrolyte increases by increasing salt concentration and the energy barrier for ion transport decreases, leading to a decrease in the activation energy (Vieira et al., 2007). This demonstrates that besides the number of charge carriers, the conductivity is also dependent on the mobility of the charge carriers. However, for the PU-NaI system, a slight difference was observed for the value of E_a although the highest conducting sample has the lowest E_a. This might be due to the number of mobility of effective charge carrier in the systems approximately the same although the concentration of NaI increases.

Table 5.3: Activation energy, E_a of PU-NaI and PU-LiI polymer electrolyte films

NaI/ LiI (wt %)	**Activation energy, E_a (eV)**	
	PU-NaI	**PU-LiI**
10	0.58	0.57
20	0.53	0.42
30	0.52	0.31
40	0.56	0.50

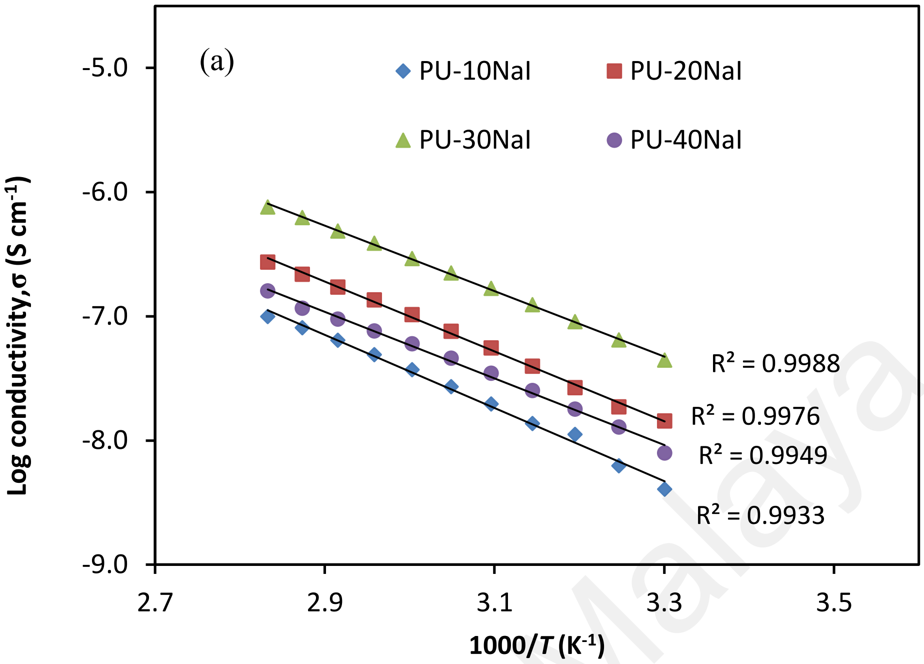

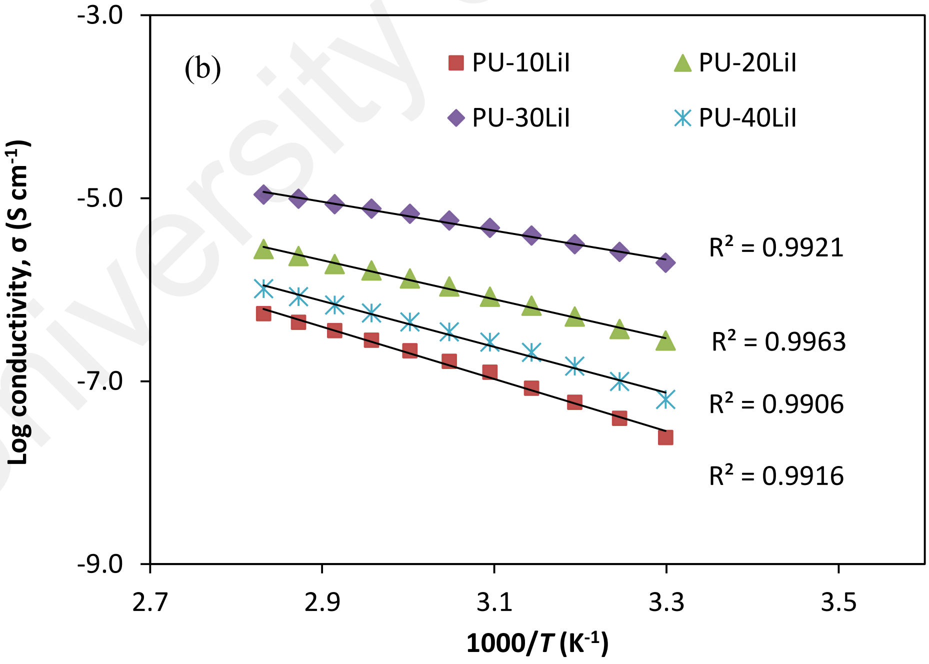

Figure 5.10: Temperature dependence of ionic conductivity of (a) PU-NaI and (b) PU-LiI polymer electrolyte films

5.5 Transference Number Measurement

5.5.1 Ionic Transference number

The transference number corresponding to ionic (t_{ion}) for PU-NaI and PU-LiI systems was evaluated using Wagner's polarization method. In this technique, the direct current (DC) is monitored as a function of time on an application of a fixed DC voltage of 1.0 V across the SS/PU polymer electrolytes/SS. After polarization, the graphs of normalized current versus time were plotted. Figure 5.11 and Figure 5.12 show the plots of normalized polarization current with respect to time for selected PU-salt samples. The values of ionic transference numbers are ~ 1 for all systems. This implies that the charge transport in PU-salt films was predominantly due to ions.

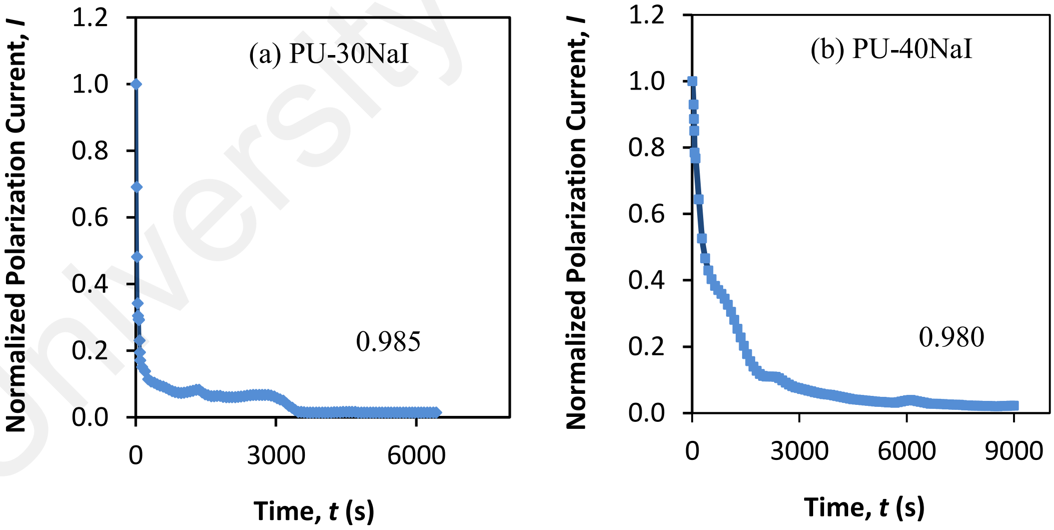

Figure 5.10: The plots of normalized polarization current versus time for selected sample of PU-NaI systems

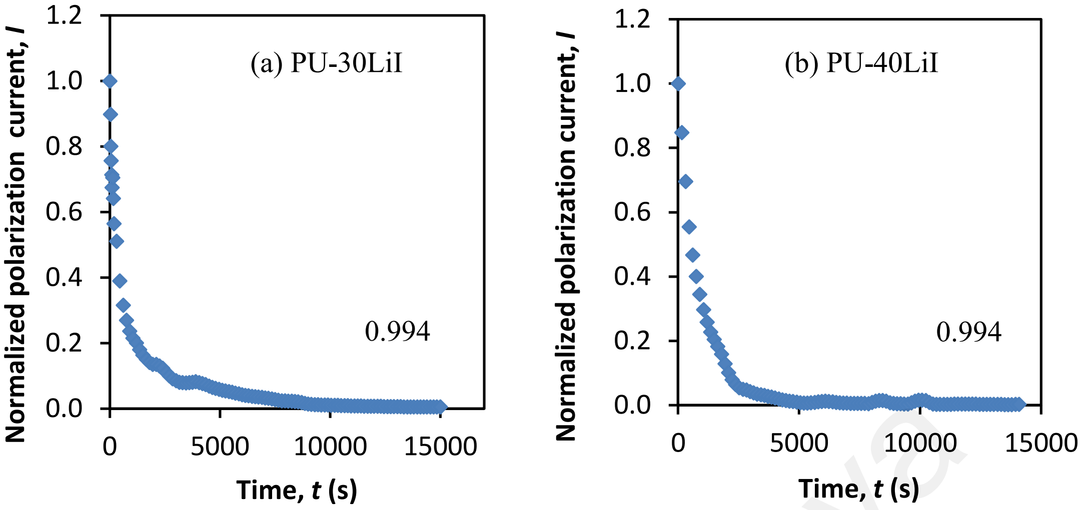

Figure 5.12: The plots of normalized polarization current versus time for selected sample of PU-LiI systems

5.5.2 Cationic Transference Number

Cationic transference number of PU electrolytes was determined using Brunce and Vincent method (Bruce et al., 1988; Musil and Vondrák, 2014). According to this method, the transference number of cation can be calculated with the following equation

$$t_+ = \frac{I_{ss}}{I_0}\left[\frac{\Delta V - I_0 R_0}{\Delta V - I_{ss} R_{ss}}\right] \tag{5.3}$$

where I_0 is initial current (t = 0), I_{ss} is steady state current, ΔV is applied voltage pulse (1.0 V), R_0 is electrolyte resistance before polarization and R_{ss} is electrolytes resistance after polarization. The frequency range of AC impedance was set from 10 Hz to 5 MHz and the arrangement of samples were Na/PU-NaI/Na and Li/PU-LiI/Li for the samples containing NaI and LiI, respectively.

Figure 5.13 and Figure 5.14 show the current versus time plots for cation transference number measurement for highest conducting PU-30NaI and PU-30LiI systems. $I_0 = 3.33 \times 10^{-4}$ A and $I_{ss} = 8.60 \times 10^{-5}$ A for PU-30NaI, whereas $I_0 = 1.83 \times 10^{-4}$ A and $I_{ss} = 2.29 \times 10^{-5}$ A for PU-30LiI. The inset graph shows the AC impedance spectra of the samples of before and after DC polarization. The PU-30NaI possessed cationic transference number, t_{Na+} of 0.180 while for highest conducting PU-30LiI showed t_{Li+} value of 0.159. The small value of cationic transference numbers might be due to ether oxygen in the polymer chains trap the cations electrostatically, and thus ionic conduction was mostly contributed by anions (Sequeira and Santos, 2010). This suggests that anionic contribution to the total ionic conduction is very significant. Higher value of anionic conduction is desired for application in DSSC (Yang et al., 2008b; Bhattacharya et al., 2009) for redox reaction in Pt/electrolytes.

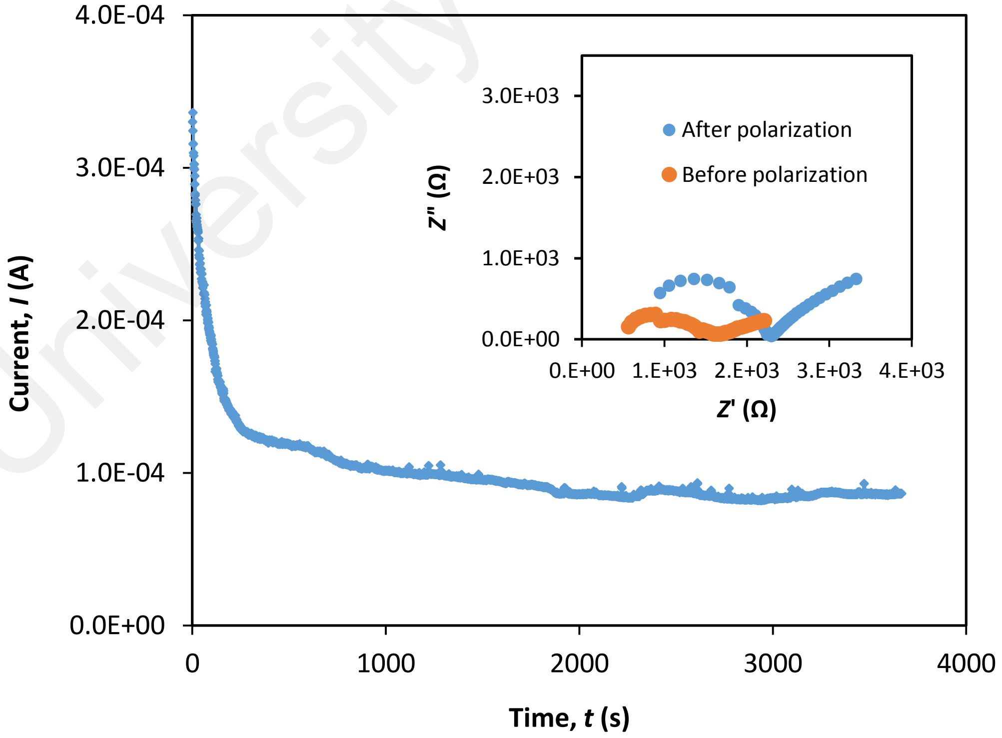

Figure 5.13: The current versus time plot of Na/PU-NaI/Na configuration. Inset graph is the impedance spectra of the sample before and after polarization

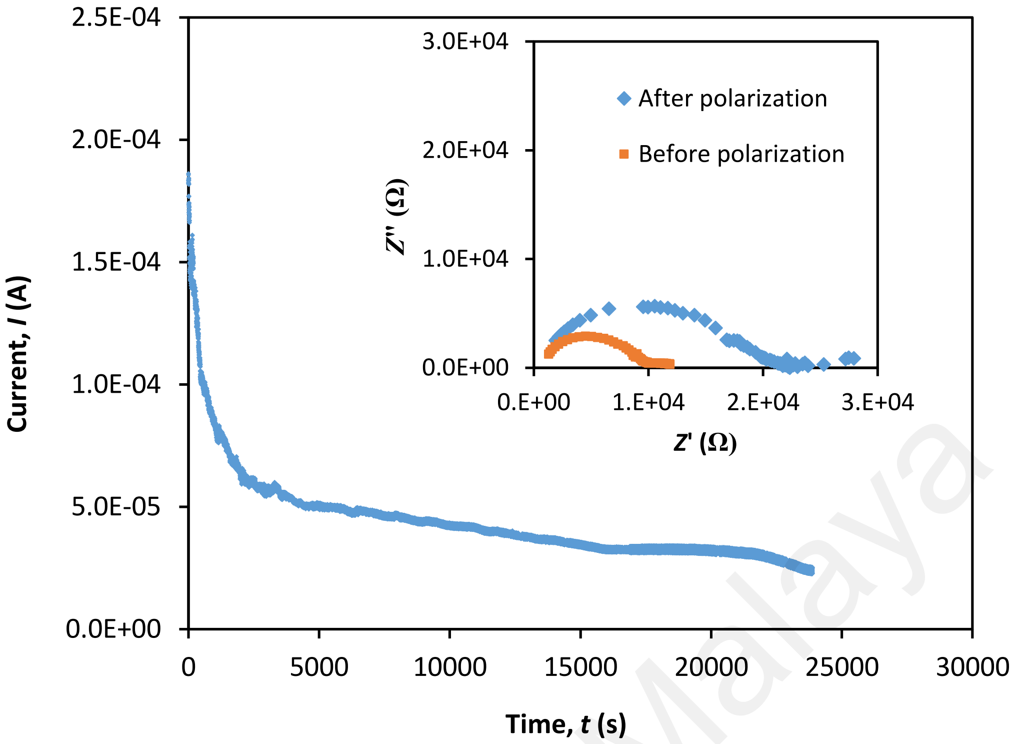

Figure 5.14: The current versus time plot of Li/PU-LiI/Li configuration. Inset graph is the impedance spectra of the sample before and after polarization

5.6 Linear Sweep Voltammetry

The electrochemical stability window of the PU electrolytes was determined by linear sweep voltammetry. Figure 5.15 and Figure 5.16 display the current-voltage response obtained for the highest conducting PU-NaI and PU-LiI polymer electrolyte systems using stainless steel as a working electrode and reference electrode measured between the potential ranges from –2.5 to 2.5 V with a scan rate of 0.5 mV s^{-1}. The onset of the current identifies the anodic decomposition voltage of the electrolytes (Reddy et al., 2003). It is observed that PU-30NaI shows a decomposition voltage at 1.9 V, whereas for PU-30LiI, the decomposition voltage is 2.0 V. The results show that the PU-LiI possessed slightly wider electrochemical stability window compared to PU-NaI. Researchers have shown that the potential window of DSSCs is ~ –1.0 to 1.0 V (Tan et al., 2012). In this work, electrochemical stability window of the PU-salt electrolytes exceed and wider than that the normal potential range of ~ –1.0 to 1.0 V, and indicates that the suitability for DSSC applications.

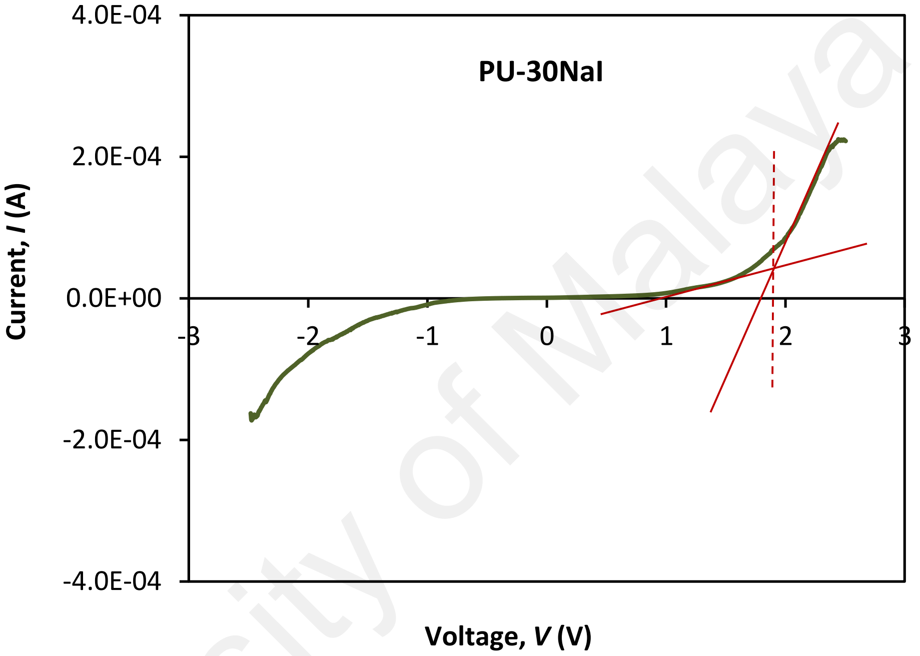

Figure 5.15: Linear sweep voltammogram of the highest conducting sample PU-NaI polymer electrolyte using stainless steel as WE, RE, CE electrodes with a scan rate of 0.5 mV s^{-1}

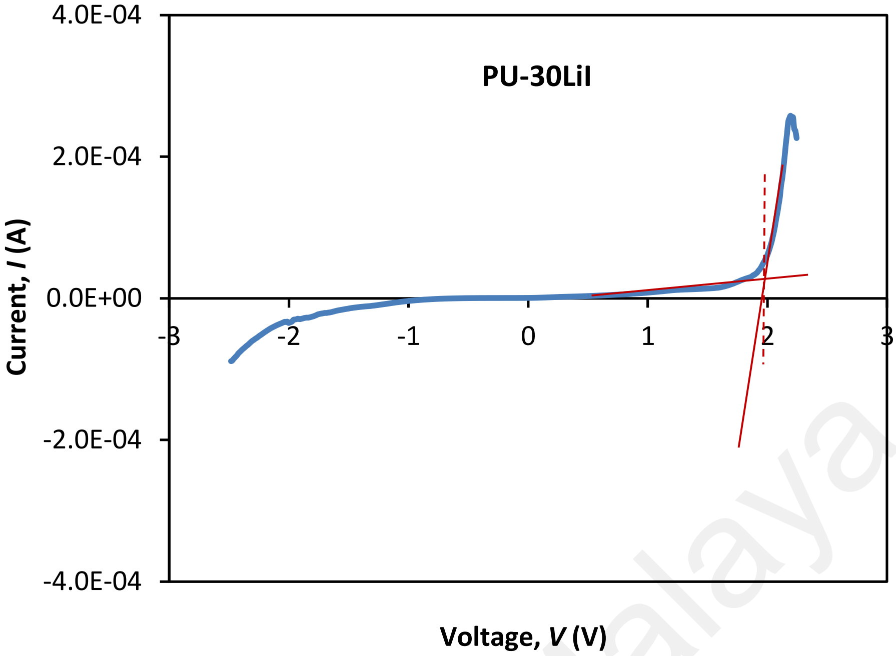

Figure 5.11 : Linear sweep voltammogram of the highest conducting sample PU-LiI polymer electrolyte using stainless steel as WE, RE, CE electrodes with a scan rate of 0.5 mV s^{-1}

5.7 Summary

PU-salt systems with NaI and LiI as doping salts have successfully prepared and characterized using FTIR, DMA, EIS, transference number measurement and LSV. In the FTIR analysis, the changes in intensity and the shifting of bands show that some interaction have occurred among PU and salts. Glass transition temperature, T_g of –15.8 °C of PU decreased upon addition of salts suggesting an increase of segmental mobility as the polymer segments became more flexible. The lowest T_g for PU-NaI system was –26.2 °C with 30 wt % NaI and for PU-LiI system was –27.3 °C with 30 wt % LiI. The PU-30NaI and PU-30LiI gave the highest conducting samples of 4.28×10^{-7} S cm^{-1} and 1.41×10^{-6} S cm^{-1} in PU-NaI and PU-LiI systems, respectively. The small cation of Li^+ also influenced the mobility of ions in the polymer. The ionic conductivity of PU-salt increased with the increase of temperature and followed the Arrhenius behaviour. Activation energy, E_a calculated from the gradient of Arrhenius plots showed that the conductivity contrary to the values of E_a. The higher conducting sample had lower activation energy. The charge transport in PU-salt was predominantly ions as confirmed from transference number measurement using Wagner's polarization method. Cationic transference number using Brunce and Vincent method suggested that the majority of ionic conduction in PU electrolytes contributed by anion. Electrochemical stability window of ~ –2.0 to 2.0 V of the PU electrolytes revealed the applicability of castor oil PU electrolytes in DSSC. However, for comparative analysis of castor oil based PU doped with NaI and LiI doping salts, the PU doped with LiI exhibited slightly better performance in terms of ionic conductivity, flexibility of polymer due to lower T_g and electrochemical stability window.

CHAPTER 6: PU-SALT-PMII POLYMER ELECTROLYTES

6.1 Introduction

The ionic conductivity is a combined effect of (a) complexation of cation with polymer backbone as well as hopping along the polymer chain and (b) motion of free anions present in the polymer matrix. The addition of salt increases the polymer chain flexibility that leads to enhanced ionic conductivity. Addition of ionic liquid to polymer matrix is one of the methods to further enhance the chain flexibility hence increases the conductivity. This chapter presents the characteristics of the highest conducting polymer of PU-NaI and PU-LiI added with 3-propyl-1-methylimidazolium iodide (PMII) ionic liquid.

6.2 FTIR Analysis

Figure 6.1 and Figure 6.2 show the FTIR spectral regions of interest of the highest conducting sample of PU-LiI and PU-NaI added with PMII. The spectra show the similar pattern. Figure 6.1 (a) and Figure 6.2 (a) present the FTIR spectra in the NH region (3700–3100 cm^{-1}). The region can be divided into 3 parts: free -NH stretching vibration (3500–3505 cm^{-1}), -NH stretching vibration where the -NH groups are H bonded to the carbonyl oxygen of the hard segment (3305–3327 cm^{-1}) and -NH stretching where the -NH groups are H bonded to the ether oxygen of the soft segment (3253–3266 cm^{-1}). The shift of peaks and increase in intensity of the peaks in these three regions as discussed in PU-salt systems could be due to the interactions between cation and lone pair electrons on the nitrogen atom, coordination of ions with the nonbonded electrons of carbonyl oxygen atoms and coordination of cations to the ether oxygen.

Figure 6.1 (b) and Figure 6.2 (b) show FTIR spectra for PU electrolytes in the region between 1760 and 1680 cm^{-1} (the carbonyl symmetric stretching vibration or amide band). The peak at 1730 cm^{-1} of PU-NaI is shifted to lower wavenumber, 1728 cm^{-1} and peak at 1732 cm^{-1} of PU-LiI shifted to 1729 cm^{-1} with the addition of PMII. Figure 6.1 (c) and Figure 6.2 (c) illustrate the ether stretching vibration region for the soft segment of PU. The broad peak at 1070 cm^{-1} of PU-NaI and PU-LiI FTIR spectra shifted to 1073 cm^{-1} upon addition of PMII. These observations suggest that some degree of coordination or complexation has occurred between PU, salt and ionic liquid.

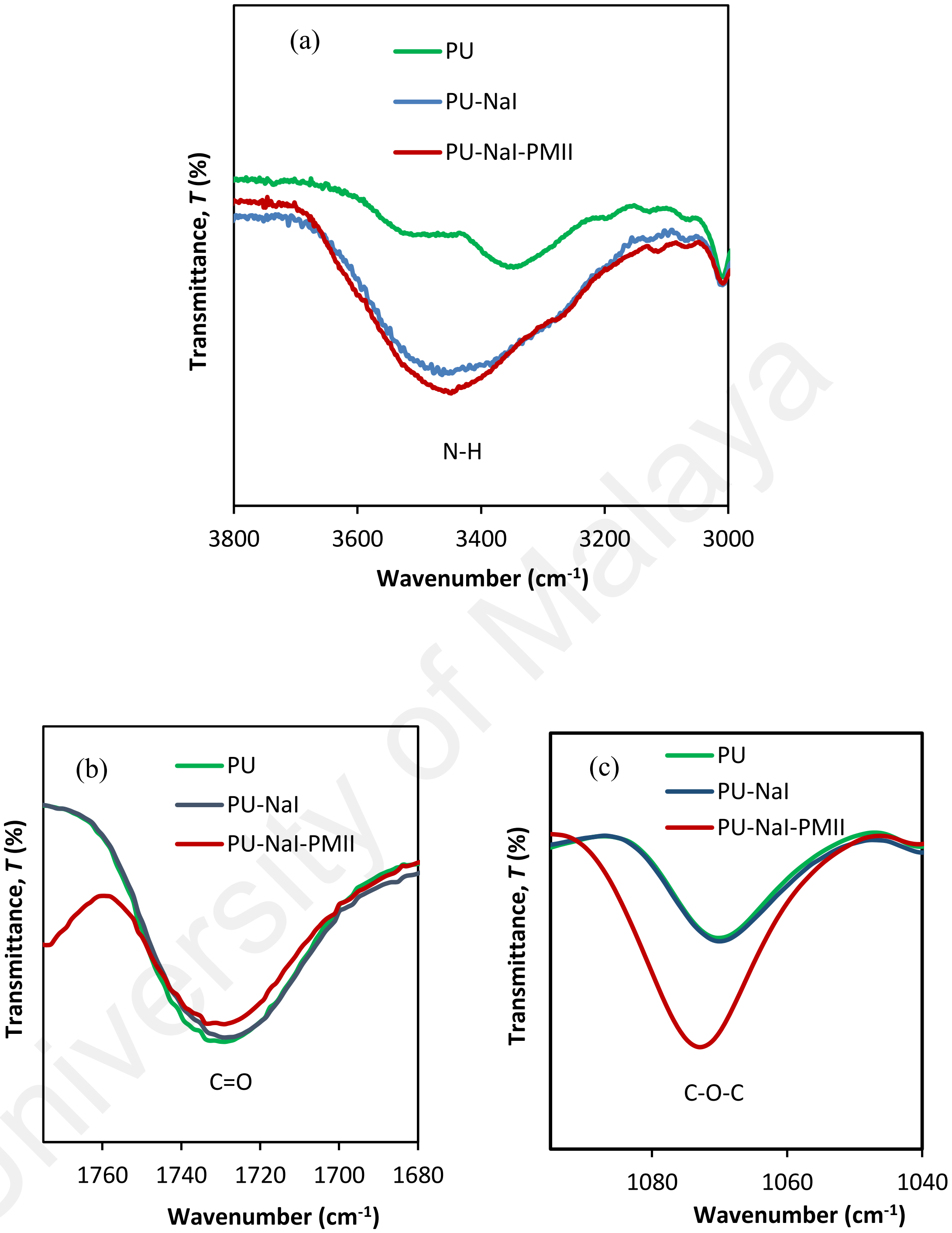

Figure 6.1: FTIR spectra of (a) N-H stretching region, (b) carbonyl stretching region and (c) ether stretching region for PU-NaI added with PMII

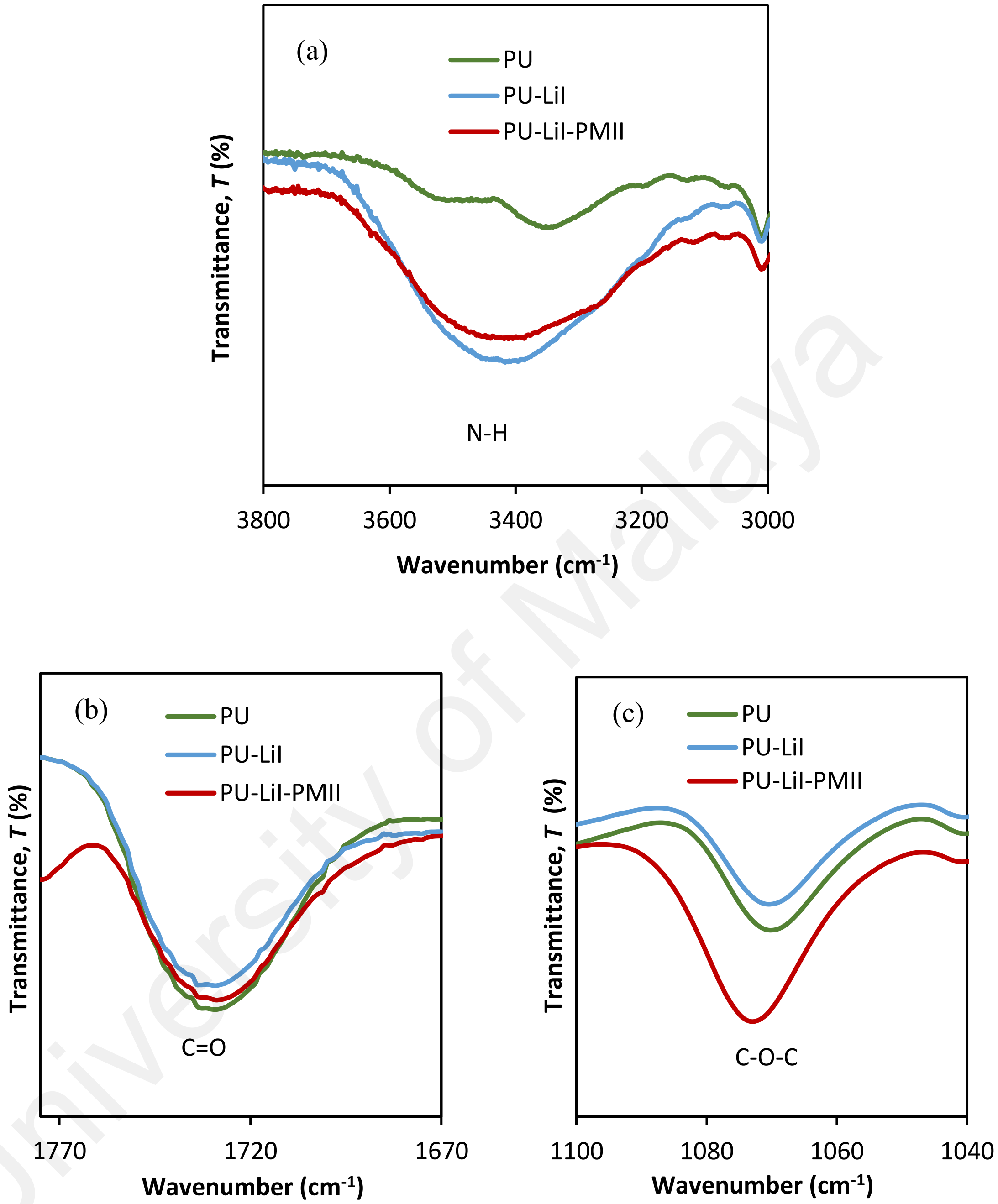

Figure 6.2: FTIR spectra of N-H stretching region, (b) carbonyl stretching region and (c) ether stretching region for PU-LiI added with PMII

6.3 Dynamic Mechanical Analysis

Figure 6.3 and Figure 6.4 present the plots of tangent delta as a function of temperature for PU-NaI-PMII and PU-LiI-PMII electrolyte films. The temperature at the peak maximum of tan δ corresponds to the T_g of the films. T_g value of –26.2 °C of PU-NaI electrolytes decreases to ~ –31.0 °C with the addition of PMII whereas T_g of PU-LiI decreases from –27.3 to ~ –33.0 °C. The decrease in T_g with inclusion of IL is due to the presence of IL that has acted as a plasticizer to soften the polymer backbone, enhances the segmental motion and hence increases the flexibility of polymer host. The plasticizing effect weakens the dipole-dipole interactions and thus disrupts the transient cross-linkage bonds among the polymer matrix. This promotes the decoupling of ions from the polymer segmental motion and improves ionic transportation (Ramesh et al., 2011).

However, no significant changes are observed on T_g value of PU-salt with wt % of PMII. The values are ~ –31 °C for PU-NaI-PMII and ~ –33 °C for PU-LiI-PMII. This result may be attributed to polymer chain movements being hindered by the inclusion of ionic liquid. The T_g values are about the same indicating that the degree of the hindrance is similar in both types of electrolytes (Tafur et al., 2013).

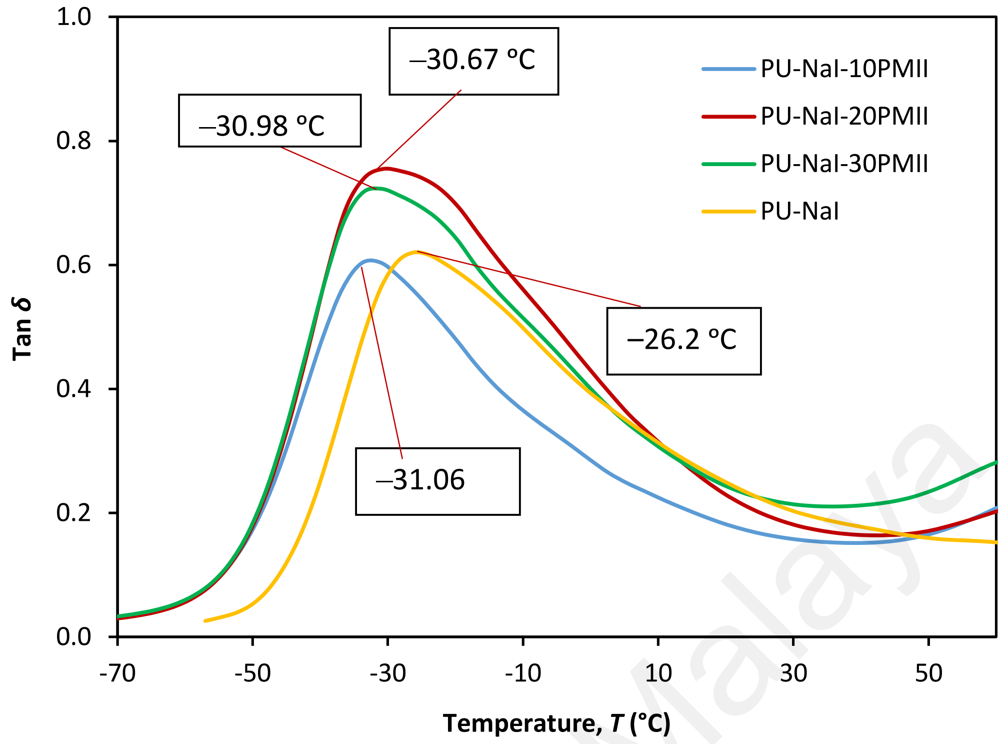

Figure 6.3: Tangent *δ* as a function of temperature for PU-NaI-PMII polymer electrolyte films

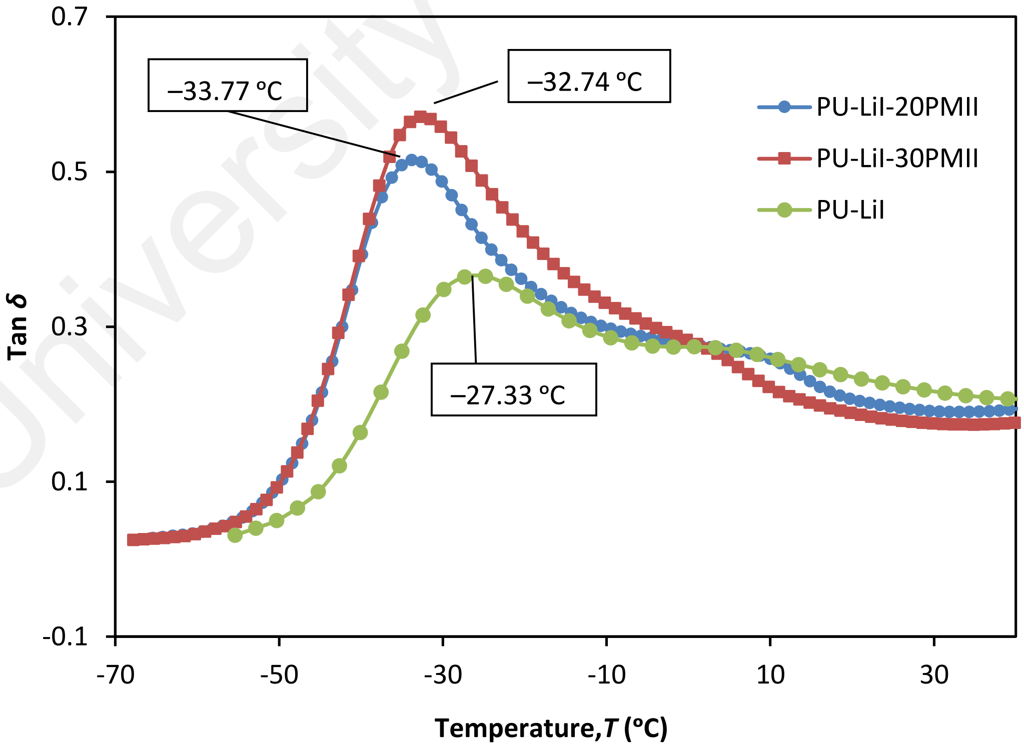

Figure 6.4: Tangent *δ* as a function of temperature for PU-LiI-PMII polymer electrolyte films

6.4 Ionic Conductivity Study

The highest conducting samples of PU-NaI and PU-LiI were added with different wt % of PMII ionic liquid and their ionic conductivity were measured. The value of ionic conductivity for PU-NaI-PMII and PU-LiI-PMII are listed in Table 6.1 and Table 6.2, respectively. Generally, ionic conductivity for both systems were found to increase about one order of magnitude upon addition of IL compared to the sample without IL. The highest conductivity of $(2.65 \pm 0.77) \times 10^{-6}$ S cm^{-1} and $(2.09 \pm 0.10) \times 10^{-5}$ S cm^{-1} were obtained by addition 20 wt % of PMII to the PU-NaI and PU-LiI systems, respectively. The increase in conductivity of PU-salt-IL might be due to the strong plasticizing effect of ionic liquid. The plasticizing effect could soften the polymer backbone and enhance the flexibility of polymer chains as evidenced by the decreased T_g value discussed earlier. Ion decoupling was initiated with higher polymer segmental motion (Liew & Ramesh, 2013). In this work, addition of IL by 10 wt % increment to polymer-salt resulted in a slight increase and then decreased in conductivity.

Table 6.1: Ionic conductivity value of PU-NaI-PMII

Sample	Conductivity, σ (S cm^{-1})
PU-30NaI	$(4.28 \pm 0.48) \times 10^{-7}$
PU-NaI-10PMII	$(1.66 \pm 0.42) \times 10^{-6}$
PU-NaI-20PMII	$(2.65 \pm 0.77) \times 10^{-6}$
PU-NaI-30PMII	$(1.81 \pm 0.30) \times 10^{-6}$

Table 6.2: Ionic conductivity value of PU-LiI-PMII

Sample	**Conductivity, σ (S cm^{-1})**
PU-30LiI	$(1.42 \pm 0.20) \times 10^{-6}$
PU-LiI-10PMII	$(8.15 \pm 0.13) \times 10^{-6}$
PU-LiI-20PMII	$(2.09 \pm 0.10) \times 10^{-5}$
PU-LiI-30PMII	$(1.71 \pm 0.20) \times 10^{-5}$

Measurement of temperature dependant ionic conductivity was carried out to analyze the mechanism of ionic conduction in the PU-salt-ionic liquid polymer electrolytes. Figure 6.5 shows the temperature dependence of PU-NaI-PMII systems in the range of 303 K to 353 K. The regression values for all plots are ~ 1 indicating that the points lie in almost straight line demonstrating that the ionic conduction mechanism is obeying the Arrhenius relationship. The E_a values were then calculated from the gradient and are listed in Table 6.3.

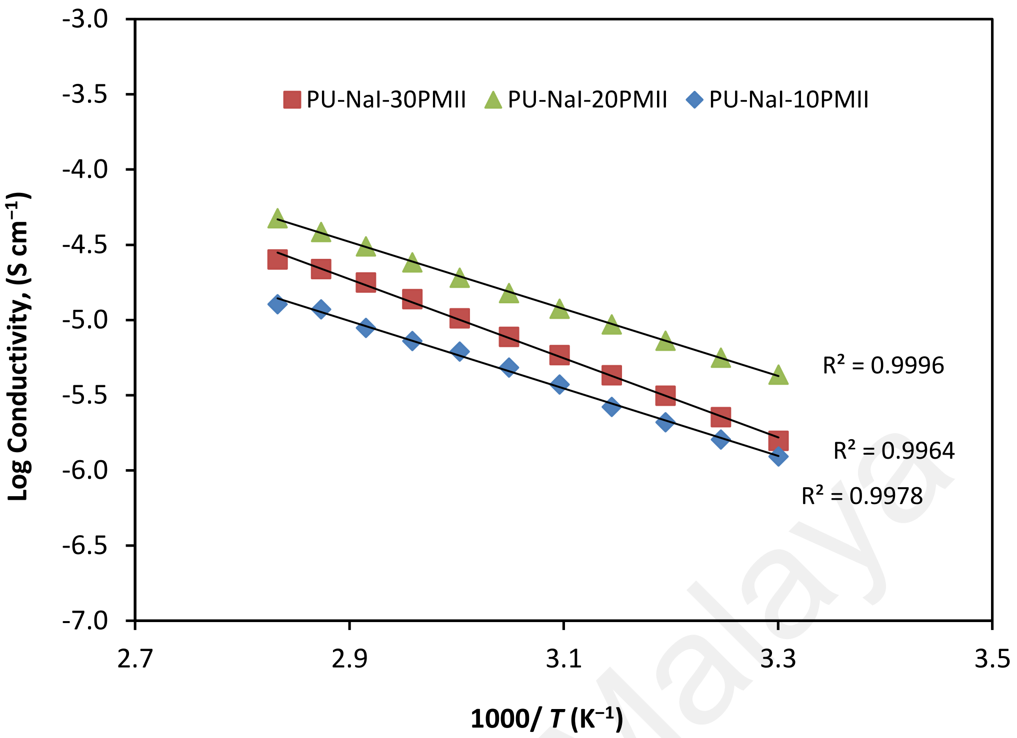

Figure 6.5: Arrhenius plots of ionic conductivity of PU-NaI-PMII polymer electrolytes

Table 6.3: Activation energy, E_a value of PU-NaI-PMII

Sample	**Activation energy, E_a (*e*V)**
PU-NaI-10PMII	0.52
PU-NaI-20PMII	0.44
PU-NaI-30PMII	0.45

For PU-LiI-PMII system, the plots of log conductivity versus $1000/T$ are not straight lines as illustrated in Figure 6.6 (a). The experimental conductivity data can be fitted into the Vogel-Tamman-Fulcher (VTF) behaviour and were plotted in Figure 6.6 (b). The VTF equation can be expressed as

$$\sigma = \sigma_o T^{1/2} exp\left(\frac{-E_a}{k_B(T-T_0}\right) \quad (5.4)$$

where σ is the conductivity, T is the absolute temperature, σ_o is a pre-exponential factor, k_B is Boltzmann constant, E_a is an activation energy and T_o is a reference temperature which is related to the equilibrium state of glass transition temperature. In this work, the measured glass transition temperature, T_g, was employed as the reference temperature, T_o for the fitting. E_a values of PU-LiI-PMII samples obtained by fitting conductivity data are summarized in Table 6.4.

E_a value for samples containing ionic liquid is lower than that E_a value of PU-salt systems. The addition of ionic liquid to the PU-NaI and PU-LiI enhanced the flexibility of polymer electrolytes as shown by the decreased value of T_g. This effect eases ions migration, thus give low E_a values.

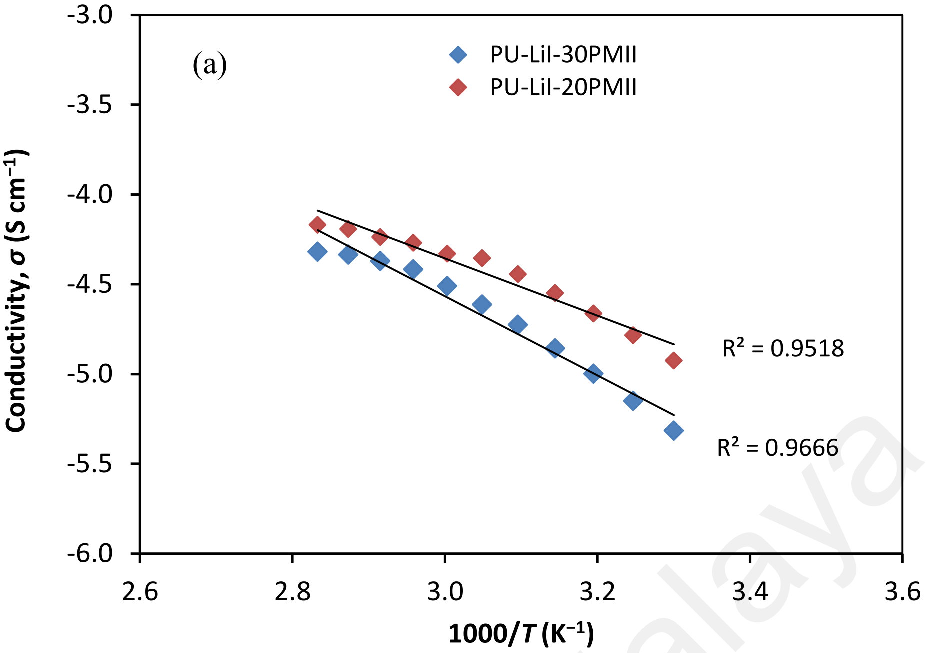

Figure 6.6 (a): Arrhenius plots of ionic conductivity of PU-LiI-20PMII and PU-LiI-30PMII polymer electrolyte films

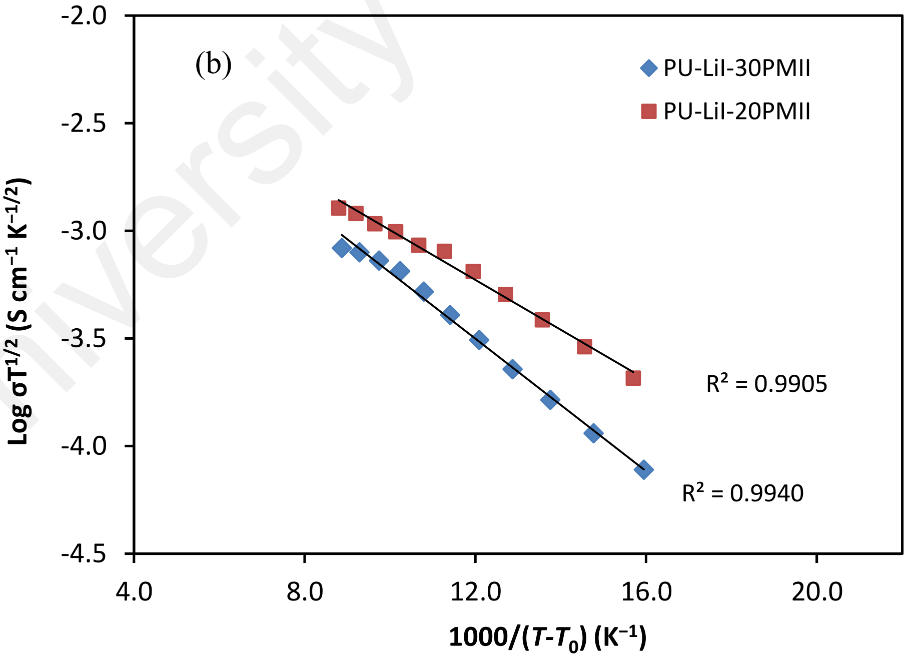

Figure 6.6 (b): VTF plots of ionic conductivity of PU-LiI-20PMII and PU-LiI-30PMII polymer electrolyte films

Table 6.4: Activation energy, E_a value of PU-LiI-PMII

Sample	**Activation energy, E_a (eV)**
PU-LiI-20PMII	0.02
PU-LiI-30PMII	0.03

6.5 Transference Number Measurement

6.5.1 Ionic Transference Number

The transference number of the highest conducting PU-salt-ionic liquid systems was evaluated using Wagner's polarization method. The direct current was recorded as a function of time upon application of a fixed DC voltage across the SS/PU polymer electrolytes/SS. After polarization, the graphs of normalized current versus time for PU-NaI-PMII and PU-LiI-PMII systems are plotted as illustrated in Figure 6.7 and Figure 6.8, respectively. The values of ionic transference numbers are 0.803 for PU-NaI-PMII and 0.854 for PU-LiI-PMII. This implies that the charge transport in PU-salt-ionic liquid polymer electrolyte films was predominantly due to ions since the values were more than 0.5. However the values obtained were smaller than that obtained from IL free systems. This due to the ionic liquid inclusion that provide electronic transport in polymer electrolyte, since the total transference number is $t = t_{\text{ion}} + t_{\text{ele}} = 1$. Österholm et al., (2011) reported their study using spectroelectrochemical characterization using in situ FTIR-ATR on the use of an IL in polymer. According to these researchers, the IL may alter not only the ion transport, but also the electronic transport and the structural changes occurring in the polymer-based films during electrochemical charging.

The values of ionic transference number of PU-salt-IL lowered compared to samples without ionic liquid contrary with the ionic conductivity value. This suggests that the increased of conductivity by incorporation of IL due to (1) contribution of electronic charge carrier and (2) improvement of polymer segmental motion and flexibility of polymer backbone and did not significantly increase the number of ionic charge carriers.

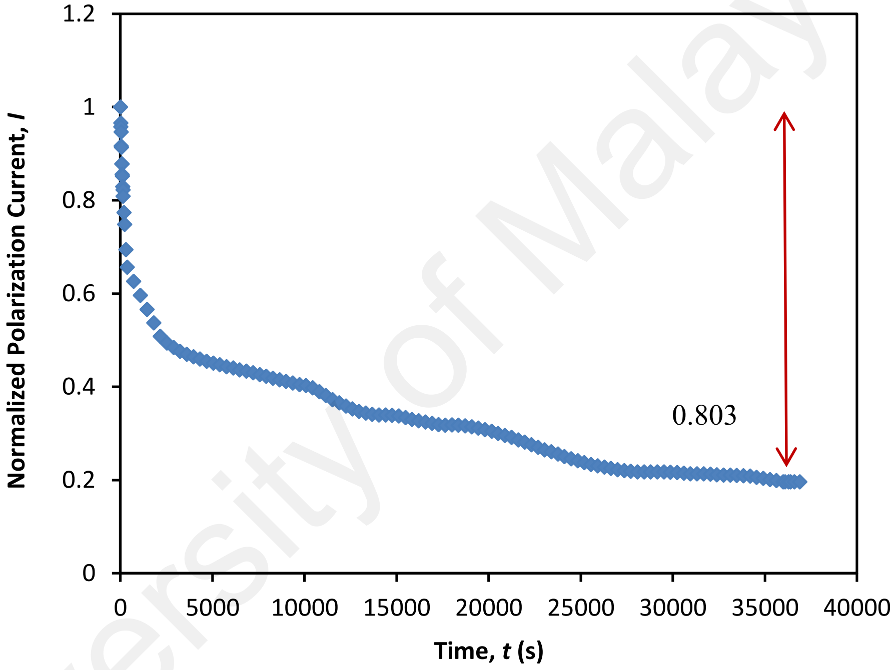

Figure 6.7: The plot of normalized polarization current versus time for PU-NaI-20PMII electrolyte

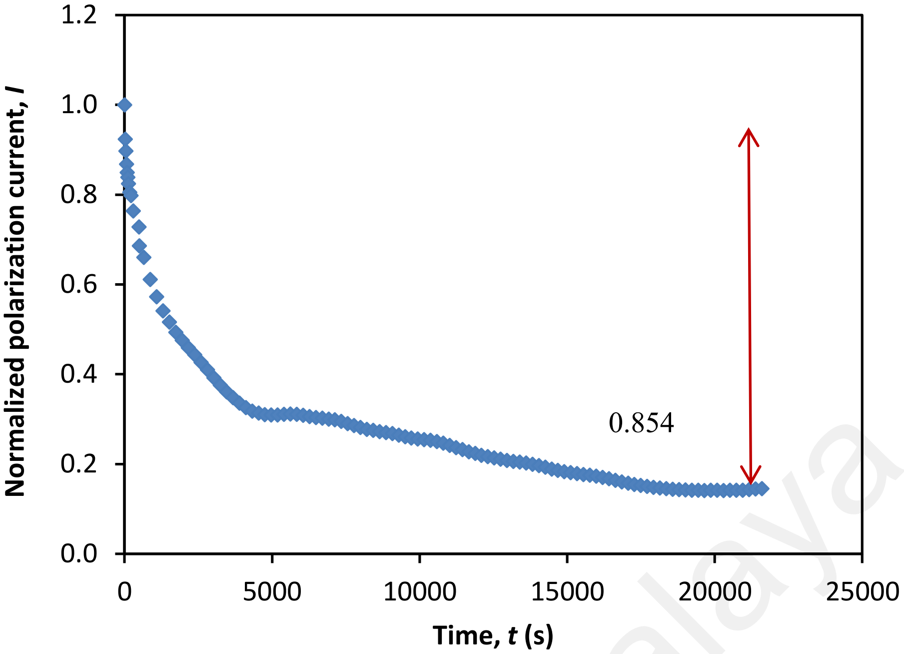

Figure 6.8: The plot of normalized polarization current versus time for PU-LiI-20PMII electrolyte

6.5.2 Cationic Transference Number

Presented in Figure 6.9 and Figure 6.10 are the plots of current versus time of the highest conducting PU-NaI-PMII and PU-LiI-PMII for sodium and lithium transference number measurement, respectively. The calculated cationic transference number using Brunce and Vincent method shows that PU-NaI-PMII has the value of t_{Na+} = 0.047, a lower value compared to that (0.180) for IL free PU-NaI. PU-LiI-PMII electrolyte has the value of cationic transference number of t_{Li+} = 0.043 decreased from 0.154 of IL free PU-LiI. This measurement confirmed the large anionic contribution to the ionic conduction in PU electrolytes.

The t_+ values are small for both systems containing IL suggesting that the cation from salt has strong interaction with PU as confirmed by shifting in wavenumbers of amine, carbonyl and ether groups in FTIR results. The cation may complexed by nucleophilic centers oxygen and nitrogen atoms in the polymer. Moreover, addition of PMII (PMI^+ and I^-) also decreased the fraction of Li^+ or Na^+ to I^- ions in the polymer. Li^+ or Na^+ ions are surrounded by a large number of I^- anions forming an ionic cluster. Other studies of cationic transference number of electrolytes containing IL also showed the small value of 0.03–0.11 range (Zygadło-Monikowska et al., 2014) and 0.07 (Menne et al., 2013). The common values of t_{Li+} for most state-of-the-art ILs are in the range of 0.02–0.04 (Niedzicki et al., 2014). The value obtained in this study is comparable with those reported in the literature. Some studies claimed that whether or not the cation is the dominant charge carrier in polymer electrolytes, the nature of polymer may also have some influence over this. From this measurement, the smaller cationic numbers give a larger value of anion and it is expected to be advantageous for the performance of DSSC.

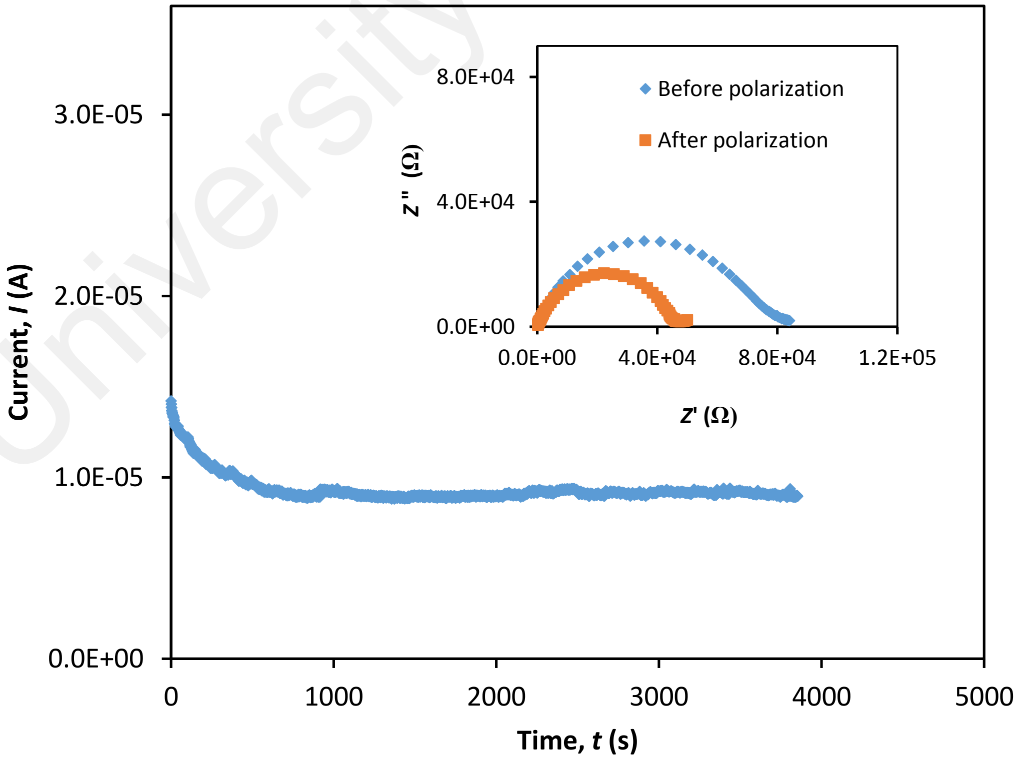

Figure 6.9: Time dependant response of DC polarization for PU-NaI-PMII electrolyte polarized with a potential 1.0 V. The inset graph shows the impedance spectra of PU-NaI-PMII electrolyte before and after polarization

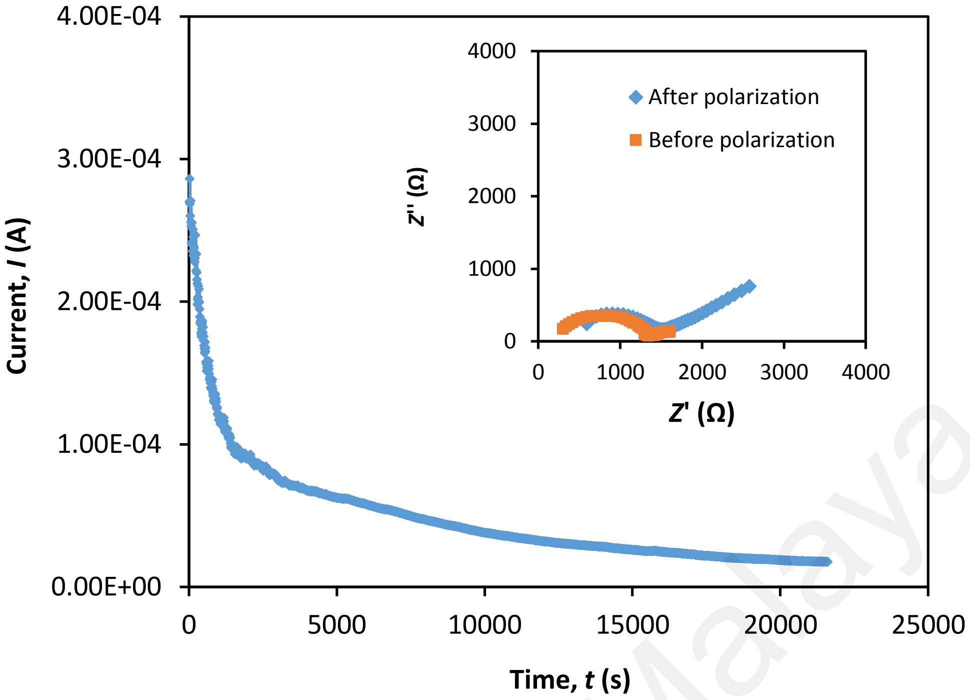

Figure 6.10: Time dependant response of DC polarization for PU-LiI-PMII electrolyte polarized with a potential 1.0 V. The inset graph shows the impedance spectra of PU-LiI-PMII electrolyte before and after polarization

6.6 Linear Sweep Voltammetry

Figure 6.11 shows linear sweep voltammogram of highest conducting sample of PU-NaI-PMII and PU-LiI-PMII polymer electrolyte films. Current increases gradually with the increase of voltage above 1.9 V for PU-NaI-PMII and 2.2 V for PU-LiI-PMII. These voltages are the decomposition voltages of the polymer electrolytes. This demonstrates that the electrochemical stability window for the PU-NaI-PMII and PU-LiI-PMII systems are up to 1.9 V and 2.2 V respectively. This observation reveals that the ionic liquid doping improved the electrochemical stability window of the PU-LiI-PMII by 0.2 V. However, the electrochemical stability window for PU-NaI-PMII remains the same as that of PU-NaI without IL. The electrochemical stability windows are wide enough for application in photoelectrochemical.

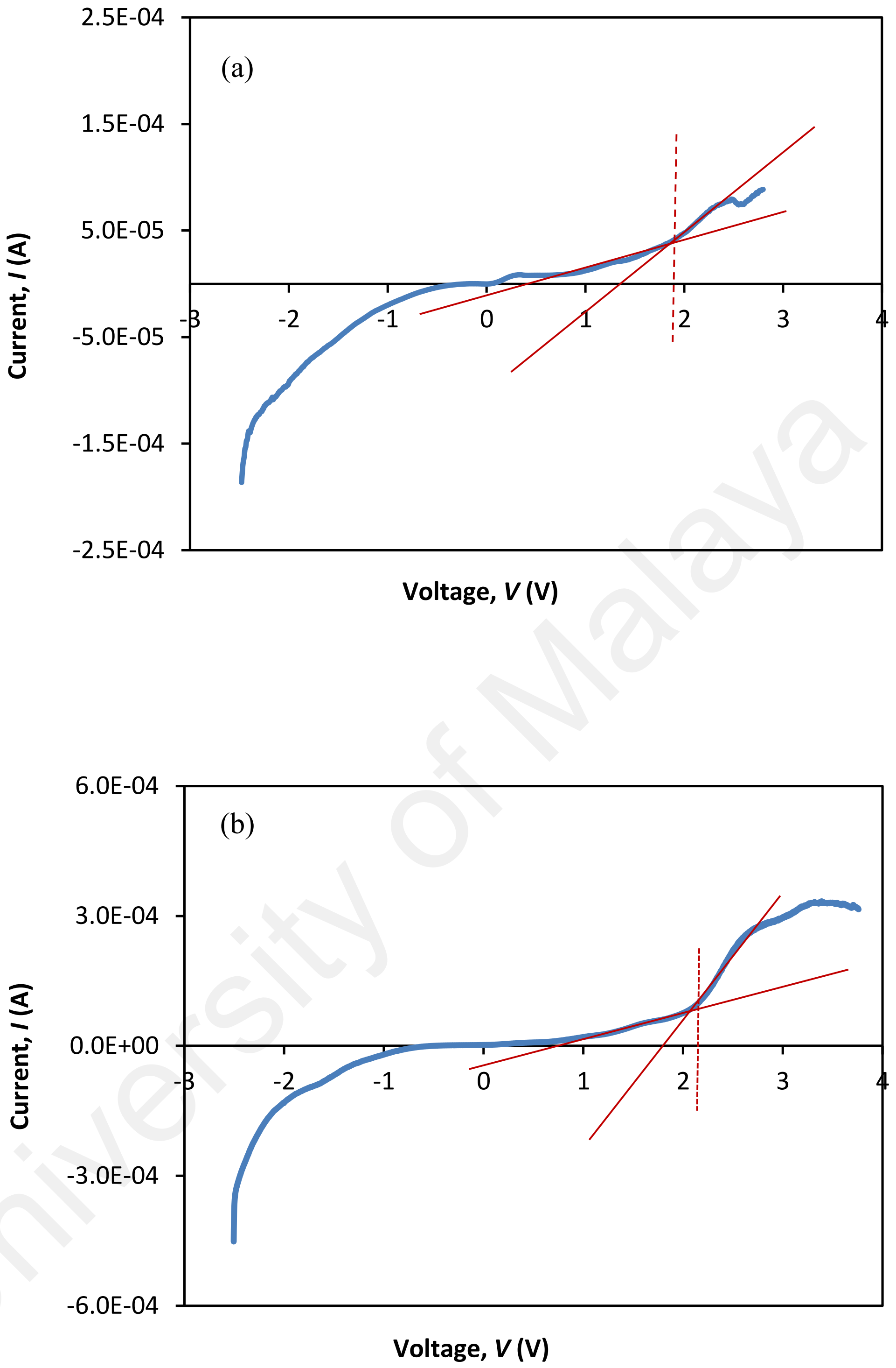

Figure 6.11: Linear sweep voltammogram of (a) PU-NaI-20PMII and (b) PU-LiI-20PMII polymer electrolytes using stainless steel as WE, RE, CE electrodes with a scan rate of 0.5 mV s^{-1}

6.7 Summary

The shifted of wavenumber and changes in intensity of amine, carbonyl and ether bands in FTIR spectra show the occurrences of interaction between PU, salt and PMII ionic liquid. Inclusion of PMII to PU-NaI and PU-LiI increased the ionic conductivity of the polymer electrolytes by an order of magnitude. The highest PU-NaI conducting sample showed a conductivity of 4.28×10^{-7} S cm^{-1} increased to 2.65×10^{-6} S cm^{-1} upon addition of 20 wt % PMII. The ionic conductivity of 1.41×10^{-6} S cm^{-1} of PU-LiI increased to 2.09×10^{-5} S cm^{-1} with 20 wt % PMII. Ionic liquid acted as plasticizer to soften the polymer backbone, therefore increase the polymer segmental motion as indicated by lowered T_g value of PU-NaI of –26.2 °C to ~ –31.0 °C and PU-LiI of –27.3 °C to ~ –33.0 °C. Temperature dependent conductivity of PU-NaI-PMII followed the Arrhenius behaviour, whereas for PU-LiI-PMII followed the VTF behaviour. Small value of cationic transference number in PU-salt-IL suggested that the anions are major contributors to the ionic conduction and this is desired for application in DSSC. Electrochemical stability window of PU-NaI-PMII was 1.9 V and which was the same as that of IL free PU-NaI. However, electrochemical stability window of PU-LiI-PMII is wider compared to the IL free PU-LiI.

CHAPTER 7: DYE-SENSITIZED SOLAR CELLS PERFORMANCE

7.1 Introduction

Polyurethane based polymer electrolytes added with iodine were employed for fabrication of DSSCs. The photocurrent density-voltage (*J–V*) characteristics of the DSSCs were measured at AM 1.5G illumination (100 mW cm^{-2}). The cell configuration was FTO | TiO_2/dye | PU electrolytes-I_2 | Pt | FTO. Electrochemical impedance analysis was also done to study the electronic and ionic transport processes in the DSSCs.

7.2 DSSC Performance

7.2.1 PU-NaI polymer electrolytes based DSSCs

The photocurrent density-voltage curves for the DSSCs employing the PU-NaI polymer electrolytes are shown in Figure 7.1. The values of the V_{oc}, J_{sc}, *FF* and η obtained from these curves are summarized in Table 7.1. It is observed that the J_{sc} increases with the increase of NaI up to 30 wt % and decreases with addition of more salt. This observation is consistent with the trend of ionic conductivity of the electrolytes (De Freitas et al., 2009). The DSSC employing PU-30NaI shows the highest current density of 3.60 mA cm^{-2} hence gives the best efficiency performance of 0.80 %.

The efficiency of DSSC fabricated using PU-10NaI is significantly lower than that of the DSSC containing PU-30NaI mostly due to difference of current density and ionic conductivity (Lee et al., 2011). Higher value of J_{sc} in PU-30 NaI originates from its higher value of ionic conductivity compared to PU-10NaI and PU-40NaI due to iodide ion concentration. Lower resistance for ion migration increases the supply of I_3^- to the Pt counter electrode and also increase the kinetic of dye generation and therefore increasing the J_{sc} (Choi & Kim, 2011). The value of V_{oc} is slightly higher for PU-30NaI. Higher V_{oc} is related to the reduction of charge recombination on the TiO_2 and electrolyte interface (Choi & Kim, 2011). Therefore, the slightly higher value of 0.49 V of V_{oc} in PU-30NaI compared to that of 0.44 V for PU-10NaI and PU-40NaI may be due to reduced recombination electron with I_3^- in the electrolytes resulting in an increase of V_{oc}.

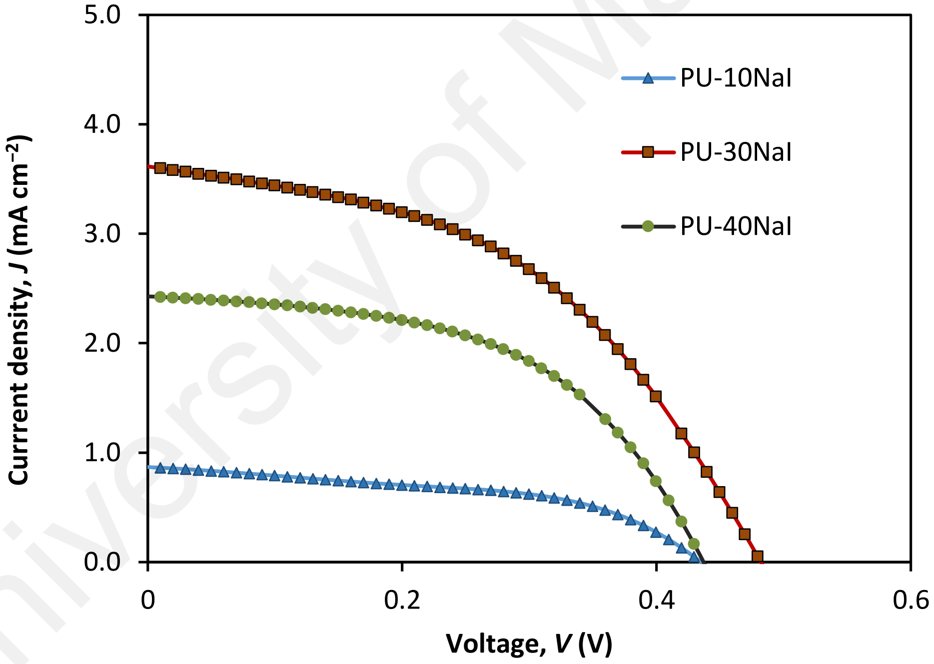

Figure 7.1: *J–V* curves of DSSCs using PU-10NaI, PU-20NaI and PU-30NaI polymer electrolytes under irradiation of 100 mW cm^{-2}

Table 7.1: *J–V* parameters of DSSCs fabricated using PU-NaI polymer electrolytes

Sample	Short circuit current density, J_{sc} (mA cm^{-2})	Open circuit voltage, V_{oc} (V)	Fill factor, *FF*	Efficiency, η (%)
PU-10NaI (+I$_2$)	0.86	0.44	0.49	0.19
PU-30NaI (+I$_2$)	3.60	0.49	0.46	0.80
PU-40NaI (+I$_2$)	2.40	0.44	0.52	0.55

7.2.2 PU-LiI polymer electrolytes based DSSCs

Figure 7.2 illustrates the photocurrent density-voltage plot of DSSCs employing PU-LiI polymer electrolytes containing 20 and 30 wt % LiI. Meanwhile, Table 7.2 lists the photovoltaic parameters for DSSCs based PU-LiI polymer electrolytes. The highest efficiency of 0.83 % was obtained from photocurrent density-voltage measurement containing PU-30LiI. The efficiency of the DSSC containing 30 wt % LiI is higher compared to that containing 20 wt % LiI. This is due to higher current density and ionic conductivity of the sample as observed in PU-NaI systems.

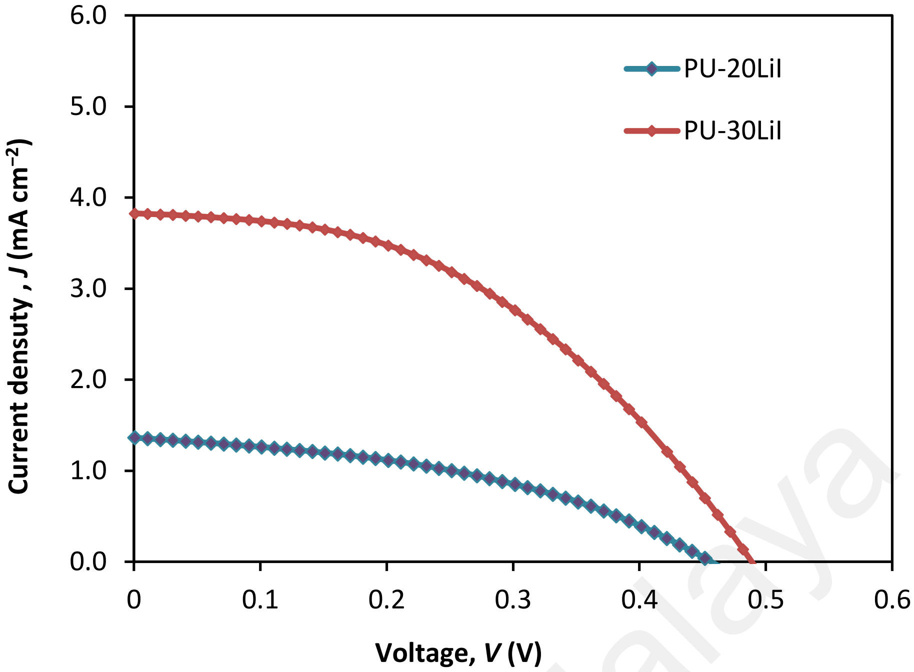

Figure 7.2: *J–V* curves of DSSCs using PU-20LiI and PU-30LiI polymer electrolytes under irradiation of 100 mW cm^{-2}

Table 7.2: *J–V* parameters of DSSCs with PU-LiI polymer electrolytes

Sample	Short circuit current density, J_{sc} (mA cm^{-2})	Open circuit voltage, V_{oc} (V)	Fill factor, *FF*	Efficiency, η (%)
PU-20LiI (+I_2)	1.36	0.46	0.41	0.26
PU-30LiI (+I_2)	3.83	0.49	0.44	0.83

The efficiency obtained in this work is comparatively higher than those reported for DSSCs developed using PU-LiI and chitosan-NaI bio polymer based electrolytes, which showed η of 0.003 % and 0.13 % respectively (Singh et al., 2010; Su'ait et al., 2014a). The higher efficiency obtained in this work may also be attributed to better adhesive property of castor oil-polyol based PU electrolytes to the working and counter electrodes of DSSC.

7.2.3 PU-salt-ionic liquid based DSSCs

Depicted in Figure 7.3 is the plots of photocurrent density-voltage of DSSCs employing the highest conducting sample of PU-NaI-PMII (PU-NaI-20PMII) and PU-LiI-PMII (PU-LiI-20PMII) systems. The measured parameters of the V_{oc}, J_{sc}, FF and η are listed in Table 7.3. The short circuit current density, open circuit voltage and efficiency of PU-salt-IL based DSSC is higher compared to that of IL free PU-LiI and PU-NaI. The improved efficiency is mainly attributed to the enhancement of J_{sc} and this can be explained by the higher conductivity of PU-salt-IL in comparison with PU-salt electrolytes. In addition, ionic liquid exhibits plasticizing effect promoting better contact of the electrolytes with the working electrode and counter electrode. Moreover, higher ionic conductivity and better contact resulting in an increase of the V_{oc} due to reduction of charge recombination on the TiO_2 and electrolyte interface (Choi and Kim, 2011). Some of injected electrons in TiO_2 recombined with I^{3-} in the electrolytes. However, diffusion of I_3^- was slower in polymer electrolytes compared to that in liquid electrolytes, the recombination reaction was depressed leading to increased V_{oc}.

Increase of J_{sc} with addition of PMII to PU-salt could also be explained in terms of the increasing iodide ion (or iodide ion transference number) as confirm in cationic transference number measurement for PU-salt-PMII electrolytes. Another reason is the intercalation of cation (Li^+ or Na^+) into TiO_2 electrode. Cation can intercalate into the TiO_2 layer and reduced the movement of electrons through the nano-porous TiO_2 layer in the working electrode. This caused positive shifting in the conduction band thus increasing the charge injection rate which in turns increases the J_{sc} (Dissanayake et al., 2014; Ng et al., 2015).

The highest overall conversion efficiency obtained in this work is comparable to the synthetic polymer based DSSCs reported by Lee and co-workers (2009) who obtained η = 2.05 % for DSSC fabricated using (PEO:PEG) + LiI/I_2, higher than that of PEO + KI/I_2 + EMImTFSI (η = 1.75 %) (Singh et al., 2008) and PVDF-HFP + NaI + EC/PC (η = 1.85 %) (Noor et al., 2014). The value is also higher than that reported by other researchers using biopolymer electrolytes based DSSCs (*k*-carrageenan + NaI + EC, η = 1.80 %) (Bella et al., 2015) and (Chitosan + NaI + EMImSCN, η = 0.73 %) (Singh et al., 2010).

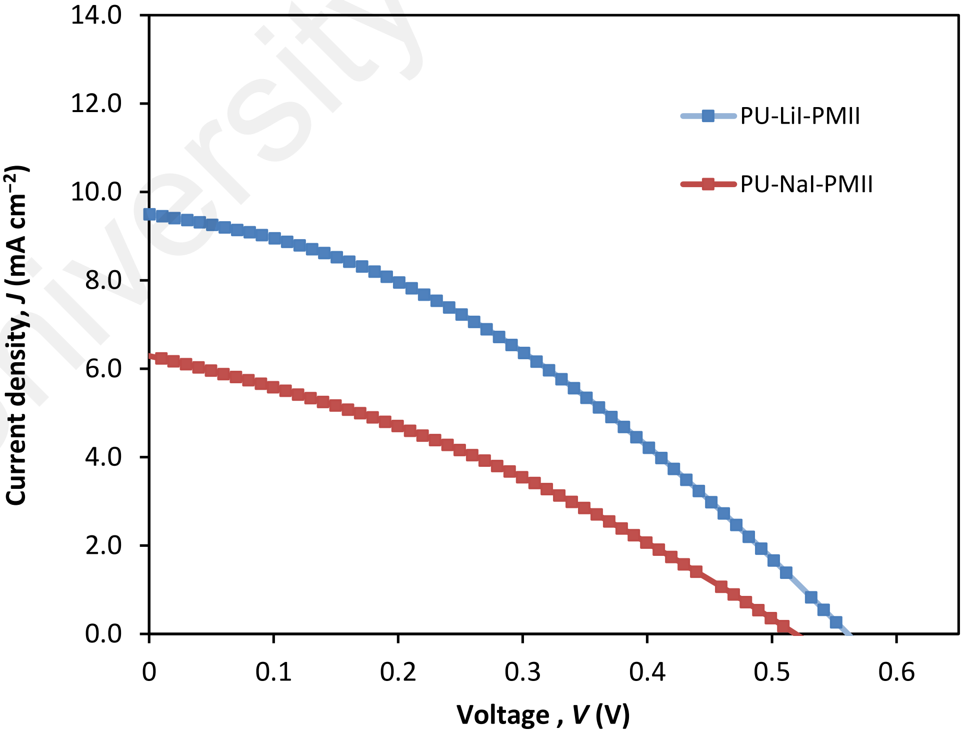

Figure 7.3: *J–V* curves of DSSC using PU-NaI-20PMII and PU-LiI-20PMII polymer electrolytes under irradiation of 100 mW cm^{-2}

Table 7.3: Characteristics of PU-salt-PMII based DSSCs

Electrolyte	**Short circuit current density, J_{sc} (mA cm^{-2})**	**Open circuit voltage, V_{oc} (V)**	**Fill factor, *FF***	**Efficiency, η (%)**
PU-NaI-20PMII (+I_2)	6.23	0.52	0.33	1.06
PU-LiI-20PMII (+I_2)	9.49	0.56	0.36	1.92

7.3 Electrochemical Impedance Spectroscopic Analysis of DSSC

To understand the electronic and ionic transport processes in the DSSCs, EIS was employed (Ahn et al., 2011; Hong et al., 2012). The impedances of the highest efficiency DSSC containing PU-salt with/without IL were measured and the Nyquist plots are depicted in Figure 7.4 and Figure 7.5. The equivalent circuit for DSSC containing PU polymer electrolytes is shown in Figure 7.6. This simple Resistor-Capacitor (RC) circuit is usually used to describe the electrochemical process in DSSCs with liquid, polymer and ionic liquids (Wang et al., 2005a; Cui et al., 2013).

The Nyquist plots of the DSSCs show three semicircles in the measured frequency range. This suggests there are at least four impedance elements in the DSSCs. From the Nyquist plots, the first and second semicircles in the high and middle frequency regions are attributed to the impedances related to charge-transfer processes occurring at the Pt counter electrode (R_{ct1}) and at the TiO_2-dye/electrolyte interface (R_{ct2}) (Wu et al., 2013). The third semicircles, in the low frequency region, referred to Warburg diffusion impedance (R_w) showing the Nernstian diffusion of I^-/I_3^- within the electrolytes. R_s is the resistance element in the high frequency range > 10^6 Hz due to the sheet resistance of transparent conductive oxide glass and electrical contacts. Similar equivalent circuit was reported by (Cui et al., 2013) in their study on DSSC containing poly(ethylene oxide/polyvinylidene fluoride-hexafluoropropylene) composite polymer electrolytes along with KI/I_2.

Higher performance of the DSSC can be achieved if the total impedance in the cell is small. In this work the value of R_{ct2} and R_w for PU-LiI and PU-NaI are big and gave main contribution to the impedance in the cells thus affects the overall performance of the DSSC. With the addition of IL, the values of R_{ct2} and R_w are comparatively low resulted in enhanced efficiency. The higher value of R_{ct2} represents the suppression of the charge recombination at the TiO_2/electrolyte interfaces in PU-salt higher compared to PU-salt-IL.

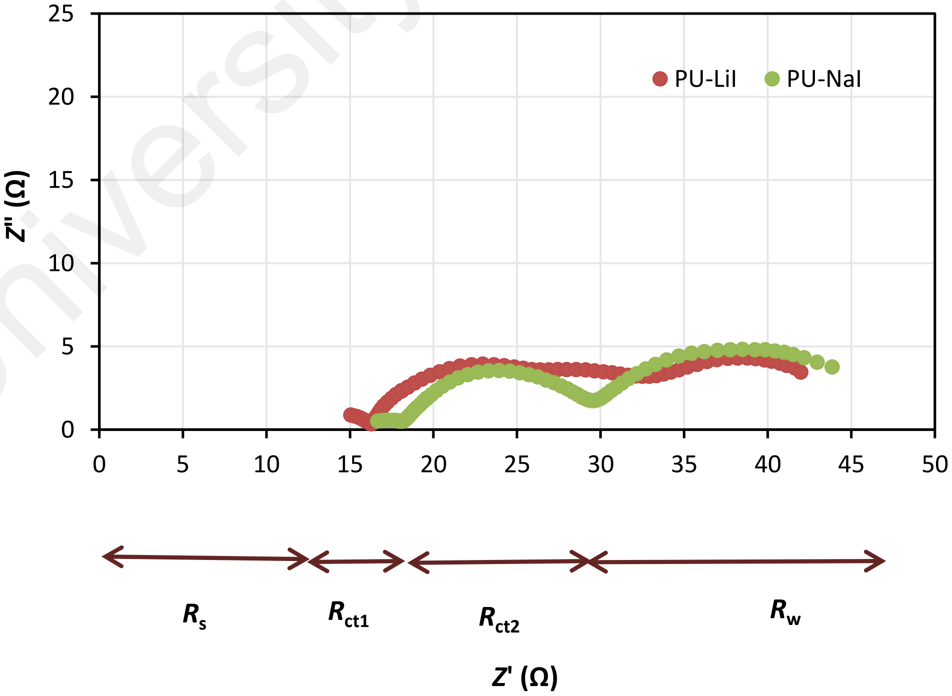

Figure 7.4: Electrochemical impedance spectrum of DSSCs with PU-30NaI and PU-30LiI electrolytes measured at 100 mW cm^{-2} light intensity

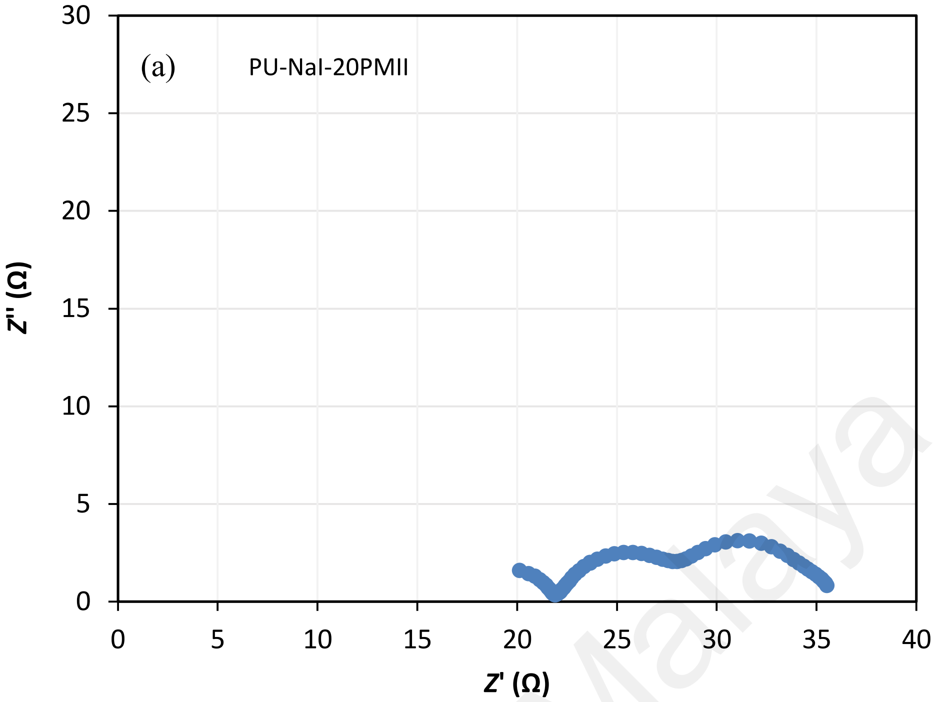

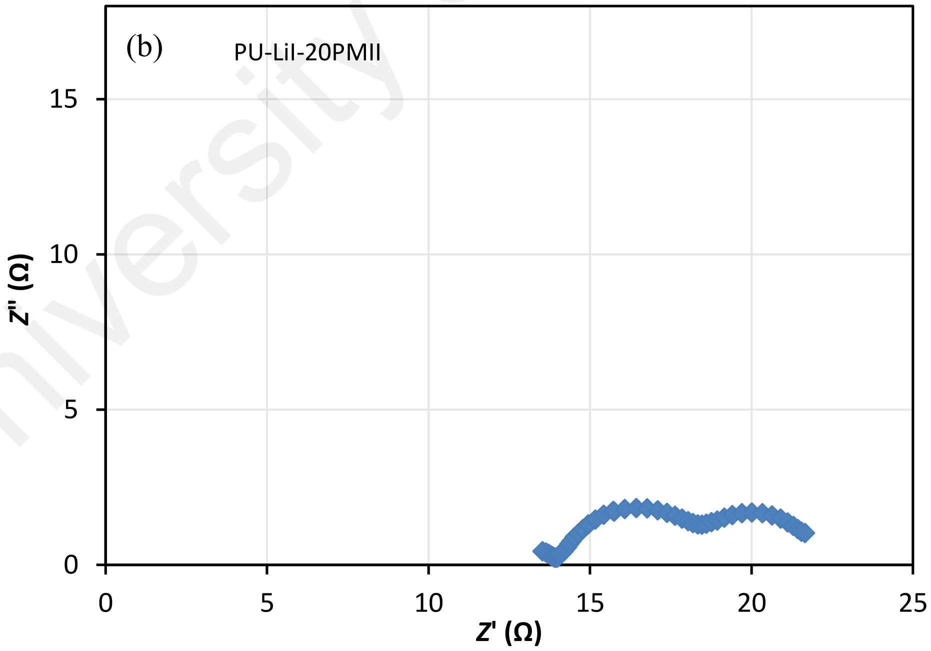

Figure 7.5: Electrochemical impedance spectrum of DSSCs with (a) PU-NaI-20PMII and (b) PU-LiI-20PMII electrolytes measured at 100 mW cm^{-2} light intensity

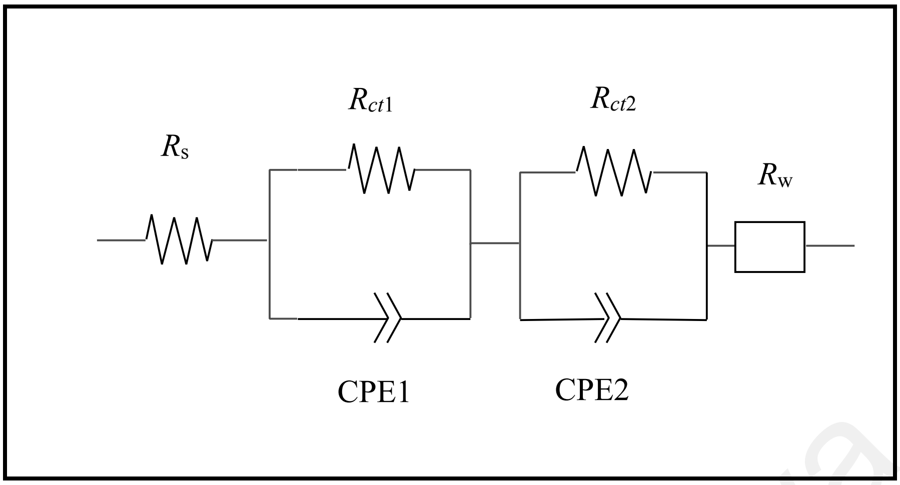

Figure 7.6: Equivalent circuit model for DSSC employing PU electrolytes

As shown in Figure 7.5 there are a decrease in the charge-transfer resistance and Warburg diffusion resistance upon addition of IL. This due to the increase of the number of injected electrons into the TiO_2 film, improves the electrical conductivity and reduces the charge recombination rate of electrons with I_3^- or the oxidized dye at the TiO_2-dye/electrolyte interfaces. It is also indicates fast electron-transfer processes in the DSSCs. These lead to a high photocurrent density and conversion efficiency (Yang et al., 2014).

7.4 Summary

DSSCs were successfully fabricated employing PU-NaI, PU-LiI, PU-NaI-PMII and PU-LiI-PMII electrolytes. The conductivity of samples influenced the performance of photovoltaic parameters. For PU-salt systems, PU-30NaI and PU-30LiI were the highest efficiency in PU-NaI and PU-LiI systems, respectively and follow the same trend as that of ionic conductivity value. The improved in efficiency mostly results from the increase in J_{sc}. The enhancement in efficiency observed for PU-salt-PMII was also attributed to the increased ionic conductivity and good retention of PMII ionic liquid. Incorporation of IL further increased the conductivity of PU-salt as well as the J_{sc} and V_{oc} due to the enhancement of transport kinetic of I^{-}/I_3^{-} redox couple that led to the enhancement of efficiency. This was also attributable to the IL that gave plasticizing effect and improved contact between electrolytes and working and counter electrodes.

CHAPTER 8: CONCLUSIONS AND SUGGESTIONS FOR FURTHER WORK

8.1 Conclusions

In this study, all the objectives set for this project have been achieved. An alternative biopolymer electrolytes based on castor oil for application in DSSC was successfully prepared and characterized.

At the first stage, castor oil based polyol (*CO-p*) was synthesized via transesterification reaction. The polyol has an acid value of 3.0 mg KOH g^{-1} and OH number of 190 mg KOH g^{-1}. These characteristics are suitable for producing flexible PU. The polyol was adapted for the preparation of polyurethane with addition of MDI isocyanate in the ratio of 20:80 (NCO:OH). The formation of PU was confirmed using FTIR analysis by the disappearance of NCO peak and appearance of amine (secondary), carbonyl and ether group in PU chain. The film prepared using the synthesized PU demonstrated highly amorphous, low T_g value of –15.8 °C and was free standing as well as good thermal stability, up to 259 °C. These results indicated that the castor oil based polyurethane possessed favourable properties for application as host in polymer electrolytes.

In the second stage, *CO-p* polyurethane based polymer electrolytes was successfully prepared using solution casting technique with addition of sodium and lithium iodide in different wt %, from 10 to 40 wt % to form PU-NaI and PU-LiI systems, respectively. All samples formed free-standing films. PMII ionic liquid with 10 to 30 wt % was added to the highest conducting sample for each system to enhance the ionic conductivity. Addition of ionic liquid of more than that formed inhomogeneous solution and did not form films. The electrolytes were characterized using FTIR, DMA, EIS, transference number measurement and linear sweep voltammetry. FTIR results confirmed the interaction between polymer-salts in PU-NaI and PU-LiI systems, and polymer-salt-ionic liquid in PU-NaI-PMII and PU-LiI-PMII systems by shifting of bands of amine, carbonyl and ether group of the polymer. The inclusion of IL to PU-salt also influences the performance of DSSC by increased the value of J_{sc}, V_{oc} and η.

Conductivity of PU-salt increased with salt concentration, reaching a maximum value at 30 wt %. The addition of more than 30 wt% decreased the ionic conductivity value. The conductivity increased due to the increased in charge carriers or mobile ions. The increase in conductivity is also consistent with the lower T_g value upon addition of salt up to 30 wt % and increased thereafter. The lower T_g increased the flexibility of polymer backbone that leads to a higher segmental motion assists ion transportation. At a high salt concentration, the distance between dissociated ions became too close to each other enabling them to recombine into neutral ion-pairs and do not contribute to conductivity. This is also due to the increase of rigidity of polymer electrolytes due to the increase of T_g value. The conductivity was higher by an order of magnitude for a system containing LiI compared to that system containing NaI. This might be due to the size of cations. The cation size of Li^+ and Na^+ are 0.76 and 1.02 Å, respectively. The smaller the cation, the higher the mobility of the cation, thus increased the ionic conductivity. However, it is known that in the polymer electrolytes, the major contribution in ionic conductivity came from anions as confirmed by the cationic transference number measurement.

Glass transition temperature, T_g of synthesized PU was -15.8 °C decreased to lower value with the addition of salt and salt-IL. PU with 30 wt % NaI was the highest conducting sample (σ of 4.28×10^{-7} S cm^{-1}) in PU-NaI system, possessed the lowest T_g

of –26.2 °C, whereas the highest conducting PU with 30 wt% LiI with σ of 1.41×10^{-6} S cm^{-1} possessed T_g of –27.3 °C. Addition of ionic liquid to the PU-NaI and PU-LiI further decreased the T_g value and enhanced the ionic conductivity by an order of magnitude. The highest conducting PU-NaI-PMII was $(2.65 \pm 0.77) \times 10^{-6}$ S cm^{-1} with 20 wt % PMII and the highest PU-LiI-PMII was $(2.09 \pm 0.10) \times 10^{-5}$ S cm^{-1} also with addition of 20 wt % PMII. The systems had T_g of –31.0 °C and –33.0 °C respectively. Ionic liquid acted as plasticizer to soften the polymer backbone, therefore increased the polymer segmental motion to ease ions migration, hence improved the ionic conductivity. However, addition of 30 wt % PMII was found to decrease the ionic conductivity. This may be due to the increased viscosity of polymer electrolytes thus slower the mobility of ions.

Temperature also influenced the conductivity of polymer electrolytes. As temperature increases, the polymer chains acquire faster internal modes in which bond rotations produce segmental motion, facilitate hopping inter-chain and intra-chain ion movements, thus increase the conductivity of the polymer electrolyte. Activation energy of ion migration in PU polymer electrolytes was calculated from the gradient of Arrhenius and Vogel-Tamman-Fulcher plots. PU-NaI, PU-LiI, PU-NaI-PMII systems followed the Arrhenius behaviour, whereas PU-LiI-PMII systems followed the VTF behaviour. The trend of conductivity contradicted the trend of E_a, which the higher conducting sample possessed lower activation energy.

Transference number measurement show that the charge transport in all PU electrolyte films was predominantly due to ions since the values of ionic transference number were ~ 1. The transference number of PU-salt of ~ 0.99 decreased to ~ 0.80 upon addition of PMII though the ionic conductivity value was increased. This suggested that the ionic conductivity increased due to segmental motion and flexibility of polymer backbones and did not significantly increase the number of charge carrier hopping and ion migrations. This is also suggested the existence of electronic charge carrier in the PU-salt-IL systems. From cationic transference number measurement, the value of Na^+ for PU-NaI was 0.180 while Li^+ for PU-LiI was 0.154. The values were further decreased to 0.047 and 0.043 upon addition of IL to PU-NaI and PU-LiI, respectively. All the PU electrolyte samples showed the small value of cationic transference number suggesting that the majority of the ionic conductance largely due to anions.

The electrochemical stability windows of PU-NaI was up to 1.9 V and remained the same with addition of PMII while for PU-LiI was 2.0 V increased to 2.2 V upon addition of the same IL. These values are due to the decomposition voltage of PU polymer electrolytes. These values were wide enough for application in DSSCs since their operating potential needed is between ~ –1.0 to 1.0 V.

The third stage in this work was the application of PU electrolytes to DSSC. DSSCs employing PU electrolytes were successfully assembled with configuration of FTO/TiO_2-dye/PU electrolytes-I_2/Pt/FTO and their photocurrent-voltage under illumination of AM 1.5G (100 mW cm^{-2}) was measured. The highest efficiency for DSSCs employing PU-NaI and PU-LiI systems were 0.80 % and 0.83 %, respectively. DSSC employing PU-LiI showed better photovoltaic parameter compared to PU-NaI consistent with the ionic conductivity value. Addition of IL further improved the photovoltaic parameter with efficiency of 1.06 % for PU-NaI-PMII and 1.92 % for PU-LiI-PMII. These results showed that the function of IL was not only improved the ionic conductivity but also energy conversion efficiency of DSSCs as well. However, polymer itself also play a significant role to the photoelectrical performance of the

DSSCs. This due to adhesive property of castor oil based polyurethane that give a good contact to the working and counter electrodes of DSSC.

EIS analysis of DSSCs demonstrated that the charge transfer resistance at the TiO_2/electrolytes and Pt/electrolytes interfaces was reduced upon addition of IL. This may be due to a higher ionic mobility of I^-/I_3^- species in PU-salt containing IL compared to that PU-salt systems. Charge transfer resistance of DSSCs also exhibited a decreasing trend upon addition of IL indicating an increase in the number of injected electrons into the TiO_2 film. It also indicated an improvement of electrical conductivity and reduction of charge recombination rate of electrons with I_3^- or the oxidized dye at the TiO_2-dye/electrolyte interfaces that leading to the increase of efficiency.

The performances of DSSCs employing castor oil polyurethane were comparable to synthetic polymer based DSSCs. The performance of the cells is believed to be improvable by improving the properties of the electrolyte with some modifications. The results of this work revealed that the new bio polymer electrolyte of castor oil based polyurethane has potential for application in DSSCs.

8.2 Suggestions for further work

As mentioned earlier, the castor oil based polymer electrolytes studied in this work have potential for application in dye-sensitized solar cell. However, further work should be done to enhance the overall conversion efficiency of the DSSC. Some suggestions that could be considered for this purpose are as follows:

a) Prepare the electrolytes in gel or quasi-solid state. In the gel form, the electrolytes may achieve conductivity value up to 10^{-2} S cm^{-1}. This will increase the overall performance of DSSC.

b) Add additives such as 4-*tert* butylpyridine (TBP) and *N*-methylbenzimidazole (NMBI) to boost the performance of DSSC (Stergiopoulos et al., 2011; Katz et al., 2014).

c) Use compact layer of TiO_2 between photoanode and FTO which is suitable to improve the performance by reducing the number of reaction sites for the recombination of triiodide with electrons on the bare FTO.

d) Study the durability of the bio-polymer electrolytes based DSSC by analysing the cycle life of the DSSCs at different temperature and times.

e) Using other types of low cost counter electrodes especially platinum free compound such as graphene and polystyrenesulfonate doped poly(3,4-ethylenedioxythiophene) (graphene/PEDOT-PSS) (Hong et al., 2008), copper zinc tin sulfide (CZTS) semiconductor thin film, (Fan et al., 2015), transition metal tellurides, CoTe and $NiTe_2$ (Guo et al., 2013) and ternary metal sulfide ($CoNi_2S_4$) nanostructure (Shi et al., 2015).

REFERENCES

Ahn, S. H., Jeon, H., Son, K. J., Ahn, H., Koh, W.-G., Ryu, D. Y., & Kim, J. H. (2011). Efficiency improvement of dye-sensitized solar cells using graft copolymer-templated mesoporous TiO_2 films as an interfacial layer. *Journal of Materials Chemistry, 21*(6), 1772-1779.

Alfani, R., Iannace, S., & Nicolais, L. (1998). Synthesis and characterization of starch-based polyurethane foams. *Journal of Applied Polymer Science, 68*(5), 739-745.

Alias, S. S., & Mohamad, A. A. (2013). Effect of NH_4I and I_2 concentration on agar gel polymer electrolyte properties for a dye-sensitized solar cell. *Ionics, 19*(8), 1185-1194.

Armand, M., Chabagno, J., & Duclot, M. (1979). Polyethers as solid electrolytes. *Fast Ion Transport in Solids*, 131-136.

Badri, K., Othman, Z., & Ahmad, S. (2004). Rigid polyurethane foams from oil palm resources. *Journal of Materials Science, 39*(16), 5541-5542.

Badri, K. H. (2012). Biobased Polyurethane from Palm Kernel Oil-Based Polyol: InTech Publication: New York.

Bandara, T., Dissanayake, M., Jayasundara, W., Albinsson, I., & Mellander, B.-E. (2012). Efficiency enhancement in dye sensitized solar cells using gel polymer electrolytes based on a tetrahexylammonium iodide and MgI 2 binary iodide system. *Physical Chemistry Chemical Physics, 14*(24), 8620-8627.

Bandyopadhyay, S., Marzke, R., Singh, R., & Newman, N. (2010). Electrical conductivities and Li ion concentration-dependent diffusivities, in polyurethane polymers doped with lithium trifluoromethanesulfonimide (LiTFSI) or lithium perchlorate (LiClO 4). *Solid State Ionics, 181*(39), 1727-1731.

Basak, P., & V Manorama, S. (2004). Poly (ethylene oxide)–polyurethane/poly (acrylonitrile) semi-interpenetrating polymer networks for solid polymer electrolytes: vibrational spectroscopic studies in support of electrical behavior. *European polymer journal, 40*(6), 1155-1162.

Baskaran, R., Selvasekarapandian, S., Kuwata, N., Kawamura, J., & Hattori, T. (2006). Conductivity and thermal studies of blend polymer electrolytes based on PVAc–PMMA. *Solid State Ionics, 177*(26), 2679-2682.

Bella, F., Imperiyka, M., & Ahmad, A. (2014). Photochemically produced quasi-linear copolymers for stable and efficient electrolytes in dye-sensitized solar cells. *Journal of Photochemistry and Photobiology A: Chemistry, 289*, 73-80.

Bella, F., Mobarak, N. N., Jumaah, F. N., & Ahmad, A. (2015). From seaweeds to biopolymeric electrolytes for third generation solar cells: An intriguing approach. *Electrochimica Acta, 151*, 306-311.

Bella, F., Nair, J. R., & Gerbaldi, C. (2013). Towards green, efficient and durable quasi-solid dye-sensitized solar cells integrated with a cellulose-based gel-polymer electrolyte optimized by a chemometric DoE approach. *RSC Advances, 3*(36), 15993-16001.

Benedetti, J. E., Goncalves, A. D., Formiga, A. L., De Paoli, M.-A., Li, X., Durrant, J. R., & Nogueira, A. F. (2010). A polymer gel electrolyte composed of a poly (ethylene oxide) copolymer and the influence of its composition on the dynamics and performance of dye-sensitized solar cells. *Journal of Power Sources, 195*(4), 1246-1255.

Bergeron, B. V., Marton, A., Oskam, G., & Meyer, G. J. (2005). Dye-sensitized SnO2 electrodes with iodide and pseudohalide redox mediators. *The Journal of Physical Chemistry B, 109*(2), 937-943.

Bhattacharja, S., Smoot, S., & Whitmore, D. (1986). Cation and anion diffusion in the amorphous phase of the polymer electrolyte $(PEO)_8$ $LiCF_3SO_3$. *Solid State Ionics, 18*, 306-314.

Bhattacharya, B., Lee, J. Y., Geng, J., Jung, H.-T., & Park, J.-K. (2009). Effect of cation size on solid polymer electrolyte based dye-sensitized solar cells. *Langmuir, 25*(5), 3276-3281.

Bhattacharya, B., Tomar, S., & Park, J.-K. (2007). A nanoporous TiO_2 electrode and new ionic liquid doped solid polymer electrolyte for dye sensitized solar cell application. *Nanotechnology, 18*(48), 485711.

Bruce, P. G., Evans, J., & Vincent, C. A. (1988). Conductivity and transference number measurements on polymer electrolytes. *Solid State Ionics, 28*, 918-922.

Buraidah, M., Teo, L., Majid, S., Yahya, R., Taha, R., & Arof, A. (2010). Characterizations of chitosan-based polymer electrolyte photovoltaic cells. *International Journal of Photoenergy, 2010*, doi:10.1155/2010/805836

Cardoso, G. T., Neto, S. C., & Vecchia, F. (2012). Rigid foam polyurethane (PU) derived from castor oil (Ricinus communis) for thermal insulation in roof systems. *Frontiers of Architectural Research, 1*(4), 348-356.

Chattopadhyay, D., & Webster, D. C. (2009). *Progress in Polymer Science, 34*(10), 1068-1133.

Chen-Yang, Y., Chen, Y., Chen, H., Lin, W., & Tsai, C. (2009). Effect of the addition of hydrophobic clay on the electrochemical property of polyacrylonitrile/LiClO 4 polymer electrolytes for lithium battery. *Polymer, 50*(13), 2856-2862.

Chen, W. C., Chen, H. H., Wen, T. C., Digar, M., & Gopalan, A. (2004). Morphology and ionic conductivity of thermoplastic polyurethane electrolytes. *Journal of Applied Polymer Science, 91*(2), 1154-1167.

Chiappone, A., Bella, F., Nair, J. R., Meligrana, G., Bongiovanni, R., & Gerbaldi, C. (2014). Structure–Performance Correlation of Nanocellulose-Based Polymer Electrolytes for Efficient Quasi-solid DSSCs. *ChemElectroChem, 1*(8), 1350–1358.

Chiu, H. T., & Wu, J. H. (2005). The effect of swelling agents and characterization of polyurethane/polymer electrolytes/clay composites. *Journal of Applied Polymer Science, 98*(3), 1206-1214.

Cho, T.-Y., Yoon, S.-G., Sekhon, S., & Han, C.-H. (2011). Effect of Ionic Liquids with Different Cations in I−/I3− Redox Electrolyte on the Performance of Dye-sensitized Solar Cells. *Bulletin of the Korean Chemical Society, 32*(6), 2058-2062.

Choi, H.-J., Song, Y.-M., Chung, I., Ryu, K.-S., & Jo, N.-J. (2009). Conducting polymer actuator based on chemically deposited polypyrrole and polyurethane-based solid polymer electrolyte working in air. *Smart Materials and Structures, 18*(2), 024006.

Choi, Y.-J., & Kim, D.-W. (2011). Photovoltaic Performance of Dye-sensitized Solar Cells assembled with Hybrid Composite Membrane based on Polypropylene Non-woven Matrix. *Bulletin of the Korean Chemical Society, 32*(2), 605-608.

Corcuera, M., Rueda, L., Saralegui, A., Martín, M., Fernández-d'Arlas, B., Mondragon, I., & Eceiza, A. (2011). Effect of diisocyanate structure on the properties and microstructure of polyurethanes based on polyols derived from renewable resources. *Journal of Applied Polymer Science, 122*(6), 3677.

Cui, Y., Zhang, X., Feng, J., Zhang, J., & Zhu, Y. (2013). Enhanced photovoltaic performance of quasi-solid-state dye-sensitized solar cells by incorporating a quaternized ammonium salt into poly (ethylene oxide)/poly (vinylidene fluoride-hexafluoropropylene) composite polymer electrolyte. *Electrochimica Acta, 108*, 757-762.

Daud, F. N., Ahmad, A., & Haji Badri, K. (2014). An Investigation on the Properties of Palm-Based Polyurethane Solid Polymer Electrolyte. *International Journal of Polymer Science, 2014*. Article ID 326716, doi:10.1155/2014/326716

De Freitas, J. N., Nogueira, A. F., & De Paoli, M.-A. (2009). New insights into dye-sensitized solar cells with polymer electrolytes. *Journal of Materials Chemistry, 19*(30), 5279-5294.

De Freitas, J. N., Nogueira, V. C., Ito, B. I., Soto-Oviedo, M. A., Longo, C., De Paoli, M.-A., & Nogueira, A. F. (2006). Dye-sensitized solar cells and solar module using polymer electrolytes: stability and performance investigations. *International Journal of Photoenergy, 2006*. Article ID 75483, doi:10.1155/IJP/2006/75483

Dean, J. A. (1985). Lange's handbook of chemistry, McGraw Hill Book Co., New York.

Deka, M., Kumar, A., Deka, H., & Karak, N. (2012). Ionic transport studies in hyperbranched polyurethane/clay nanocomposite gel polymer electrolytes. *Ionics, 18*(1-2), 181-187.

Digar, M., Hung, S.-L., Wang, H.-L., Wen, T.-C., & Gopalan, A. (2002). Study of ionic conductivity and microstructure of a cross-linked polyurethane acrylate electrolyte. *Polymer, 43*(3), 681-691.

Dissanayake, M., Bandara, L., Bokalawala, R., Jayathilaka, P., Ileperuma, O., & Somasundaram, S. (2002). A novel gel polymer electrolyte based on polyacrylonitrile (PAN) and its application in a solar cell. *Materials Research Bulletin, 37*(5), 867-874.

Dissanayake, M., Rupasinghe, W., Seneviratne, V., Thotawatthage, C., & Senadeera, G. (2014). Optimization of iodide ion conductivity and nano filler effect for efficiency enhancement in polyethylene oxide (PEO) based dye sensitized solar cells. *Electrochimica Acta, 145*, 319-326.

Dutta, N., Karak, N., & Dolui, S. (2004). Synthesis and characterization of polyester resins based on Nahar seed oil. *Progress in Organic Coatings, 49*(2), 146-152.

Dzulkurnain, N. A., Ahmad, A., & Mohamed, N. S. (2015). P (MMA-EMA) Random Copolymer Electrolytes Incorporating Sodium Iodide for Potential Application in a Dye-Sensitized Solar Cell. *Polymers, 7*(2), 266-280.

Fan, M.-S., Chen, J.-H., Li, C.-T., Cheng, K.-W., & Ho, K.-C. (2015). Copper zinc tin sulfide as a catalytic material for counter electrodes in dye-sensitized solar cells. *Journal of Materials Chemistry A, 3*(2), 562-569

Firdaus, M., & Meier, M. A. (2013). Renewable polyamides and polyurethanes derived from limonene. *Green Chemistry, 15*(2), 370-380.

Gao, Y., Chu, L., Wu, M., Wang, L., Guo, W., & Ma, T. (2012). Improvement of adhesion of Pt-free counter electrodes for low-cost dye-sensitized solar cells. *Journal of Photochemistry and Photobiology A: Chemistry, 245*, 66-71.

Goetzberger, A., Luther, J., & Willeke, G. (2002). Solar cells: past, present, future. *Solar Energy Materials and Solar Cells, 74*(1), 1-11.

Grätzel, M. (2000). Perspectives for dye-sensitized nanocrystalline solar cells. *Progress in Photovoltaics: Research and Applications, 8*(1), 171-185.

Grätzel, M. (2001). Photoelectrochemical cells. *Nature, 414*(6861), 338-344.

Guo, J., Shi, Y., Chu, Y., & Ma, T. (2013). Highly efficient telluride electrocatalysts for use as Pt-free counter electrodes in dye-sensitized solar cells. *Chemical Communications, 49*(86), 10157-10159.

Hagfeldt, A., & Graetzel, M. (1995). Light-induced redox reactions in nanocrystalline systems. *Chemical Reviews, 95*(1), 49-68.

Hepburn, C. (1992). Trends in polyurethane elastomer technology. *Iranian Journal of Polymer Science and Technology, 1*(2), 84-110.

Hong, L., & Shi, L. (2007). Composite polymer electrolytes based on the low crosslinked copolymer of linear and hyperbranched polyurethanes. *Journal of Applied Polymer Science, 104*(6), 3607-3613.

Hong, L., Shi, L., & Tang, X. (2003). Conductivities and spectroscopic studies of polymer electrolytes based on linear polyurethane and hybrid and copolymer of linear and hyperbranched polyurethanes. *Macromolecules, 36*(13), 4989-4994.

Hong, S. C., Nguyen-Thai, N. U., Hong, S. B., & Kang, P.-H. (2012). UV-cross-linked block copolymers for initiator-free, controlled in situ gelation of electrolytes in dye-sensitized solar cells. *Journal of Materials Chemistry, 22*(36), 18854-18863.

Hong, W., Xu, Y., Lu, G., Li, C., & Shi, G. (2008). Transparent graphene/PEDOT–PSS composite films as counter electrodes of dye-sensitized solar cells. *Electrochemistry Communications, 10*(10), 1555-1558.

Howard, G. T. (2002). Biodegradation of polyurethane: A review. *International Biodeterioration & Biodegradation, 49*(4), 245-252.

Hug, H., Bader, M., Mair, P., & Glatzel, T. (2014). Biophotovoltaics: natural pigments in dye-sensitized solar cells. *Applied Energy, 115*, 216-225.

Ibrahim, S., Ali, H., Aishah, S., & Nor Sabirin, M. (2010). *Characterization of PVDF-HFP-$LiCF_3SO_3$-ZrO_2 Nanocomposite Polymer Electrolyte Systems.* Paper presented at the Advanced Materials Research.

Idris, R., Glasse, M., Latham, R., Linford, R., & Schlindwein, W. (2001). Polymer electrolytes based on modified natural rubber for use in rechargeable lithium batteries. *Journal of Power Sources, 94*(2), 206-211.

Ileperuma, O., Dissanayake, M., & Somasundaram, S. (2002). Dye-sensitised photoelectrochemical solar cells with polyacrylonitrile based solid polymer electrolytes. *Electrochimica Acta, 47*(17), 2801-2807.

Ileperuma, O., Dissanayake, M., Somasunderam, S., & Bandara, L. (2004). Photoelectrochemical solar cells with polyacrylonitrile-based and polyethylene oxide-based polymer electrolytes. *Solar Energy Materials and Solar Cells, 84*(1), 117-124.

Imperiyka, M., Ahmad, A., Hanifah, S., & Bella, F. (2014). A UV-prepared linear polymer electrolyte membrane for dye-sensitized solar cells. *Physica B: Condensed Matter, 450*, 151-154.

Jena, A., Mohanty, S. P., Kumar, P., Naduvath, J., Gondane, V., Lekha, P., Das, J., Narula, H. K., Mallick, S., & Bhargava, P. (2012). Dye sensitized solar cells: a review. *Transactions of the Indian Ceramic Society, 71*(1), 1-16.

Júnior, A., Santos, J. H., Bertuol, D. A., Meneguzzi, A., Ferreira, C. A., & Amado, F. D. R. (2013). Castor oil and commercial thermoplastic polyurethane membranes modified with polyaniline: a comparative study. *Materials Research, 16*(4), 860-866.

Kang, J., Li, W., Wang, X., Lin, Y., Li, X., Xiao, X., & Fang, S. (2004). Gel polymer electrolytes based on a novel quaternary ammonium salt for dye-sensitized solar cells. *Journal of Applied Electrochemistry, 34*(3), 301-304.

Kang, M.-S., Ahn, K.-S., & Lee, J.-W. (2008). Quasi-solid-state dye-sensitized solar cells employing ternary component polymer-gel electrolytes. *Journal of Power Sources, 180*(2), 896-901.

Katz, M. J., DeVries Vermeer, M. J., Farha, O. K., Pellin, M. J., & Hupp, J. T. (2014). Dynamics of Back Electron Transfer in Dye-Sensitized Solar Cells Featuring 4-*tert*-Butyl-Pyridine and Atomic-Layer-Deposited Alumina as Surface Modifiers. *The Journal of Physical Chemistry B*, *119*(24), 7162-7169.

Khanmirzaei, M., & Ramesh, S. (2014). Nanocomposite polymer electrolyte based on rice starch/ionic liquid/TiO_2 nanoparticles for solar cell application. *Measurement, 58*, 68-72.

Kim, K. M., Park, N., Kang, M. G., Ryu, K. S., & Chang, S. H. (2006). Effect of TiO_2 Inclusion in the Poly (vinylidene fluoride-co-hexafluoropropylene)-Based Polymer Electrolyte of Dye-Sensitized Solar Cell. *Bulletin Korean Chemical Society, 27*(2), 322.

Kumar, M., Tiwari, T., & Srivastava, N. (2012). Electrical transport behaviour of bio-polymer electrolyte system: Potato starch + ammonium iodide. *Carbohydrate Polymers, 88*(1), 54-60.

Kuo, C.-W., Li, W.-B., Chen, P.-R., Liao, J.-W., Tseng, C.-G., & Wu, T.-Y. (2013). Effect of plasticizer and lithium salt concentration in PMMA-based composite polymer electrolytes. *International Journal of Electrochemical Science*.

Kuo, H.-H., Chen, W.-C., Wen, T.-C., & Gopalan, A. (2002a). A novel composite gel polymer electrolyte for rechargeable lithium batteries. *Journal of Power Sources, 110*(1), 27-33.

Kuo, P. L., Liang, W. J., & Lin, C. L. (2002b). Solid Polymer Electrolytes, 2. Preparation and Ionic Conductivity of Solid Polymer Electrolytes Based on Segmented Polysiloxane-Modified Polyurethane. *Macromolecular Chemistry and Physics, 203*(1), 230-237.

Lan, Z., Wu, J., Wang, D., Hao, S., Lin, J., & Huang, Y. (2006). Quasi-solid state dye-sensitized solar cells based on gel polymer electrolyte with poly (acrylonitrile-co-styrene)/NaI+ I_2. *Solar Energy, 80*(11), 1483-1488.

Lavall, R., Ferrari, S., Tomasi, C., Marzantowicz, M., Quartarone, E., Magistris, A., Mustarelli, P., Lazzaroni, S., & Fagnoni, M. (2010). Novel polymer electrolytes based on thermoplastic polyurethane and ionic liquid/lithium bis (trifluoromethanesulfonyl) imide/propylene carbonate salt system. *Journal of Power Sources, 195*(17), 5761-5767.

Lee, C.-P., Lin, J.-J., Ho, K.-C., Chang, L.-Y., & Chu, T.-C. (2013). *Solid-State Ionic Liquid Based Electrolytes for Dye-Sensitized Solar Cells*: INTECH Open Access Publisher.

Lee, H.-S., Han, C.-H., Sung, Y.-M., Sekhon, S., & Kim, K.-J. (2011). Gel electrolyte based on UV-cured polyurethane for dye-sensitized solar cells. *Current Applied Physics, 11*(1), S158-S162.

Lee, J. J., Ahammad, A. S., Lee, J. K., Rahman, M. M., Nath, N. D., & Sarker, S. (2011). *Metal oxides and their composites for the photoelectrode of dye sensitized solar cells*. INTECH Open Access Publisher.

Lee, J. Y., Bhattacharya, B., Kim, Y. H., Jung, H.-T., & Park, J.-K. (2009). Self degradation of polymer electrolyte based dye-sensitized solar cells and their remedy. *Solid State Communications, 149*(7), 307-309.

Liang, G., Zhong, Z., Qu, S., Wang, S., Liu, K., Wang, J., & Xu, J. (2013). Novel in situ crosslinked polymer electrolyte for solid-state dye-sensitized solar cells. *Journal of Materials Science, 48*(18), 6377-6385.

Liew, C.-W., & Ramesh, S. (2013). Studies on ionic liquid-based corn starch biopolymer electrolytes coupling with high ionic transport number. *Cellulose, 20*(6), 3227-3237.

Liu, D., Tian, H., Zhang, L., & Chang, P. R. (2008). Structure and properties of blend films prepared from castor oil-based polyurethane/soy protein derivative. *Industrial & Engineering Chemistry Research, 47*(23), 9330-9336.

Liu, L., Wu, X., & Li, T. (2014). Novel polymer electrolytes based on cationic polyurethane with different alkyl chain length. *Journal of Power Sources, 249*, 397-404.

Louwrier, A. (1998). Industrial products-the return to carbohydrate-based industries. *Biotechnology and Applied Biochemistry, 27*, 1-8.

Mengistie, D. A., Wang, P.-C., & Chu, C.-W. (2013). Effect of molecular weight of additives on the conductivity of PEDOT: PSS and efficiency for ITO-free organic solar cells. *Journal of Materials Chemistry A, 1*(34), 9907-9915.

Menne, S., Kühnel, R.-S., & Balducci, A. (2013). The influence of the electrochemical and thermal stability of mixtures of ionic liquid and organic carbonate on the performance of high power lithium-ion batteries. *Electrochimica Acta, 90*, 641-648.

Mohamed, N., & Arof, A. (2004). Conductivity studies of $LiCF_3SO_3$-doped and DMF-plasticized PVDF-based solid polymer electrolytes. *Physica Status Solidi (a), 201*(14), 3096-3101.

Mohamed, N., Subban, R., & Arof, A. (1995). Polymer batteries fabricated from lithium complexed acetylated chitosan. *Journal of Power Sources, 56*(2), 153-156.

Mortley, A., Bonin, H., & Bui, V. (2007). Synthesis and properties of radiation modified thermally cured castor oil based polyurethanes. *Nuclear Instruments and Methods in Physics Research Section B: Beam Interactions with Materials and Atoms, 265*(1), 98-103.

Musil, M., & Vondrák, J. (2014). Transference Number Measurements on Gel Polymer Electrolytes for Lithium-Ion Batteries. *ECS Transactions, 63*(1), 315-319.

Mutlu, H., & Meier, M. A. (2010). Castor oil as a renewable resource for the chemical industry. *European Journal of Lipid Science and Technology, 112*(1), 10-30.

Narine, S. S., Kong, X., Bouzidi, L., & Sporns, P. (2007). Physical properties of polyurethanes produced from polyols from seed oils: II. Foams. *Journal of the American Oil Chemists' Society, 84*(1), 65-72.

Ng, H., Ramesh, S., & Ramesh, K. (2015). Efficiency improvement by incorporating 1-methyl-3-propylimidazolium iodide ionic liquid in gel polymer electrolytes for dye-sensitized solar cells. *Electrochimica Acta*, *175*, 169-175.

Niedzicki, L., Karpierz, E., Zawadzki, M., Dranka, M., Kasprzyk, M., Zalewska, A., Marcinek, M., Zachara, J., Domańska, U., & Wieczorek, W. (2014). Lithium cation conducting TDI anion-based ionic liquids. *Physical Chemistry Chemical Physics, 16*(23), 11417-11425.

Niitani, T., Shimada, M., Kawamura, K., Dokko, K., Rho, Y.-H., & Kanamura, K. (2005). Synthesis of Li^+ ion conductive PEO-PSt block copolymer electrolyte with microphase separation structure. *Electrochemical and Solid-State Letters, 8*(8), A385-A388.

Ning, W., Xingxiang, Z., Haihui, L., & Benqiao, H. (2009). 1-Allyl-3-methylimidazolium chloride plasticized-corn starch as solid biopolymer electrolytes. *Carbohydrate Polymers, 76*(3), 482-484.

Noda, A., & Watanabe, M. (2000). Highly conductive polymer electrolytes prepared by in situ polymerization of vinyl monomers in room temperature molten salts. *Electrochimica Acta, 45*(8), 1265-1270.

Nogueira, A., Longo, C., & De Paoli, M.-A. (2004). Polymers in dye sensitized solar cells: overview and perspectives. *Coordination Chemistry Reviews, 248*(13), 1455-1468.

Nogueira, A. F., Alonso-Vante, N., & De Paoli, M.-A. (1999). Solid-state photoelectrochemical device using poly (o-methoxy aniline) as sensitizer and an ionic conductive elastomer as electrolyte. *Synthetic Metals, 105*(1), 23-27.

Nogueira, A. F., & De Paoli, M.-A. (2000). A dye sensitized TiO 2 photovoltaic cell constructed with an elastomeric electrolyte. *Solar Energy Materials and Solar Cells, 61*(2), 135-141.

Nogueira, A. F., Durrant, J. R., & De Paoli, M. A. (2001). Dye-Sensitized Nanocrystalline Solar Cells Employing a Polymer Electrolyte. *Advanced Materials, 13*(11), 826-830.

Noor, M., Buraidah, M., Careem, M., Majid, S., & Arof, A. (2014). An optimized poly (vinylidene fluoride-hexafluoropropylene)–NaI gel polymer electrolyte and its application in natural dye sensitized solar cells. *Electrochimica Acta, 121*, 159-167.

Noor, S., Ahmad, A., Talib, I., & Rahman, M. (2010). Morphology, chemical interaction, and conductivity of a PEO-ENR50 based on solid polymer electrolyte. *Ionics, 16*(2), 161-170.

O'Regan, B., & Grätzel, M. (1991). A low-cost, high-efficiency solar cell based on dye-sensitized colloidal TiO_2 films. *nature, 353*(6346), 737-740.

Österholm, A., Damlin, P., Kvarnström, C., & Ivaska, A. (2011). Studying electronic transport in polyazulene–ionic liquid systems using infrared vibrational spectroscopy. *Physical Chemistry Chemical Physics, 13*(23), 11254-11263.

Patton, T. (1962). Alkyd Resin Technology Interscience. *New York.*

Periasamy, P., Tatsumi, K., Shikano, M., Fujieda, T., Saito, Y., Sakai, T., Mizuhata, M., Kajinami, A., & Deki, S. (2000). Studies on PVdF-based gel polymer electrolytes. *Journal of Power Sources, 88*(2), 269-273.

Petrović, Z. S. (2008). Polyurethanes from vegetable oils. *Polymer Reviews, 48*(1), 109-155.

Petrovic, Z. S., Zhang, W., & Javni, I. (2005). Structure and properties of polyurethanes prepared from triglyceride polyols by ozonolysis. *Biomacromolecules, 6*(2), 713-719.

Pfister, D. P., Xia, Y., & Larock, R. C. (2011). Recent Advances in Vegetable Oil-Based Polyurethanes. *ChemSusChem, 4*(6), 703-717.

Puguan, J. M. C., Chinnappan, A., Appiah-Ntiamoah, R., & Kim, H. (2015). Enhanced Ionic conductivity and optical transmissivity of functionalized ZrO_2/PVdF-HFP hybrid electrolyte for energy efficient windows. *Solar Energy Materials and Solar Cells, 137*, 265-273.

Quartarone, E., Mustarelli, P., & Magistris, A. (1998). PEO-based composite polymer electrolytes. *Solid State Ionics, 110*(1), 1-14.

Rajendran, S., Sivakumar, M., Subadevi, R., & Nirmala, M. (2004). Characterization of PVA–PVdF based solid polymer blend electrolytes. *Physica B: Condensed Matter, 348*(1), 73-78.

Rajendran, S., Sivakumar, P., & Babu, R. S. (2006). Investigation on poly (vinylidene fluoride) based gel polymer electrolytes. *Bulletin of Materials Science, 29*(7), 673.

Ramesh, S., Liew, C.-W., & Ramesh, K. (2011). Evaluation and investigation on the effect of ionic liquid onto PMMA-PVC gel polymer blend electrolytes. *Journal of Non-Crystalline Solids, 357*(10), 2132-2138.

Rani, M. S. A., Rudhziah, S., Ahmad, A., & Mohamed, N. S. (2014). Biopolymer electrolyte based on derivatives of cellulose from kenaf bast fiber. *Polymers, 6*(9), 2371-2385.

Rashmi, B., Rusu, D., Prashantha, K., Lacrampe, M., & Krawczak, P. (2013). Development of bio-based thermoplastic polyurethanes formulations using corn-derived chain extender for reactive rotational molding. *Express Polymer Letter, 7*(10), 852-862.

Reddy, C. V. S., Sharma, A., & Rao, V. N. (2003). Conductivity and discharge characteristics of polyblend (PVP+ PVA+ KI) electrolyte. *Journal of Power Sources, 114*(2), 338-345.

Rodrigues, L., Barbosa, P., Silva, M. M., & Smith, M. J. (2007). Electrochemical and thermal properties of polymer electrolytes based on poly (epichlorohydrin-co-ethylene oxide-co-ally glycidyl ether). *Electrochimica Acta, 53*(4), 1427-1431.

Rogers, M. E., & Long, T. E. (2003). *Synthetic methods in step-growth polymers*: Wiley Online Library.

Rudhziah, S., Ahmad, A., Ahmad, I., & Mohamed, N. (2015a). Biopolymer electrolytes based on blend of kappa-carrageenan and cellulose derivatives for potential application in dye sensitized solar cell. *Electrochimica Acta*.

Rudhziah, S., Rani, M., Ahmad, A., Mohamed, N., & Kaddami, H. (2015b). Potential of blend of kappa-carrageenan and cellulose derivatives for green polymer electrolyte application. *Industrial Crops and Products*.

Samsudin, A., Lai, H., & Isa, M. (2014). Biopolymer Materials Based Carboxymethyl Cellulose as a Proton Conducting Biopolymer Electrolyte for Application in Rechargeable Proton Battery. *Electrochimica Acta, 129*, 1-13.

Santhosh, P., Vasudevan, T., Gopalan, A., & Lee, K.-P. (2006). Preparation and properties of new cross-linked polyurethane acrylate electrolytes for lithium batteries. *Journal of Power Sources, 160*(1), 609-620.

Sapp, S. A., Elliott, C. M., Contado, C., Caramori, S., & Bignozzi, C. A. (2002). Substituted polypyridine complexes of cobalt (II/III) as efficient electron-transfer mediators in dye-sensitized solar cells. *Journal of the American Chemical Society, 124*(37), 11215-11222.

Sedlaří, M., Velická, J., Klápště, B., & Reiter, J. (2001). Gel polymer electrolytes based on PMMA. *Electrochimica Acta, 46*(13), 2047-2048.

Sequeira, C., & Santos, D. (2010). *Polymer Electrolytes: Fundamentals and Applications*. UK: Woodhead Publishing.

Shen, X., Xu, W., Xu, J., Liang, G., Yang, H., & Yao, M. (2008). Quasi-solid-state dye-sensitized solar cells based on gel electrolytes containing different alkali metal iodide salts. *Solid State Ionics, 179*(35), 2027-2030.

Shi, Z., Deng, K., & Li, L. (2015). Pt-free and efficient counter electrode with nanostructured $CoNi_2S_4$ for dye-sensitized solar cells. *Scientific reports, 5*.

Singh, P. K., Bhattacharya, B., Nagarale, R., Kim, K.-W., & Rhee, H.-W. (2010). Synthesis, characterization and application of biopolymer-ionic liquid composite membranes. *Synthetic Metals, 160*(1), 139-142.

Singh, P. K., Kim, K.-W., & Rhee, H.-W. (2008). Electrical, optical and photoelectrochemical studies on a solid PEO-polymer electrolyte doped with low viscosity ionic liquid. *Electrochemistry Communications, 10*(11), 1769-1772.

Singh, P. K., Kim, K. W., & Rhee, H. W. (2009). Ionic liquid (1-methyl 3-propyl imidazolium iodide) with polymer electrolyte for DSSC application. *Polymer Engineering & Science, 49*(5), 862-865.

Singh, P. K., Nagarale, R., Pandey, S., Rhee, H., & Bhattacharya, B. (2011). Present status of solid state photoelectrochemical solar cells and dye sensitized solar cells using PEO-based polymer electrolytes. *Advances in Natural Sciences: Nanoscience and Nanotechnology, 2*(2), 023002.

Singh, R., Bhattacharya, B., Rhee, H.-W., & Singh, P. K. (2014). New Biodegradable Polymer Electrolyte for Dye Sensitized Solar Cell. *Int. J. Electrochem. Sci, 9*, 2620-2630.

Singh, R., Jadhav, N. A., Majumder, S., Bhattacharya, B., & Singh, P. K. (2013). Novel biopolymer gel electrolyte for dye-sensitized solar cell application. *Carbohydrate polymers, 91*(2), 682-685.

Singh, V. K., Bhattacharya, B., Shukla, S., & Singh, P. K. (2015). Dye-sensitized solar cell comprising polyethyl methacrylate doped with ammonium iodide solid polymer electrolyte. *Applied Physics A, 118*(3), 877-883.

Singh, V. V., Nigam, A. K., Batra, A., Boopathi, M., Singh, B., & Vijayaraghavan, R. (2012). Applications of ionic liquids in electrochemical sensors and biosensors. *International Journal of Electrochemistry, 2012*.

Somani, K. P., Kansara, S. S., Patel, N. K., & Rakshit, A. K. (2003). Castor oil based polyurethane adhesives for wood-to-wood bonding. *International journal of adhesion and adhesives, 23*(4), 269-275.

Su'ait, M., Ahmad, A., Badri, K., Mohamed, N., Rahman, M., Ricardo, C., & Scardi, P. (2014a). The potential of polyurethane bio-based solid polymer electrolyte for photoelectrochemical cell application. *International Journal of Hydrogen Energy, 39*(6), 3005-3017.

Su'ait, M., Ahmad, A., Badri, K., Mohamed, N., Rahman, M., Ricardo, C. A., & Scardi, P. (2014b). The potential of polyurethane bio-based solid polymer electrolyte for photoelectrochemical cell application. *International Journal of Hydrogen Energy, 39*(6), 3005-3017.

Su'ait, M., Ahmad, A., Hamzah, H., & Rahman, M. (2009). Preparation and characterization of PMMA–MG49–$LiClO_4$ solid polymeric electrolyte. *Journal of Physics D: Applied Physics, 42*(5), 055410.

Stergiopoulos, T., Rozi, E., Karagianni, C. S., & Falaras, P. (2011). Influence of electrolyte co-additives on the performance of dye-sensitized solar cells. *Nanoscale Research Letters*, *6*(1), 1-7.

Suhaimi, S., Shahimin, M. M., Alahmed, Z., Chyský, J., & Reshak, A. (2015). Materials for Enhanced Dye-sensitized Solar Cell Performance: Electrochemical Application. *Int. J. Electrochem. Sci, 10*, 2859-2871.

Szycher, M. (2013). Szycher's handbook of polyurethanes. Boca Raton, Taylor & Francis, 2013, xvii, 1126 s: ISBN 14-398-3958-1.

Tafur, J. P., Santos, F., & Romero, A. J. F. (2015). Influence of the Ionic Liquid Type on the Gel Polymer Electrolytes Properties. *Membranes, 5*(4), 752-771.

Tan, W. C., Alias, S. S., Ismail, A. B., & Mohamad, A. A. (2012). Effect of styrene–acrylonitrile content on 0.5 M NaI/0.05 M I_2 liquid electrolyte encapsulation for dye-sensitized solar cells. *Journal of Solid State Electrochemistry, 16*(6), 2103-2112.

Tsai, C.-H., Lu, C.-Y., Chen, M.-C., Huang, T.-W., Wu, C.-C., & Chung, Y.-W. (2013). Efficient gel-state dye-sensitized solar cells adopting polymer gel electrolyte based on poly (methyl methacrylate). *Organic Electronics, 14*(11), 3131-3137.

Ueki, T., & Watanabe, M. (2008). Macromolecules in ionic liquids: progress, challenges, and opportunities. *Macromolecules, 41*(11), 3739-3749.

Uyama, H., Kuwabara, M., Tsujimoto, T., Nakano, M., Usuki, A., & Kobayashi, S. (2003). Green nanocomposites from renewable resources: plant oil-clay hybrid materials. *Chemistry of Materials, 15*(13), 2492-2494.

Van Heumen, J., & Stevens, J. (1995). The role of lithium salts in the conductivity and phase morphology of a thermoplastic polyurethane. *Macromolecules, 28*(12), 4268-4277.

Vieira, D. F., Avellaneda, C. O., & Pawlicka, A. (2007). Conductivity study of a gelatin-based polymer electrolyte. *Electrochimica Acta, 53*(4), 1404-1408.

Vu, C. (1989). Castor oil based polyurethane for bridge deckings and related applications: US Patent.

Wang, G., Zhou, X., Li, M., Zhang, J., Kang, J., Lin, Y., Fang, S., & Xiao, X. (2004). Gel polymer electrolytes based on polyacrylonitrile and a novel quaternary ammonium salt for dye-sensitized solar cells. *Materials Research Bulletin, 39*(13), 2113-2118.

Wang, H.-L., Kao, H.-M., & Wen, T.-C. (2000). Direct 7Li NMR Spectral Evidence for Different Li^+ Local Environments in a Polyether Poly (urethane urea) Electrolyte. *Macromolecules, 33*(19), 6910-6912.

Wang, P., Zakeeruddin, S. M., Comte, P., Charvet, R., Humphry-Baker, R., & Grätzel, M. (2003a). Enhance the performance of dye-sensitized solar cells by co-grafting amphiphilic sensitizer and hexadecylmalonic acid on TiO_2 nanocrystals. *The Journal of Physical Chemistry B, 107*(51), 14336-14341.

Wang, P., Zakeeruddin, S. M., Moser, J. E., Nazeeruddin, M. K., Sekiguchi, T., & Grätzel, M. (2003b). A stable quasi-solid-state dye-sensitized solar cell with an amphiphilic ruthenium sensitizer and polymer gel electrolyte. *Nature materials, 2*(6), 402-407.

Wang, Q., Moser, J.-E., & Grätzel, M. (2005a). Electrochemical impedance spectroscopic analysis of dye-sensitized solar cells. *The Journal of Physical Chemistry B, 109*(31), 14945-14953.

Wang, S. (2007). *Development of solid polymer electrolytes of polyurethane and polyether-modified polysiloxane blends with lithium salts.* The University of Akron.

Wang, S., Jeung, S., & Min, K. (2010). The effects of anion structure of lithium salts on the properties of in-situ polymerized thermoplastic polyurethane electrolytes. *Polymer, 51*(13), 2864-2871.

Wang, S., & Min, K. (2010). Solid polymer electrolytes of blends of polyurethane and polyether modified polysiloxane and their ionic conductivity. *Polymer, 51*(12), 2621-2628.

Wang, X., Zhang, Y., Xu, Q., Xu, J., Wu, B., Gong, M., Chu, J., & Xiong, S. (2015). A low-cost quasi-solid DSSC assembled with PVDF-based gel electrolyte plasticized by PC–EC & electrodeposited Pt counter electrode. *Journal of Photochemistry and Photobiology A: Chemistry, 311*, 112-117.

Wang, Y. (2009). Recent research progress on polymer electrolytes for dye-sensitized solar cells. *Solar Energy Materials and Solar Cells, 93*(8), 1167-1175.

Wang, Z.-S., Sayama, K., & Sugihara, H. (2005b). Efficient eosin y dye-sensitized solar cell containing Br^-/Br_3^- electrolyte. *The Journal of Physical Chemistry B, 109*(47), 22449-22455.

Wen, T.-C., Du, Y.-L., & Digar, M. (2002). Compositional effect on the morphology and ionic conductivity of thermoplastic polyurethane based electrolytes. *European Polymer Journal, 38*(5), 1039-1048.

Wen, T.-C., Luo, S.-S., & Yang, C.-H. (2000). Ionic conductivity of polymer electrolytes derived from various diisocyanate-based waterborne polyurethanes. *Polymer, 41*(18), 6755-6764.

Wen, T.-C., Wang, Y.-J., Cheng, T.-T., & Yang, C.-H. (1999a). The effect of DMPA units on ionic conductivity of PEG–DMPA–IPDI waterborne polyurethane as single-ion electrolytes. *Polymer, 40*(14), 3979-3988.

Wen, T.-C., Wu, M.-S., & Yang, C.-H. (1999b). Spectroscopic investigations of poly (oxypropylene) glycol-based waterborne polyurethane doped with lithium perchlorate. *Macromolecules, 32*(8), 2712-2720.

Wen, T. C., Fang, J. C., Lin, H. J., & Yang, C. H. (2001). Characteristics of PPG-based thermoplastic polyurethane doped with lithium perchlorate. *Journal of Applied Polymer Science, 82*(2), 389-399.

Wright, P. V. (1975). Electrical Conductivity in Ionic Complexes of poly(ethylene oxide). *British Polymer Journal, 7*, 319-327.

Wu, C., Jia, L., Guo, S., Han, S., Chi, B., Pu, J., & Jian, L. (2013). Open-Circuit Voltage Enhancement on the Basis of Polymer Gel Electrolyte for a Highly Stable Dye-Sensitized Solar Cell. *ACS applied materials & interfaces, 5*(16), 7886-7892.

Wu, F., Feng, T., Wu, C., Bai, Y., Ye, L., & Chen, J. (2010). Thermally stable hyperbranched polyether-based polymer electrolyte for lithium-ion batteries. *Journal of Physics D: Applied Physics, 43*(3), 035501.

Xu, Y., Petrovic, Z., Das, S., & Wilkes, G. L. (2008). Morphology and properties of thermoplastic polyurethanes with dangling chains in ricinoleate-based soft segments. *Polymer, 49*(19), 4248-4258.

Yang, H., Huang, M., Wu, J., Lan, Z., Hao, S., & Lin, J. (2008a). The polymer gel electrolyte based on poly (methyl methacrylate) and its application in quasi-solid-state dye-sensitized solar cells. *Materials Chemistry and Physics, 110*(1), 38-42.

Yang, J. H., Bark, C. W., Kim, K. H., & Choi, H. W. (2014). Characteristics of the Dye-Sensitized Solar Cells Using TiO_2 Nanotubes Treated with $TiCl_4$. *Materials, 7*(5), 3522-3532.

Yang, Y., Zhang, J., Zhou, C., Wu, S., Xu, S., Liu, W., Han, H., Chen, B., & Zhao, X.-z. (2008b). Effect of lithium iodide addition on poly (ethylene oxide)− poly (vinylidene fluoride) polymer-blend electrolyte for dye-sensitized nanocrystalline solar cell. *The Journal of Physical Chemistry B, 112*(21), 6594-6602.

Yeganeh, H., & Shamekhi, M. A. (2006). Novel polyurethane insulating coatings based on polyhydroxyl compounds, derived from glycolysed PET and castor oil. *Journal of Applied Polymer Science, 99*(3), 1222-1233.

Zainal, N., Mohamed, N., & Idris, R. (2013). Properties of ENR-50 Based Electrolyte System. *Sains Malaysiana 42*(4), 481-485.

Zhou, L., Cao, Q., Jing, B., Wang, X., Tang, X., & Wu, N. (2014). Study of a novel porous gel polymer electrolyte based on thermoplastic polyurethane/poly (vinylidene fluoride-co-hexafluoropropylene) by electrospinning technique. *Journal of Power Sources, 263*, 118-124.

Zygadło-Monikowska, E., Florjańczyk, Z., Kubisa, P., Biedroń, T., Sadurski, W., Puczyłowska, A., Langwald, N., & Ostrowska, J. (2014). Lithium electrolytes based on modified imidazolium ionic liquids. *International Journal of Hydrogen Energy, 39*(6), 2943-2952.

LIST OF PUBLICATIONS

Ibrahim, S., Ahmad, A., & Mohamed, N. S. (2015). Characterization of Novel Castor Oil-Based Polyurethane Polymer Electrolytes. *Polymers, 7*(4), 747-759.

Ibrahim, S., Ahmad, A., & Mohamed, N. S. (2015). Synthesis and Characterization of Castor Oil-Based Polyurethane for Potential Application as Host in Polymer Electrolytes. *Bulletin of Materials Science*, *38*(5) 1155-1161.

Ibrahim, S., Ahmad, A., & Mohamed, N. S., Comprehensive Studies on Polymer Electrolyte and Dye-Sensitized Solar Cell Developed Using Castor Oil based Polyurethane, *Submitted to ISI-Cited Publication.*

LIST OF CONFERENCES ATTENDED

1. XIV International Symposium on Polymer Electrolytes, 24th-29th August 2014, Geelong, Australia.
   Title: Novel Castor Oil based Polyurethane Quasi-Solid Polymer Electrolytes for Dye-Sensitized Solar Cell Application.
   Poster presenter

2. Regional Conference on Solid State Science and Technology (RCSSST), 25th-27th November 2014, Cameron Highlands, Pahang.
   Title: Polyurethane based Biopolymer Electrolytes for Dye-Sensitized Solar Cells
   Oral presenter.

LIST OF AWARD

1. **Silver Medal**
   Title: Alternative Bio-Based Polymer Electrolytes for High Efficiency DSSC.
   Invention, Innovation and Design Exposition (IIDEX 2015) at Universiti Teknologi MARA UiTM Shah Alam, Malaysia. 27th-30th April 2015.

2. **Student Travel Award**
   XIV International Symposium on Polymer Electrolytes, 24th-29th August 2014, Geelong, Australia.